Alternative Approaches to Orbital Optimisation in First Row Transition Metal Systems

By

Matthew John Tilling

A thesis submitted in partial fulfilment of the requirements for the degree of Doctor of Philosophy in Chemistry

University of Warwick

Department of Chemistry

June 2015

Contents

List of Figures

List of Tables

Acknowledgements

Over my years at The University of Warwick I have met many people without whose help and support I would not have reached this far.

First of all, I would like to thank my supervisor Professor Peter Taylor whose help and support has been instrumental in producing this thesis. Without his guidance and sparks of genius none of this would have been possible.

During my PhD I have meet many wonderful people who both as friends and colleagues have provided much needed support and guidance whenever it has been needed. For this I would like to thank Dr. Guilherme Arantes, Devan Bailey, Jay Bomphrey, Dr. James Burnside, Dr. Christian Diedrich, Dr. Natalie Gilka, Dr. Remco Havenith, Dr. Rob Hawtin, Dr. David Quigley, Dr. Adam Skelton, Dr. Espen Tangen. A special thank you goes to Dr. Kaz Yousaf and Dave Haggart who have helped and supported me at every turn.

I would also like to thank members of the University of Warwick archery club and it's associates who are too numerous to name for their friendship and support throughout my university career.

Finally I would like to thank my parents Sheila and Lenard for their unending support and encouragement.

Declaration

This thesis represents original material, and is the author's own work. No part of this thesis has been previously created or published by a person other than the author, unless otherwise acknowledged in the text. This thesis has not been submitted for a degree at an establishment other than the University of Warwick.

Summary

Two new methods to aid in the calculation of *ab initio* energies are presented.

The first method sets out to change the way that systems that have multiple elements that would benefit from a multireference treatment are handled. The method proposes splitting the system into multiple small active spaces in order to avoid the computational issues present with a single large active space. The method is developed using localised orbitals and tested on Cr_2 and the molecule N_2 both at long bond lengths.

The second method proposes and develops a method for the production of starting orbitals for CASSCF and CASPT2 calculations. This method requires multiple subunits of the system which are then optimised to produce subsets of orbitals. These orbitals are then combined using a custom script (detailed within) to form a coherent orbital set for the entire system. This method is then tested on two transition metal complexes, one of which could not be successfully treated using traditional methods. Along with the two new methods, two studies of individual transition metal systems are presented. The first covers a comparison between a published DFT/OLYP study of complexes of the form (nacnac)M^{III}(NPh) with a DFT/B3-LYP, CASSCF, CASPT2 and CCSD(T) study of similar systems presented here. The second studies the complex $[Cr^{II}(CN)_5]^{3-}$. It produces a possible transition state, and discussed its role in a Berry pseudorotation-like mechanism for this system.

List of Abbreviations

ACPF Averaged coupled-pair functional

ANO Atomic natural orbital

AO Atomic orbital

AUG-CC Augmented correlation consistent

B3 Becke three parameter exchange functional

BSSE Basis set superposition error

CASPT2 Second order multireference perturbation theory

CAS Complete active space

CCSD(T) Coupled cluster with single and doubles and pseudo-triples

CC Correlation consistent

CGTO Contracted Gaussian type orbital

CI Configuration Interaction

CSF Configuration State function

DFT Density functional theory

GTO Gaussian type orbital

HF Hartree-Fock

HOMO-x The orbital x below the HOMO

HOMO Highest occupied molecular orbital

IVO Improved virtual orbitals

LDA Local density approximation

LSDA Local spin density approximation

LUMO Lowest unoccupied molecular orbital

LYP Lee, Yang and Parr correlation functional

MO Molecular orbital

MPx The x-th order Møller-Plesset Perturbation Theory

Me The methyl functional group

O OPTX exchange functional

PBE Perdew, Berke and Ernzerhof correlation functional

PGTO Primitive Gaussian type orbital

PVDZ Valence double-zeta with polarisation

Ph The phenyl functional group

RAS Restricted active space

RHF Restricted Hartree-Fock

SCF Self consistent field

STO Slater-type orbital

SVP Split valence plus polarisation

TZVP Triple-zeta valence plus polarisation

J Heisenberg exchange coupling constant

Chapter 1

Introduction

1.1 Background

"It is unworthy of excellent men to lose hours like slaves in the labor of calculation which could be relegated to anyone else if machines were used."

Gottfried Wilhelm von Leibniz

Without the invention of the computer the modelling of real world chemical systems would be impossible; hand calculation of matrices of the size used in most modern computational methods would be ludicrously time consuming. However just as hand calculation reached a limit some time ago even with the perpetual increase in compute power that the world currently enjoys, some things are still at the edge or beyond the capabilities of even the larger supercomputers. This is not due to a lack of compute power but simply a matter of practicality. Yes if you wait long enough and have enough memory and storage any calculation is possible. However after a certain point the risk of accidental loss of data or the need for results outweighs any benefits. One such problem is multireference calculations with large active spaces. Once the active space exceeds about twenty electrons in twenty orbitals the number of processor hours of work becomes insurmountable. However these types of calculation are becoming more important as large, multi-metal complexes are becoming more widely investigated. The metal centres in these compounds require large active spaces when treated individually. This means that when multiple centres are com-

bined a calculation can quickly expand to a size where multireference methods are no longer feasible.

1.2 Aims

The aim of this thesis was to find new and inventive procedures to aid in the calculation of the type of large transition metal systems so popular at the moment. These systems have many important uses from solar power [1] to models of enzyme behaviour [2]. These systems are normally too large or complex for the kind of accurate post Hartree-Fock methods that produce the best results.

In order to meet this aim two methods have been presented which tackle the main problems preventing the use of these methods for large transition metal systems. These problems include the presence of multiple metal centres and the complexity of the orbital interactions around those metal centres.

1.3 Overview

This thesis can be split into three sections, one for each of the proposed methods and a third containing investigations into two interesting systems discovered during the course of this thesis. A short summary of each section is detailed below.

A method for the calculation of multi-metal centre containing compounds using a number of small localised active spaces is proposed and investigated in chapters 3 and 4. Chapter 3 introduces the methods and initial test system used in this investigation the Cr_2 dimer. Chapter 4 investigates in detail a a second test system the N_2 molecule. This chapter also presents some extensions of the method.

Chapter 7 covers a proposed method for the production of better optimised molecular orbitals for the calculation of CASSCF and CASPT2 wave functions using a multi-stage process. This process calculates orbitals in discrete units, produced by subdividing the system of interest. The units are then reassembled, to produce a complete orbital set using a custom piece of Python code. This code is detailed in Chapter 7, along with two

practical examples of the method in use on transition metal centred complexes.

An investigation into the use of a an interesting DFT functional and its applications are covered in chapter 5. Here DFT/B3-LYP, CASSCF, CASPT2 and CCSD(T) calculations are used to assess the validity of information produced about complexes of the form (nacnac)M^{III}(NPh) using OLYP, a functional constructed with the OPTX exchange functional and the LYP correlation functional.

The discovery of a possible new transition state in the complex $[Cr^{II}(CN)_5]^{3-}$ is discussed in chapter 6. The discovery of the transition state is explained along with a proposed variation on the Berry pseudorotation mechanism for this system.

Chapter 2

Theory

2.1 References

A number of books and sets of lecture notes were used in the production of this thesis and particularly in this chapter. Rather than quote each part used, the references for the entire books and sets of notes are presented here.

The books used were Introduction to Computational Chemistry [3] and the European Summerschool in Quantum Chemistry 2005 books [4, 5, 6]. Also lecture notes by Prof. Peter Taylor, and notes by Prof. Jeremy Harvey were used [7].

2.2 Introduction

Chemistry is the study of how atoms interact with each other. In the world of Experimental Chemistry this is usually done through the mixing and reacting of various chemical compounds (collections of atoms formed in to complex molecules) to form new and novel compounds. In the world of Computational and Theoretical Chemistry, however, the study of these interactions is done at a more fundamental level.

In Theoretical and Computational Chemistry, mathematical equations are used to characterise the interactions that, when put together, describe how atoms interact to form molecules, and how these molecules react to, and with, each other.

To understand how molecules are formed we must first understand the fundamental

particles that make up the atoms. These particles can be split in to two groups: the nucleus, consisting of protons and neutrons, and the electrons that surround the nucleus.

There are two ways of looking at the interactions between particles in a system. The classical Newtonian method which works well for heavy slow moving objects such as buildings and people, and quantum mechanics which works better when the objects of interest are extremely light and small.

An atom, in general, is on the borderline between the classical and quantum mechanical regimes. Atoms moving with respect to one another can be described within both regimes, but if the interaction between the nucleus and electrons, or between a number of individual electrons is needed, a quantum mechanical method is required.

This thesis will concentrate on the interactions between electrons within atoms and molecules as they relate to chemical bonds and and other properties of these systems. As such this section will be limited to the use of quantum mechanics as a method for understanding these interactions.

2.2.1 Atomic Units

In order to simplify the representations of the various equations in this thesis the system of units used is atomic units (au). This system of units simplifies the equations by setting various important physical quantities involved in electronic structure and quantum mechanics to one. The quantities involved are the mass of an electron (m_e), (e) represents minus the charge on an electron, the Bohr radius (a_0) and the reduced Plank's constant ($\hbar$). This incidentally leads to a new unit for energy in an atomic system called the Hartree (E_H) which is equal to 4.360×10^{-18} J.

2.3 The Schrödinger Equation

Quantum mechanics is a way of producing a set of equations using the fundamental behaviour of the particles in a system. This set of equations can be used to determine how the particles in the system interact with each other, and from these interactions, how the

system as a whole can be described.

The basic equation used for quantum mechanics at a molecular level is the time-independent Schrödinger, equation which can be represented as shown in equation (2.1),

$$\mathbf{H}(\tau_1, \tau_2 \ldots \tau_N)\Psi(\tau_1, \tau_2 \ldots \tau_N) = E\Psi(\tau_1, \tau_2 \ldots \tau_N) \tag{2.1}$$

In equation (2.1) $\mathbf{H}$ is the Hamiltonian operator, Ψ is the wave function of the system, E is total energy of the system and τ_i the co-ordinates of the i^{th} particle in the system. The Hamiltonian operator is the sum of the kinetic energy ($\mathbf{T}$) and potential energy ($\mathbf{V}$). The wave function Ψ contains all the information about the system.

This equation can be solved exactly, but only for systems with up to two bodies such as in the Hydrogen atom which consists of one proton in the nucleus and one electron surrounding it. For larger systems such as the helium atom or any molecule, the equation has a larger number of variables. There is no way of solving the set of equations generated by such a system for all variables analytically. As such the use of the full time-independent Schrödinger equation is not possible for the study of the type of systems of interest to today's Chemists.

In order to make the time-independent Schrödinger equation useful to Chemists, simplifications of the equation are needed to allow a solution for a many body system. The simplified equation must be able to accurately predict the properties of systems comprising many atoms.

The first thing to consider when looking at ways to simplify the time-independent Schrödinger equation is what parts of the system require quantum mechanical treatment. In an atom, most of the mass is in the nucleus (in the form of protons and neutrons). Comparing a proton and an electron, the proton is approximately two thousand times more massive than the electron. From this comparison an assertion can be made that the electrons, being much lighter, are also moving at a much higher speed and are therefore the parts of the system most requiring quantum mechanical treatment.

The Born-Oppenheimer approximation is a formalisation of the above assertion which states that one can ignore coupling between nuclear motion (slow) and electronic motion

(fast). This approximation allows the separation of the electronic and nuclear parts of the time-independent Schrödinger equation.

The Born-Oppenheimer approximation gives rise to a new form of the Schrödinger equation as a separate electronic Schrödinger equation, as shown in (2.2), and a nuclear Schrödinger equation.

$$\mathbf{H}(r_i;R_A)\Psi(r_i;R_A) = E(R_A)\Psi(r_i;R_A) \tag{2.2}$$

In equation (2.2) i runs over the electrons in the system and A runs over the nuclei. This gives $\Psi(r_i;R_A)$ as a set of different electronic wave functions over R_A the co-ordinates of fixed nuclei. $E(R_A)$, then defines the potential energy surface for nuclear motion, and $\mathbf{H}(r_i;R_A)$ is the Hamiltonian operator.

For the electronic Schrödinger equation the form of the Hamiltonian operator $\mathbf{H}(r_i;R_A)$ can be seen in (2.3).

$$\mathbf{H} = -\sum_i \frac{1}{2}\nabla_i^2 - \sum_A \sum_i \frac{Z_A}{r_{Ai}} + \sum_{i>j} \frac{1}{r_{ij}} + \sum_{A>B} \frac{Z_A Z_B}{R_{AB}} \tag{2.3}$$

In equation (2.3) ∇_i^2 is defined as in (2.4), Z_a is the charge on nucleus A, r_{Ai} is the distance between nucleus A and electron i, r_{ij} is the distance between electron i and electron j and R_{AB} is the distance between nucleus A and nucleus B.

$$\nabla_i^2 = \left(\frac{\partial^2}{\partial X_i^2} + \frac{\partial^2}{\partial Y_i^2} + \frac{\partial^2}{\partial Z_i^2} \right) \tag{2.4}$$

2.4 Hartree-Fock

Even using the Born-Oppenheimer approximation, the electronic Schrödinger equation is still too complex to be able to find an analytical solution for the size of systems that are regarded as chemically important. Therefore, further simplifications to the model used must be made to produce a calculable method. A start in this simplification is to make the assumption that the traditional chemistry model of an atom holds. This models the atom as

systems of electrons orbiting a central nucleus, in set orbitals each holding up to two spin paired (i.e. one electron spin up (α) and one electron spin down (β)) electrons. From this model a wave function can be constructed by allocating electrons pair-wise, to molecular orbitals ψ. These molecular orbitals can then be modelled by Slater determinants which are the antisymmetrised orbital products.

The first step in forming the Hartree-Fock equations is to look at the problem at a very basic level. The electronic Schrödinger equation can be solved for the case of the Hydrogen atom. This solution can also be shown for other one electron systems such as He^+ as the electronic Schrödinger equation has no reliance on the mass of the nucleus, only on its position. In order to move beyond a one-electron problem the interaction between electrons must be considered. The obvious place to start is to consider a case of non-interacting electrons. For this a model system of H^- is used. If the electrons are non-interacting, the Hamiltonian could be separated into a sum of one electron Hamiltonians. The separation of the Hamiltonian results in a separation of the total electronic wave function $\Psi(r_1, r_2)$ into a a number of atomic wave function. The separation of the total electronic wave function for H^- would result in two atomic Hydrogen wave functions as shown in equation (2.5).

$$\Psi(r_1, r_2) = \Psi_{\mathrm{H}}(r_1)\Psi_{\mathrm{H}}(r_2) \tag{2.5}$$

The assumption of non-interacting electrons is a large one, but it is a starting point for an approach to multi-electron systems. This approach can be extended to the general form as shown in equation (2.6) which is known as the Hartree Product.

$$\Psi_{HP}(r_1, r_2, \ldots, r_N) = \phi_1(r_1)\phi_2(r_2)\ldots\phi_N(r_N) \tag{2.6}$$

In equation (2.6) Ψ_{HP} is the Hartree product wave function and $\phi_N(r_N)$ represents the N^{th} spatial orbital.

This approach is a good starting point, however it violates a fundamental principle of quantum mechanics which states that any like elementary particles in a system are

indistinguishable from one another.

Consider a two electron wave function (2.7) formed using a Hartree product as described in equation (2.6).

$$\Psi(r_1, r_2) = \phi_1(r_1)\phi_2(r_2) \tag{2.7}$$

The wave function (2.7) produced is not a valid expression as it does not give the same product as the equally valid wave function (2.8) below.

$$\Psi(r_2, r_1) = \phi_1(r_2)\phi_2(r_1) \tag{2.8}$$

The solution to the problem of indistinguishable electrons is to take a linear combination of the Hartree products with the the electrons in different positions. For the two electron system used previously this produces two solutions as shown in equations (2.9).

$$\Psi(r_1, r_2) = \begin{cases} \phi_1(r_1)\phi_2(r_2) + \phi_1(r_2)\phi_2(r_1) \\ \phi_1(r_1)\phi_2(r_2) - \phi_1(r_2)\phi_2(r_1) \end{cases} \tag{2.9}$$

Either of these wave functions are, in principle, a valid solution to the system however, experimental observation has shown that in electron containing systems, the wave function changes sign on exchange of electrons. This is the heart of the Pauli Principle. The Pauli principle states that "*Valid electronic wave functions must change sign upon exchanging the co-ordinates of any two electrons*".

Of the two linear combinations, only the second of the two forms shown in (2.9) has this property.

However, there are still problems with this wave function as it stands. This can be seen by constructing a wave function for the helium atom, which has two electrons in the first orbital labelled $1s$. The result is shown in equation (2.10).

$$\begin{aligned}\Psi(\mathrm{He}) &= \phi_{1s}(r_1)\phi_{1s}(r_2) - \phi_{1s}(r_2)\phi_{1s}(r_1) \\ &= 0 \end{aligned} \tag{2.10}$$

Obviously this result which suggests that helium would not form, is not correct as helium is a well documented element. There is obviously still a flaw in the construction of the wave function. The current model used to represent an atomic or molecular system takes in to account only the the electronic properties of the electrons and their position in space. There is another property of electrons that can be used to distinguish one electron from another, this property is called spin. Spin is an intrinsic property of electrons related to how they interact with a magnetic field. Electrons have two possible spin states, here represented as α and β which are equivalent to a positive one half spin or a negative one half spin respectively.

When creating orbital representations of a system it is possible to put two electrons in a single orbital only if the two electrons have opposite spins. This property must therefore be represented in the wave function to get a non-zero product in doubly occupied orbitals.

In order to represent spin in a wave function a new co-ordinate must be introduced, this fourth co-ordinate is ω or the spin "co-ordinate" . From this new model a one electron wave function is represented as follows in equation (2.11).

$$\begin{aligned}\chi(e^-) &= \chi(x_{e^-}, y_{e^-}, z_{e^-}, \omega_{e^-}) \\ &= \chi(r, \omega) \\ &= \chi(X) \end{aligned} \tag{2.11}$$

In equation (2.11) $\chi(X)$ is a spin orbital which can be derived from a spatial orbital $\phi(r)$ in two ways as shown in equation (2.12).

$$\chi(X) = \begin{cases} \phi(r) \times \alpha(\omega) = \phi(r)\alpha = \phi(r) \\ \text{Or} \\ \phi(r) \times \beta(\omega) = \phi(r)\beta = \overline{\phi(r)} \end{cases} \tag{2.12}$$

The use of spin orbitals ($\chi(X)$) provides a way to write the helium wave function in a way that produces a non-zero sum as shown in equation (2.13).

$$\Psi(\text{He})(x_1, x_2) = \chi_1(x_1)\chi_2(x_2) - \chi_1(x_2)\chi_2(x_1)$$
$$\text{Where} \begin{cases} \chi_1 & = \phi 1s(r)\alpha \\ \chi_2 & = \phi 1s(r)\beta \end{cases} \tag{2.13}$$

Writing wave functions as the antisymmetrised products of spin orbitals soon becomes tedious as the size of the system increases, therefore a simpler general representation is required, this comes in the form of Slater determinants as shown for the general case below in (2.14).

$$\Psi(x_1, x_2, x_3, \ldots x_n) = \frac{1}{\sqrt{n_{elec}!}} \begin{vmatrix} \chi_1(x_1) & \chi_2(x_1) & \chi_3(x_1) & \cdots & \chi_n(x_1) \\ \chi_1(x_2) & \chi_2(x_2) & \chi_3(x_2) & \cdots & \chi_n(x_2) \\ \chi_1(x_3) & \chi_2(x_3) & \chi_3(x_3) & \cdots & \chi_n(x_3) \\ \vdots & \vdots & \vdots & \ddots & \vdots \\ \chi_1(x_n) & \chi_2(x_n) & \chi_3(x_n) & \cdots & \chi_n(x_n) \end{vmatrix} \tag{2.14}$$

These Slater determinants are still time consuming to write, a simpler way of representing them is shown in (2.15) where Bra-ket notation is used.

$$\Psi = |\chi_1\chi_2\chi_3 \ldots \chi_n\rangle \tag{2.15}$$

With the various methods above it is now possible to write an approximate molecular wave function in terms of Slater determinants (Ψ_{SD}) as shown below in equation (2.16).

$$\Psi_{SD}(x_1, x_2, \ldots x_n) = \mathcal{A}\left\{\prod_{i=1}^{n_{elec}} \chi_1(x_i)\right\}$$
$$\text{where:} \quad \chi_i(x_i) = \psi_i(r_i)\alpha \text{ or } \psi_i(r_i)\beta \tag{2.16}$$

here $\mathcal{A}$ is the antisymmetrisation operator.

The unknown molecular orbital $\Psi_i(r_i)$ is universally expanded as a set of "basis functions" as shown in (2.17). For further information on these "basis functions" see section 2.4.1.

$$\psi_i(r_i) = \sum_{j}^{n_{basis}} c_{ij}\phi_j(r_i) \tag{2.17}$$

In (2.17) c_{ij} is the expansion coefficient for a known basis function ϕ_j.

The next step is to find the values of the coefficients c_{ij}, this is achieved by approximating a solution to the electronic Schrödinger equation. In order to find the best approximate solution the variational principle is used. The variational principle states that any approximate wave function will produce a higher energy solution than the exact wave function would. Therefore the approximate wave function that produces the lowest energy solution will give the best description of the exact wave function.

In order to use the variational principle an energy must be calculated from the electronic Schrödinger equation. The equations below show how the energy of an approximate wave function can be calculated in longhand or using a normalised wave function in Bra-ket notation (2.18).

$$E = \begin{cases} \dfrac{\int \Psi(x)\hat{H}_{elec}\Psi(x)dx}{\int \Psi(x)\Psi(x)dx} \\ \text{Or} \\ \dfrac{\langle\Psi|H|\Psi\rangle}{\langle\Psi|\Psi\rangle} \end{cases} \tag{2.18}$$

In order to calculate an energy for a Slater determinant wave function (Ψ_{SD}) the mathematical expression is substituted in to (2.18) as shown below in (2.19). In order for this transformation to work the wave function must be normalised. The normalisation of the wave function when Slater determinants are used is achieved by constraining the orbitals such that they are orthonormal.

$$E = \int \Psi_{SD} \hat{H}_{elec} \Psi_{SD} dx \tag{2.19}$$

In equation (2.19) Ψ_{SD} is as shown in (2.14) and $\hat{H}_{elec}$ can be represented as shown in (2.20).

$$\hat{H}_{elec} = \sum_{A}^{N} \sum_{B>A}^{N} \frac{Z_A Z_B}{R_{AB}} + \sum_{i=1}^{n} \hat{h}_i + \sum_{i}^{n} \sum_{j>i}^{n} \frac{1}{r_{ij}} \tag{2.20}$$

In (2.21) the Hamiltonian operator has been split into three parts the first part of the sum does not depend on electron co-ordinates, the second part is a sum of one electron operators ($\hat{h}_i$) of a form shown in (2.21) and the final part is a sum of two electron contributions.

$$\hat{h}_i = -\frac{\nabla_i^2}{2} - \sum_{A}^{N} + \frac{Z_A}{r_{iA}} \tag{2.21}$$

The result of the expanding (2.19) using $\hat{H}_{elec}$ from (2.20) is shown in (2.22) below.

$$\begin{aligned} E_{SD} = & \int \Psi \left\{ \sum_{A}^{N} \sum_{B>A}^{N} \frac{Z_A Z_B}{R_{AB}} \right\} \Psi dx \\ & + \int \Psi \left\{ \sum_{i=1}^{n} \hat{h}_i \right\} \Psi dx \\ & + \int \Psi \left\{ \sum_{i}^{n} \sum_{j>i}^{n} \frac{1}{r_{ij}} \right\} \Psi dx \end{aligned} \tag{2.22}$$

The equation is complex to read but the terms can be summarised to more descriptive ones. As before, the first term is an integral over a constant as it only involves internuclear terms. This term is written as V_{NN} as shown in (2.23) and represents the potential

energy of inter-nuclear coulombic repulsion.

$$\int \Psi \left\{ \sum_{A}^{N} \sum_{B>A}^{N} \frac{Z_A Z_B}{R_{AB}} \right\} \Psi dx = \sum_{A}^{N} \sum_{B>A}^{N} \frac{Z_A Z_B}{R_{AB}} = V_{NN} \tag{2.23}$$

The other two terms can be re-written as sums of integrals (2.24).

$$E_{SD} = V_{NN} + \sum_{i=1}^{n} \left\{ \int \Psi \hat{h}_i \Psi dx \right\} + \sum_{i}^{n} \sum_{j>i}^{n} \left\{ \int \Psi \frac{1}{r_{ij}} \Psi dx \right\} \tag{2.24}$$

The first sum represents the one-electron interactions. These can be simplified to $T_{e,i}$ the electronic kinetic energy and V_{Ne} the potential energy due to nuclear-electronic coulombic attraction, via the one-electron energies of an orbital h_{ii} as shown in (2.25) and (2.26) where i is an electron in the orbital.

$$\begin{aligned} \sum_{i=1}^{n} h_{ii} &= \sum_{i=1}^{n} \left\{ \int \Psi \hat{h}_i \Psi dx \right\} \\ &= \sum_{i=1}^{n} \left\{ \int \chi_i \hat{h}_i \chi_i dx d\omega \right\} \end{aligned} \tag{2.25}$$

$$\begin{aligned} h_{ii} &= \int \chi_i \left(-\frac{\nabla_i^2}{2} - \sum_{A}^{N} \frac{Z_A}{r_{iA}} \right) \chi_i dr d\omega \\ &= -\int \chi_i \left(\frac{\nabla_i^2}{2} \right) \chi_i dr d\omega - \int \chi_i \left(\sum_{A}^{N} \frac{Z_A}{r_{iA}} \right) \chi_i dr d\omega \\ &= T_{e,i} + V_{Ne,i} \end{aligned} \tag{2.26}$$

The final sum represents the two electron interactions called V_{ee}: the potential energy due to electron-electron coulombic repulsion.

Each term in the final sum can be reduced to a four term sum of double integrals as shown in (2.27). In some cases some of the terms in the sum will vanish due to integration over spins.

$$
\begin{aligned}
&\iint \chi_i(x_1)\chi_j(x_2)\frac{1}{r_{12}}\chi_i(x_1)\chi_j(x_2)dx_1dx_2 \\
-&\iint \chi_i(x_1)\chi_j(x_2)\frac{1}{r_{12}}\chi_i(x_2)\chi_j(x_1)dx_1dx_2 \\
-&\iint \chi_i(x_2)\chi_j(x_1)\frac{1}{r_{12}}\chi_i(x_1)\chi_j(x_2)dx_1dx_2 \\
+&\iint \chi_i(x_2)\chi_j(x_1)\frac{1}{r_{12}}\chi_i(x_2)\chi_j(x_1)dx_1dx_2
\end{aligned} \tag{2.27}
$$

In (2.27) the first and last term and the second and third term are identical pairs. These pairs of identical terms represent the two main two electron interactions.

The first pair form J_{ij} the coulomb integral (which represents the coulombic interaction between electrons) and is shown in terms of real spatial orbitals and co-ordinates in (2.28)

$$
J_{ij} = \iint \psi_i^2(r_1)\frac{1}{r_{12}}\psi_j^2(r_2)dr_1dr_2 \tag{2.28}
$$

The second pair form K_{ij} the exchange integral (which represents a quantum mechanical effect related to the exchange of electrons in a wave function) and is shown in terms of real spatial orbitals and co-ordinates in (2.29)

$$
K_{ij} = \iint \psi_i(r_1)\psi_j(r_2)\frac{1}{r_{12}}\psi_i(r_2)\psi_j(r_1)dr_1dr_2 \tag{2.29}
$$

These integrals are related to V_{ee} as shown in (2.30).

$$
V_{ee} = J_{ee} - K_{ee} = \sum_{i}^{n_{elec}} \sum_{j>i}^{n_{elec}} (J_{ij} - K_{ij}) \tag{2.30}
$$

The result of the simplified energy equation is shown below in (2.31).

$$
E_{SD} = V_{NN} + T_e + V_{Ne} + V_{ee} \tag{2.31}
$$

2.4.1 The Self-Consistent Field (SCF) Method

There is now a set of equations that describe the relationship between the Slater determinant wave function and the energy, which means the orbital coefficients c_{ij} (as defined in (2.17)) can be found. However some of the terms in the energy expression such as the two electron terms, are dependent on the form of the orbitals. This creates a situation where an exact value for the energy is needed to calculate the orbital coefficients, and an exact description of the orbital coefficients is required to calculate the energy. There is a method for solving this kind of contradiction, this method is the Self-Consistent Field (SCF) method, which takes an iterative approach to a solution. The general procedure for the SCF method for solving this system is:

1. Guess a set of orbital coefficients
2. Construct a set of orbitals
3. Calculate new orbital coefficients (by minimising the energy)
4. Compare to previous set of coefficients. If the two sets match to a given threshold stop or else repeat from 2 with new orbitals.

Now a method is required to minimise the energy with respect to the orbitals. This takes the form of a set of simultaneous equations with the orbital coefficients as the variables. This set of equations is usually expressed as a matrix equation shown below for the closed shell case in (2.32) where the variables are collected into matrices.

$$\sum_j F_{ij} C_{jx} = \sum_j S_{ij} C_{jx} \varepsilon_x$$

where

$$F_{ij} = h_{ij} + \sum_{mn} D_{mn} \left[(ij|mn) - \frac{1}{4}(im|jn) - \frac{1}{4}(in|jm) \right]$$

and

$$D_{mn} = 2\sum_{x}^{occ} C_{mx}C_{nx} \tag{2.32}$$

In (2.32) **F** is the Fock matrix, **S** is the overlap matrix, **D** is the density matrix and $\mathbf{C_{jx}}$ is the matrix of orbital coefficients. The indices ij represent occupied orbitals whilst mn represent the unoccupied orbitals.

This matrix equation produces a new set of orbital coefficients which can then be used in the SCF procedure.

In order to form the Fock matrix (**F**) integrals over the one and two electron operators in the Hamiltonian must be calculated. In order to calculate the Fock matrix both h_{ij} and $(ij|mn)$ must be calculated. h_{ij} is part of the one electron operators as shown in (2.33)

$$h_{ij} = \int \psi_i(r_1)\left(-\frac{1}{2}\nabla^2 - \sum_A Z_A r_{A_1}^{-1}\right)\psi_j(r_1)dr_1 \tag{2.33}$$

and $(ij|mn)$ is part of the two electron operators as shown in (2.34).

$$\begin{aligned}(ij|mn) &= \iint \psi_i(r_1)\psi_j(r_1)\frac{1}{r_{12}}\psi_m(r_2)\psi_n(r_2)dr_1dr_2 \\ &= \iint \psi_i(r_1)\psi_m(r_2)\frac{1}{r_{12}}\psi_j(r_1)\psi_n(r_2)dr_1dr_2 \quad \text{(from (2.27))}\end{aligned} \tag{2.34}$$

In order to make the calculation of the integrals possible for larger systems the molecular orbitals are created as a Linear Combination of Atomic Orbitals (LCAO). These "atomic orbitals" are expressed as a system of mathematical functions. These functions are the basis functions mentioned previously. A collection of all the basis functions required for the production of a molecular orbital is the basis set. From the Hydrogen atom the preferred form for atomic orbitals would appear to be Slater type exponential functions but these are hard to calculate integrals over. Instead a related function, the Gaussian function, is used to produce molecular orbitals as they are easily combined to

produce the desired orbitals, and much easier to calculate integrals over. These so called Gaussian type orbitals use one or more Gaussian functions of the form shown in (2.35). In practise in many techniques higher angular momenta orbitals are expressed as true spherical harmonic Gaussians. The true spherical harmonic Gaussians produce an equal or smaller number of basis functions at higher angular momenta and thus reduce calculation times [8].

$$X_A^l Y_A^m Z_A^n e^{-\alpha r_A^2} \tag{2.35}$$

In early calculations a single basis function (set of Gaussian functions) was used to represent each atomic orbital occupied in a molecular orbital. This minimal, or single-zeta (SZ), basis is too small and inflexible to describe how the atomic orbitals deform in a molecular orbital and so give poor results. A larger basis set is required to produce a good representation of a molecular orbital. These larger basis sets are produced by increasing the number of functions of a type in the set. One way to increase the number of functions is to include more functions describing each orbital, for example two functions per orbital is a double-zeta (DZ) basis set.

There is now enough information to construct a Hartree-Fock wave function and solve the SCF equations to minimise the orbitals and get an energy. However with all the approximations the variational principle says that the energy produced by this method will always be higher than the true energy of the system. There is still a part of the system left undescribed, this part is represented by a correction to the energy called the correlation energy, and is the representation of another quantum mechanical interaction between electrons.

The correlation energy can be expressed as shown in the following equation (2.36)

$$E_{corr} = E_{exact} - E_{HF} \tag{2.36}$$

Where E_{corr} is the correlation energy E_{exact} is the exact energy of the system and E_{HF} is the energy calculated by Hartree-Fock.

In the next few sections, a variety of methods which attempt to account for this correlation energy will be described.

2.5 Density Functional Theory (DFT)

Density Functional Theory (DFT) attempts to provide an improvement to the representation of a quantum system, when compared to methods such as Hartree-Fock. It does so by including a representation of both the exchange and correlation quantum phenomenon, whereas the Hartree-Fock method only represents exchange.

The full expression for the energy of a system can be expanded with correlation as shown below in (2.37).

$$E_{exact} = V_{NN} + T_{ee} + V_{Ne} + V_{coul} + V_x + V_c \tag{2.37}$$

Equation (2.37) is an extended version of (2.31). Here V_{ee} has been expanded as V_{coul} the energy due to electron-electron coulomb interactions and V_x the energy due to electron exchange. The energy due to correlation has been added in the form of V_c.

The correlation energy describes the energy of an effect known as correlation. Correlation describes the fact that there is an amount of correlated interaction between electrons. This interaction affects the movement of these electrons relative to one another; this effect, like exchange, is a quantum effect.

In defining DFT the first thing to realise is that the exchange and correlation energy terms can be combined into a single term V_{xc}. With a suitable functional form for V_{xc}, the energy only depends on the electron density ($D_{\lambda\sigma}$).

The density $D_{\lambda\sigma}$ can be written as a product of LCAO orbitals (ψ_i) just as in the SCF method as shown below in (2.38).

$$\psi_i = \sum_{\mu} \chi_\mu C_{\mu i}$$

$$D_{\lambda\sigma} = 2\sum_{i} C_{\lambda i} C_{\sigma i} \tag{2.38}$$

Molecular orbitals formed this way are called Kohn-Sham orbitals. These orbitals do not represent a physical property or the form of an electronic orbital of the system, rather they describe an area of electronic density. They are often used for interpretation in the same way that LCAO orbitals are in Hartree-Fock, but as they do not represent the same property this can lead to errors in interpretation.

The energy of a system can now be written as a function of the density $D_{\lambda\sigma}$ as shown in (2.39) below.

$$E_{DFT}[D_{\lambda\sigma}] = V_{NN}[D_{\lambda\sigma}] + T_{ee}[D_{\lambda\sigma}] + V_{Ne}[D_{\lambda\sigma}] + V_{coul}[D_{\lambda\sigma}] + V_{xc}[D_{\lambda\sigma}] \tag{2.39}$$

The functional form of each term in (2.39) is known and can be easily calculated using various methods except for V_{xc} . There is no known exact functional form for V_{xc} so approximations must be made. There are three main methods for defining a functional for V_{xc}, Local Density Approximation (LDA) [9, 10], gradient-corrected methods or hybrid methods. All these methods with the exception of LDA involve a certain amount of fitting the parameters in the functional to a given data set. DFT sits somewhere between *Ab Initio* methods, where everything can be defined from first principles, and semi-empirical methods which use empirical data to fit many of the parameters for calculation.

2.5.1 Functionals

As stated above there are three main methods for approximation of the functional for V_{xc} each method will be detailed below.

The Local Density Approximation (LDA) [9, 10] is based solely on the properties of

the electron density. The critical assumption in LDA is that the local density at any point in a molecule can be satisfactorily described as a uniform electron gas, and therefore the density seen by each electron is uniform throughout the molecule. This assumption obviously does not hold up for most single molecules, as there are obvious areas of high electron density about bonds and areas of low electron density or no electron density at the nuclei. This approach might work better in extremely large and diffuse molecules where the density is more uniform, or in large systems such as metals or semi-conductors. Here the electrons form bands which have a relatively uniform density. The LDA can be expanded to include separate orbitals and densities for α and β spin electrons; in this form it is called the Local Spin Density Approximation (LSDA) [11, 10]. The LSDA has a number of advantages, the most obvious being that it allows calculations of systems in which the electrons are not spin paired, such as radicals and some ions.

Built upon the LDA or LSDA are gradient-corrected methods. These methods combine the electron density with a first order correction in the form of the gradient of the density. This allows for a non-uniformity of the density seen by each electron. The inclusion of the first-order correction to the exchange term produces a better total energy, whilst the first order correction to the correlation term often results in a positive energy for correlation, counteracting the improvement in the exchange term. This simple application of the method actually produces a worse performing model than an LSDA model. To solve this the gradient is often included as a variable, and the terms are fitted to produce a better representation of the correlation energy. This approach is know as the generalised gradient approximation (GGA).

The final method is a hybrid functional. In this type of functional the realisation is that Hartree-Fock already provides an exact representation of the exchange energy. This method takes that exchange energy from Hartree-Fock and uses an LSDA or gradient corrected functional to represent the correlation energy. However it is not as simple as just putting these two energies together to form V_{xc}. The most common method is to use a known exchange-correlation functional, and include a part of the Hartree-Fock exchange energy with a fitting function to produce a better representation of the energy.

Generally, functionals are of the hybrid type and split into an exchange part and a correlation part. These parts are often developed separately and put together in a mix and match approach in order to produce a good fit for certain quantities of interest in a given system.

One of the most popular general purpose functionals, and the one used for most DFT calculations in this thesis, is B3-LYP. It is a form of hybrid functional using the Becke three term exchange Functional (B3) [12], and the Lee, Yang and Parr correlation functional (LYP) [13]. This functional combines contributions from a number of different exchange and correlation functionals with appropriate fitting functions as shown in (2.40). The constants used are as follows $a_0 = 0.2$, $a_x = 0.72$ and $a_c = 0.81$.

$$\begin{aligned} V_{xc} = (1-a_0)V_x(LDA) + a_0V_x(HF)a_xV_x(B88_x) \\ + a_cV_c(LYP88_c) + (1-a_c)V_c(VWN80_c) \end{aligned} \tag{2.40}$$

The B3-LYP Functional was optimised on a number of properties of first and second row atoms. However B3-LYP is also often used to calculate properties outside those it was optimised for, and for calculations on elements outside the first and second rows.

2.5.2 Performance

DFT has a number of advantages and disadvantages as a method of calculation. Its major advantage is its relatively low scaling of computational workload with the size of a system. This allows it to scale to molecules of sizes that no other method which includes a correlation treatment can achieve. The disadvantages to this method are mostly due to its semi-empirical approach where, if a calculation looks at properties or atoms outside those it was optimised to treat, varying degrees of error can be introduced by the different environments. Further, DFT can show a preference for certain arrangements of electrons, especially when the system contains transition metal atoms where multiple electronic configurations can be very close in energy. In these cases DFT tends to favour higher oxidation states and low spin state systems. This effect, especially in relation to

spin state, is less noticeable using hybrid functionals.

The next few sections will detail a number of methods that attempt to incorporate correlation using a purely *Ab Initio* approach rather than the semi-empirical approach used in DFT.

2.6 Single Reference Correlation

The previous section detailed the use of DFT in order to add correlation to the description of a molecular system using semi-empirical functionals. The next two sections will focus on introducing correlation using an *Ab Initio* approach.

The first thing to look at is what makes up correlation. Correlation can be divided into two separate effects. The first of these effects is dynamical correlation. This describes what happens to a wave function when two electrons approach each other. The other type of correlation is non-dynamical correlation, also known as static correlation. Static correlation is due to near degeneracy of different electron configurations in the wave function. In order to fully describe a system, both forms of correlation must be properly accounted for.

Non-dynamical correlation can be included in a system quite easily by allowing a mixing of more than one configuration in the wave function. Methods for doing this will be discussed in the next section. Dynamical correlation is very difficult to include in a system. It takes many different configurations in order to properly describe these interactions.

There are broadly three classes of method for including dynamical correlation in a wave function, all closely related in theory. These methods are perturbation theory, configuration interaction (CI) and coupled cluster.

In perturbation theory it is assumed that the new problem only differs slightly from a problem that has already been solved, either exactly or approximately. In this case correlated wave functions differ only in the inclusion of correlation compared to an already solved wave function such as Hartree-Fock.

Perturbation theory solves the new problem by introducing a small change or perturbation into the problem. In the case of correlation this is done by defining a two part Hamiltonian consisting of a reference Hamiltonian, H_0, and a perturbation, H', with the magnitude of λ. The relationship is shown in (2.41).

$$\mathbf{H} = \mathbf{H_0} + \lambda \mathbf{H'} \tag{2.41}$$

The perturbed wave function is given by (2.42).

$$\mathbf{H}\Psi = W\Psi \tag{2.42}$$

As the perturbation increases to a finite value the new energy (W) and wave function also changes continuously. The new wave function and energy can be expanded in a power series in the perturbation parameter λ as shown in (2.43).

$$\begin{aligned} W &= \lambda^0 W_0 + \lambda^1 W_1 + \lambda^2 W_2 + \lambda^3 W_3 + \ldots \\ \Psi &= \lambda^0 \Psi_0 + \lambda^1 \Psi_1 + \lambda^2 \Psi_2 + \lambda^3 \Psi_3 + \ldots \end{aligned} \tag{2.43}$$

Inserting the results from (2.42) and (2.43) into the Schrödinger equation and collecting terms of the same order in λ gives (2.44).

$$\begin{aligned} \mathbf{H_0}|\Psi_0\rangle &= W_0|\Psi_0\rangle \\ (\mathbf{H_0} - W_0)|\Psi_1\rangle &= (W_1 - \mathbf{H_1})|\Psi_0\rangle \\ (\mathbf{H_0} - W_0)|\Psi_2\rangle &= (W_1 - \mathbf{H_1})|\Psi_1\rangle + W_2|\Psi_0\rangle \end{aligned} \tag{2.44}$$

It can be assumed that the perturbed wave functions are orthogonal to the zeroth order wave function. This orthogonality allows a normalisation of the total wave function such that $\langle\Psi|\Psi_0\rangle = 1$. This normalisation is used to produce energy expressions up to second order as shown in (2.45).

$$W_0 = \langle \Psi_0 | \mathbf{H_0} | \Psi_0 \rangle$$
$$W_1 = \langle \Psi_0 | \mathbf{H_1} | \Psi_0 \rangle$$
$$W_2 = \langle \Psi_0 | \mathbf{H_1} | \Psi_1 \rangle \tag{2.45}$$

The most popular form of perturbation theory is Møller-Plesset Perturbation Theory (MP) which chooses the sum over Fock operators as the zeroth-order Hamiltonian and uses the exact V_{ee} operator minus twice the $\langle V_{ee} \rangle$ operator. There are different orders of perturbation theory based on how far along the power series the perturbation extends. The most popular form of (MP) is second order Møller-Plesset (MP) Perturbation theory (MP2) as it is computationally cheap, although not as cheap as DFT, and seldom gives a more accurate result as it often overshoots the correlation energy.

The second method is Configuration Interaction (CI) which is similar to mixing millions of different configurations. In CI the wave function is built from a linear combination of Configuration State functions (CSF). These CSF's are constructed using a ground state Hartree-Fock determinant expanded with a number of excited state determinants.

A CI method is generally limited by the number of additional determinants used in the construction of the CSF's. For example if any occupied orbital is replaced by a virtual orbital this is a single excitation, two is a double excitation and so on. CI methods are usually limited by the number of excitations allowed. Just single excitations are no use as all matrix elements between the single excitations and the Hartree-Fock determinants are all zero. but CID (just double excitations) and CISD (singles and doubles) are popular forms.

CI is generally less widely used than both MP2 and coupled cluster methods as it is extremely expensive computationally (although no worse than coupled cluster), especially at higher excitation levels or when used on larger systems. It only produces better results than MP2 in small systems and does not scale correctly with the number of electrons.

The final method is Coupled Cluster (CC) theory. CC provides the best single refer-

ence treatment of correlation. It is size-extensive (it scales correctly with the number of electrons) giving it the advantage over CI methods and gives a much better result than MP2. Unfortunately these advantages come at the expense of computational speed.

In the perturbation theory method outlined above all types of correction to the reference wave function are added to a given order (2,3,4, etc.). The idea with coupled cluster methods is to include all corrections of a given type to infinite order. To do this an excitation operator $\mathbf{T}$ as shown in (2.46) is used to act on a Hartree-Fock reference wave function Φ_0 where $\mathbf{T}_i$ generates all i^{th} excited Slater determinants. As shown in (2.47).

$$\mathbf{T} = \mathbf{T}_1 + \mathbf{T}_2 + \mathbf{T}_3 + \cdots + \mathbf{T}_{N_{elec}} \tag{2.46}$$

$$\mathbf{T}_1\Phi_0 = \sum_{i}^{occ}\sum_{a}^{vir} t_i^a \Phi_i^a$$

$$\mathbf{T}_2\Phi_0 = \sum_{i<j}^{occ}\sum_{a<b}^{vir} t_{ij}^{ab} \Phi_{ij}^{ab} \tag{2.47}$$

A CI wave function can be generated by allowing $\mathbf{T}$ to work on a Hartree-Fock wave function. The corresponding CC wave function is defined as the exponential of the excitation operator acting on the same Hartree-Fock wave function. Both are shown in (2.48).

$$\begin{aligned}\Psi_{CI} &= (1+\mathbf{T})\Phi_0 \\ &= (1+\mathbf{T}_1+\mathbf{T}_2+\mathbf{T}_3+\mathbf{T}_4+\cdots)\Phi_0 \\ \Psi_{CC} &= e^{\mathbf{T}}\Phi_o\end{aligned}$$

Where

$$\begin{aligned}e^{\mathbf{T}} &= 1+\mathbf{T}+\frac{1}{2}\mathbf{T}^2+\frac{1}{6}\mathbf{T}^3+\ldots \\ &= \sum_{k=0}^{\infty}\frac{1}{K!}\mathbf{T}^k\end{aligned} \tag{2.48}$$

The exponential operator $e^{\mathbf{T}}$ can be also be written as in (2.49) where each term generates all excitations of a given order. For example the second term in parentheses generates

all triple excitations (triples).

$$e^{\mathbf{T}} = 1 + \mathbf{T}_1 + (\mathbf{T}_2 + \frac{1}{2}\mathbf{T}_1^2) + (\mathbf{T}_3 + \mathbf{T}_2\mathbf{T}_1 + \frac{1}{6}\mathbf{T}_1^3) + (\mathbf{T}_4 + \mathbf{T}_3\mathbf{T}_1 + \frac{1}{2}\mathbf{T}_2^2 + \frac{1}{2}\mathbf{T}_2\mathbf{T}_1^2 + \frac{1}{24}\mathbf{T}_1^4)\ldots \tag{2.49}$$

So far, this wave function generates an exact solution equivalent to a full CI. However, as with a full CI, this is just not possible for anything but the smallest systems and in the same way that a CI is usually truncated to only include certain excitations, the same is applied to CC methods. For example CCSD, one of the most popular CC methods, includes only contributions from $\mathbf{T} = \mathbf{T}_1 + \mathbf{T}_2$.

The addition of a full treatment of triples (CCSDT) causes a lot of added computational complexity to coupled cluster calculations; however for only a small amount of extra computational work over CCSD, a perturbative treatment of triples can be used. The perturbative treatment uses equations derived from MP4 and MP5, but using CCSD amplitudes (t) rather than perturbation coefficients, this gives CCSD(T).

2.7 Multiconfigurational Effects

In order to recover a large amount of the non-dynamical correlation in a system a single reference wave function is unsuitable, as it treats only one of the many possible near degenerate electron states. This may not be a problem in a ground state system of simple atoms, near its equilibrium geometry. However, once the system moves away from an equilibrium geometry, or if the system includes atoms which can exhibit a number of different and low lying valence electron configurations (such as many transition metal complexes), the number and importance of near degenerate electron states and by extension non-dynamical correlation becomes much more important.

A simple example of this is the dissociation of a H_2. The H_2 molecular orbitals can be written in the form shown in (2.50) where χ_{iA} and χ_{iB} are functions on H_A and H_B respectively and N_i is a normalisation constant.

$$\varphi_i = N_i(\chi_{iA} \pm \chi_{iB}) \tag{2.50}$$

At the equilibrium geometry the ground state is dominated by the doubly occupied φ_1 orbital ($(\varphi_1)^2$) which is made up from the atomic orbitals χ_{1A} and χ_{1B} whose main contribution is the Hydrogen $1s$ orbital with some "small corrections". A qualitative representation of φ_1 is shown in (2.51), here the small corrections are neglected.

$$\varphi_1 = N_1(1s_A + 1s_B) \tag{2.51}$$

In the restricted Hartree-Fock (RHF) model the wave function is formed by doubly occupying φ_1 as shown in (2.52), where $\Theta_{2,0}$ is the singlet spin function.

$$\begin{aligned} &\Psi_1 = \varphi_1(r_1)\varphi_1(r_2)\Theta_{2,0} \\ &\text{Where} \\ &\Theta_{2,0} = \sqrt{\tfrac{1}{2}}(\alpha_1\beta_2 - \beta_1\alpha_2) \end{aligned} \tag{2.52}$$

The RHF model like all Hartree-Fock models, works well at the equilibrium bond length; however as the bond length is changed away from equilibrium, such as when measuring a potential curve, there is a problem. In the RHF wave function as described in (2.51) as the bond length changes the form of the molecular orbital does not. The problem with this becomes clear if the wave function is expanded as the product of atomic orbitals as shown in (2.53).

$$\Psi_1 = N_1^2[1s_A(r_1)1s_A(r_2) + 1s_A(r_1)1s_B(r_2) + 1s_B(r_1)1s_A(r_2) + 1s_B(r_1)1s_B(r_2)] \tag{2.53}$$

As can be seen from (2.53) the RHF wave function at all distances has components where both electrons appear on the same nucleus. At the equilibrium geometry this is a valid contribution, but as the H_2 molecule disassociates these contributions would result in ionic terms ($H^+ + H^-$) in the product.

These "ionic structures" are a known feature of RHF calculations and mean that they

are unsuitable where there are open shell products associated. A method is therefore needed to correct for these "ionic structures". An easy solution to this problem would be to divide the wave function into an ionic and covalent part and use inter-nuclear distance to weight the contributions of each part as shown in (2.54)

$$\begin{aligned}
&\Psi_{VB} = C_{ion}\Psi_{ion} + C_{cov}\Psi_{cov} \\
&\text{Where} \\
&\Psi_{ion} = N_{ion}[1s_A(r_1)1s_A(r_2) + 1s_B(r_1)1s_B(r_2)]\Theta_{2,0} \\
&\text{and} \\
&\Psi_{cov} = N_{cov}[1s_A(r_1)1s_B(r_2) + 1s_B(r_1)1s_A(r_2)]\Theta_{2,0}
\end{aligned} \tag{2.54}$$

This method produces a valence bond description of the chemical bond which gives it appeal as a chemical description; however this chemical understanding comes at the cost of mathematical simplicity. The formulation in (2.54) relies on atomic orbitals which are formed from nonorthogonal basis functions which add a great deal of complexity to the mathematical treatment. The added mathematical complexity has meant that this method is not widely used in chemistry.

The main problem with the formulation in (2.54) is the nonorthogonal basis functions, therefore an alternative formulation is required using an orthogonal basis. Rather than thinking about the problem as a competition of ionic and covalent configurations, this method introduces the principle of an anti-bonding orbital φ_2 (2.55). In a bonding molecular orbital the components of the constituent atomic orbitals have the same phase creating a favourable environment for electrons. In an anti-bonding molecular orbital the components of the constituent atomic orbitals are out of phase creating an unfavourable environment for electrons.

$$\varphi_2 = N_2(1s_A - 1s_B) \tag{2.55}$$

The inclusion of an anti-bonding orbital provides the key to writing a multiconfigurational (MC) molecular orbital formulation of the wave function for the chemical bond in

H_2. The wave function is shown in (2.56) where Ψ_2 is the wave function using electronic configuration (φ_2). C_1 and C_2 are coefficients to weight the influence of the different configurations.

$$\Psi_{MC} = C_1\Psi_1 + C_2\Psi_2 \tag{2.56}$$

The dissociation of the Hydrogen bond is a simplistic example of the power of multiconfigurational methods and also does not really show its limitations. For the most part a multiconfigurational wave function can be built in a similar way to that shown for H_2 but instead of using the full atomic orbital basis, more complex examples are generally constructed from an appropriate molecular orbital basis.

As the number of orbitals which are directly involved in bonding increase, it is obvious that the number of configuration state functions (CSF's) involved will increase. This increase is very rapid. For example, without taking into account symmetry the number of configuration state functions involved in the dissociation of the bond in H_2 is just two, whereas one hundred and seventy five are required to describe the dissociation of the triple bond in N_2, whilst the number of orbitals involved has only increased from two (φ_1 and φ_1) to six ($3\sigma_g$, $3\sigma_u$, $1\pi_{ux}$, $1\pi_{gx}$, $1\pi_{uy}$ and $1\pi_{gy}$). The orbitals involved directly in the multiconfigurational calculation are called the 'active' orbitals.

The general equation for an MCSCF wave function is shown in (2.57)

$$\Psi_{MCSCF} = \sum_k \Phi_K A_K$$

Where

$$\Phi_K = A\left\{\prod_{i\subset k}\phi_i\right\}$$

and

$$\phi_i = \sum_\mu \chi_\mu C_{\mu i} \tag{2.57}$$

(2.57) shows a liner combination of a number of configurations. These configurations

are the CSF's Φ_K. A_K are the associated configuration mixing coefficients. Each CSF is a product of MOs ϕ_i shown expanded in an AO basis chi_μ.

An MCSCF calculation can be viewed as a CI calculation where as well as configuration mixing coefficients A_K, the orbital coefficients ($C_{\mu i}$ themselves are optimised. This optimisation is similar to the SCF optimisation method used in Hartree-Fock. A problem with the MCSCF wave function is that it is hard to converge and often does not find a minimum. In Hartree-Fock SCF a check that the first derivatives of the energy with respect to the orbital coefficients is zero is usually sufficient to check convergence although does not guarantee a minimum. In order to ensure convergence to a minimum in MCSCF a further check is made. The second derivatives of the energy with respect to the orbital coefficients is calculated. If the diagonalisation of these second derivatives produces only positive eigenvalues a minimum has been found.

A number of methods have been used to optimise the MCSCF wave function some of them are discussed below.

The Optimised Valence Configuration (OVA) method was the first practical method for optimising a MCSCF wave function. The OVA used a two step process in which first the configuration mixing or CI coefficients A_K are optimised by diagonalisation of the Hamiltonian followed by an update of the orbitals. The new optimised orbital coefficients were produced by a set of coupled Fock matrix diagonalisations using a generalisation of the open and closed shell SCF techniques. This technique suffered from poor convergence due to poorly selected CSF's and the step-wise optimisation process.

The Generalised Brillouin Theorem (GBT) was the first technique to allow the creation of reliably convergent poly-atomic MCSCF algorithms. The Brillouin Theorem states that a stationary one-determinant wave function does not interact with configurations created by single excitations (SX). In the case of the MCSCF wave function a generalisation of the Brillouin Theorem allows that there is an equivalence between the convergence criterion used in Fock matrix techniques and the vanishing of certain single excitation (SX) matrix elements. These single excitations are excitations from all configurations of the MCSCF wave function, with unrelaxed CI coefficients, and thus possess

multiconfigurational character themselves. The states arising from these excitations along with reference MCSCF state form the super-CI. At convergence, the Hamiltonian matrix elements between the MCSCF wave function and the SX space must vanish. This led to several optimisation techniques attempting to drive these matrix elements to zero. A more efficient method of calculating updated orbitals was also developed at the time the GBT optimisation techniques were being developed replacing natural orbitals of the MCSCF wave function with natural orbitals of the super-CI. There was a problem with early implementations of this method due to the large amount of elements needing calculation in a super-CI. This is due to each single excitation being a linear combination of as many CSF's as were contained in the MCSCF wave function. This means that in order to calculate a single element of the Super-CI Hamiltonian a large number of smaller matrix calculations are required, this created a bottleneck in the calculation. A solution to this problem was shown by Björn Roos [14]. He presented a method for approximating the super-CI Hamiltonian. The method used Fock matrix elements to approximate some parts of the SX-SX interactions while still maintaining exact calculation of the MCSCF-SX elements used by GBT to track optimisation.

The most common methods currently in use for the optimisation of MCSCF calculation fall into the category of second order optimisation. These methods use the second derivative of the energy (the Hessian) as a convergence criterion as well as the first derivative (the gradient). This was achieved by applying the Newton-Raphson method to the MCSCF wave function.

The most common method for calculating a multiconfigurational wave function is the Complete Active Space SCF (CASSCF) method. This method can be seen as a generalisation of the Hartree-Fock method in which the restrictions in orbital occupation have been relaxed.

2.7.1 CASSCF

CASSCF avoids a problem with the MCSCF method namely how to chose the MO configurations. Instead of hand picking different MO configurations in CASSCF a number of

MOs are chosen as those critical to the system under investigation and a "full CI" of all possible configurations of electrons within that selection of MOs is created.

In order to differentiate the important MOs they are divided in three subsets:

1. Inactive orbitals
2. Active orbitals
3. Virtual orbitals

The inactive orbitals are generally those which represent the core atomic orbitals of the atoms in the molecule, and are kept doubly occupied in the calculation. The virtual orbitals are those orbitals formed from the basis set, which are not part of either the active or inactive spaces and are therefore not occupied in any CSF. The active orbitals are most often those which form the valence orbitals in atoms, the bonding, anti-bonding or non-bonding orbitals in molecules or some important subset of these orbitals. The active orbitals are used to build the CSF's by filling them with the remaining electrons known as the active electrons. These CSF's are then optimised as shown in (2.56) along with the molecular orbitals. The total wave function is a linear combination of all the CSF's that fulfil a given space and spin symmetry. This tends to lead to a spectrum of occupation numbers for the active orbitals that fall between zero and two. This method is called CASSCF because all CSF's generated by the combination of active electrons and orbitals are included in the calculation.

There is an amount of skill required in the generation of a CASSCF calculation. The number of CSF's generated increases rapidly with any increase in the number of active orbitals, especially if the ratio between the number of active electrons and active orbitals is large. The key to this selection is to include only those orbitals most likely to be affected by dissociation and near degeneracy effects. All others should be moved into either the inactive space for orbitals not likely to be affected but occupied, or the virtual space for unoccupied orbitals that are unlikely to interact. It is best to start with the minimum active space that can conceivably work. Once a calculation in the minimum active space has been carried out, a study of the orbital coefficients can give clues to improving the

active space. As a general rule of thumb any orbital with an orbital occupation of less than 1.95 or greater than 0.05 should be included in the active space if possible. There is a practical limit to the size of the active space where the number of CSF's generated makes the calculation unfeasible. This generally lies somewhere around fifteen electrons in fifteen orbitals.

2.7.2 Improvements on MCSCF Results.

The CASSCF method is based on a Hartree-Fock wave function, as such it suffers from the same problem as Hartree-Fock in that there is no treatment of dynamical correlation. The methods described so far fall broadly into two camps: those that treat dynamical correlation well, such as coupled cluster, and those that treat non-dynamical correlation well, such as CASSCF. For best results a method that combined these two treatments would be preferable.

The obvious solution to combining non-dynamical and dynamical correlation would be to take the two best methods coupled cluster and CASSCF and combine them. Many people have tried to formulate a solution to combining the two approaches and none has been generally applicable due to the great complexity of the results.

The first successful attempts at creating a multi-reference system that included dynamical correlation was a multi-reference formation of the CI method, however, this shared many of the problems of the CI method it was based on. It worked well for small systems with a small reference configuration and that produced a small number of basis functions. Like any CI method however, the computational workload scales vary rapidly, therefore the use of larger reference configurations or larger basis sets results in unfeasibly large computational requirements both in terms of processing time and memory.

There are several multi-reference methods that have incorporated a treatment of dynamical correlation. These include CASSCF with second order perturbation (CASPT2), restricted active space SCF (RASSCF) and multi-reference CI (MR-CI).

The first method to be look at seriously was MR-CI as it was an extension of previous well known techniques. MR-CI takes the CI methodology and applies it to a MCSCF

reference wave function. Due to the extremely large number of configurations created by this technique the size of the CI is usually truncated to a subset of excitations. The most common truncations are single (MR-CIS) or single and double (MR-CISD) excitations from reference state.

The most common and widely used of the two methods is CASPT2 which takes a CASSCF wave function and expands it using a second order perturbation in a similar way to MP2.

Looking back to the discussion of MP2 in section 2.6 the equations that form the basis of perturbation theory are detailed. Equation (2.41) shows a Hamiltonian constructed from a zeroth order term and a perturbation of strength λ, and equation (2.43) shows the corresponding effect on the wave function and energy (W).

The perturbation treatment in the case of CASPT2 is applied to a CASSCF wave function. This second order treatment refines the CASSCF energy to extract more of the dynamical correlation. CASPT2 however does not offer this improved accuracy for free. There is a trade off in compute time due to the more complex equations that require large amounts of data and processing to solve.

The other method mentioned for including dynamical correlation into a multi-reference system is RASSCF. RASSCF is in many ways similar to CASSCF in that it uses the idea of splitting the inactive, active and virtual orbitals into different spaces; however with the RAS treatment the split is more complex, with five spaces rather than the three in CAS:

1. Inactive orbitals
2. The RAS1 space
3. The RAS2 space
4. The RAS3 space
5. External orbitals

The inactive and virtual orbitals have the same properties as their counterparts in a

CASSCF system. The RAS spaces each have rules governing what may happen to electrons and orbitals within them.

The RAS1 space contains orbitals which would normally be doubly occupied in a CAS calculation. The RAS1 space allows a specific number of electrons to be excited out to a specific level, for example singles and doubles.

The RAS2 space has the same properties as the active space in a CAS calculation.

The RAS3 space contains orbitals that are normally unoccupied in a CAS calculation. The RAS3 space allows a specific number of electrons to be excited into it.

By changing the occupations of the RAS spaces a number of different types of wave function can be created. For example, with an empty RAS2 space and a limit on excitations in the RAS1 to singles and doubles a CISD wave function with a single reference is created. Addition of orbitals and electrons in the RAS2 space produces a wave function analogous to a multi-reference CISD with a CAS reference. Due to the structure of the RAS spaces there can be convergence problems as the wave function is no longer complete in the active space which makes the result dependant on orbital rotations between the RAS spaces.

2.8 Basis Sets

The most common technique for solving all the computational methods mentioned so far requires the wave function to be expanded in a set of orbitals constructed from basis functions. An appropriate collection of basis functions for a given atom type is called a basis set. The basic idea of a basis set has already been discussed in this chapter.

The types of basis sets used in this thesis have a number of properties to improve computational efficiency and accuracy.

As stated previously, a basis set for computational chemistry is generally constructed of Gaussian type orbitals (GTO's). These GTO's are collected to form a set representing the orbitals in an atom. These atomic basis sets can be classified by how these orbitals are constructed. The most obvious way to construct a basis set for an atom is to use

GTO's to build a set of orbitals matching those occupied in the atom, for example the $1s$, $2s$ and $2p$ orbitals in Carbon. This kind of basis set is a minimal basis set. This type is not very reliable when constructing molecular orbitals as there is not much flexibility in optimising the size and shape of orbitals. In order to increase the flexibility of the orbitals one or more additional GTO's of the same orbital type can be included. If two orbitals of each type are included this is called a Double Zeta (DZ) basis set, as more orbitals are added so the zeta value increases. Increasing the number of GTO's of the same type is a good start in increasing flexibility in basis sets, however as atomic orbitals (AO) combine to create molecular orbitals (MO) they tend to deform away from their original shape. In order to represent this change in shape, an orbital of a different type is often useful so the next extension to a basis set is often to include GTO's of higher angular momentum such as p orbitals in a Hydrogen basis set. These higher angular momentum functions are called polarisation functions.

Once a basis set has been configured with an appropriate selection of primary functions and polarisation functions, the exponents of the GTO's must be optimised to produce a usable basis set. The process for optimising these exponents is usually to use a variational approach to minimising the energy of the atom using the exponents as variational parameters. This is most often done at the Hartree-Fock level although sometimes a correlated method is used. This method works for core and valence basis functions, but as the orbitals represented in polarisation functions are unoccupied in the atom in Hartree-Fock, these functions are not treated. In order to optimise polarisation functions, a Hartree-Fock optimisation of small molecules or a correlated treatment of the atom is required.

Energy optimised basis sets have a disadvantage however: the core electrons in an atom, because they are closer to the nucleus, have a much higher energy than those in the valence shells. As such, a tighter optimisation of core orbitals results in a greater improvement in the energy than the same optimisation of valence orbitals. This results in basis sets that have well optimised cores and less well optimised valence orbitals. This, in most cases, is the opposite of what is required in calculations as most interactions of interest happen in the valence shells. In order to increase the accuracy of a basis set,

more GTO's are added, yet most of these GTO's are used to better describe the core orbitals. This means that in order to increase the accuracy of the valence orbitals, many more GTO's of each type are needed, leading to very large basis sets. These can be reduced somewhat by introducing diffuse functions to the optimised basis set. These diffuse functions have small exponents (larger radii) that combine with the optimised functions to improve the descriptions of valence orbitals in a similar way to polarisation functions.

The size of basis set needed to describe the valence orbitals well, is large with many of the functions primarily used for describing the chemically less significant core orbitals. In a calculation using these basis sets, the coefficients for each orbital must be re-calculated each iteration. This is both time consuming and requires large amounts of compute power. However, the coefficients of core orbitals change very little in a calculation on a molecule, so a way of reducing the need to calculate coefficients for core orbitals will drastically increase the efficiency of a calculation. Contracted basis sets fulfil this requirement.

In a contracted basis set the coefficients for the group of functions used in describing each orbital in the core region is frozen and grouped together. Each core orbital is now described by a *fixed* linear combination of functions. This leaves just the important valence and supplementary orbitals to be optimised separately, greatly reducing the computational load. The full uncontracted basis set consists of the primitive GTO's (PGTO's) which are contracted to form a new set of contracted GTO's (CGTO's), this contraction is usually written as shown below in (2.58).

$$(10s4p1d/4s1p) \longrightarrow [3s2p1d/2s1p] \tag{2.58}$$

Here heavy atoms are shown before the / and Hydrogen's after.

There are two methods for contracting a basis set based on how the coefficients are calculated. The older method is a segmented contraction, where the basis set is divided into discrete segments of PGTO's and the coefficients calculated on each segment with each PGTO only used once. The other method is a general contraction, where all PGTO's are used in each CGTO with different coefficients. Most basis sets in use today are some-

where in between, with generally contracted basis sets with uncontracted valence orbitals or segmented basis sets, with some basis functions appearing in multiple contractions.

One final way of cutting down on the number of basis functions in a basis set is to build a basis set where the core orbitals are described with a relatively small basis, and the valence orbitals with a higher level basis. This type of basis set is called a split valence basis set, or a valence double zeta basis for the example of a minimal core and double zeta valence.

Below is a selection of pre-constructed basis sets which demonstrate those used in this thesis.

2.8.1 Dunning-Huzinaga Basis Sets

These basis sets are built using energy optimised, uncontracted basis sets up to (10s6p) determined by Huzinaga [15] and expanded by van Duijneveldt (14s9p) [16] and Partridge (18s13p) [17]. Dunning used the Huzinaga basis sets to produce a number of contracted basis set jointly known as the Dunning-Huzinaga [18] basis sets. Huzinaga's optimised second row basis sets have been adapted in a similar way by McLean and Chandler [19]. These sets are rarely used in this work.

2.8.2 Correlation Consistent (cc) Basis Sets

These basis sets proposed by Dunning and co-workers [20] are designed to recover the correlation energy of valence electrons. Correlation consistent refers to the design of the basis sets such that orbitals that contribute similar amounts of correlation energy are included at the same stage. For example the first d-function contributes a large correlation energy, but a second only contributes as much as the first f-function; therefor the first d-function is added in one stage and the second d-function and first f-function would be added in the same stage. These basis sets are designated as correlation consistent polarised valence X zeta (cc-pVXZ). These basis sets can also be augmented with diffuse functions producing the aug-cc-pVXZ basis sets [21].

2.8.3 Ahlrichs Type Basis Sets

These basis sets were designed by the group of R. Ahlrichs [22, 23] and comprise of DZ, TZ and more recently QZ basis sets [24] for elements up to Krypton. These basis sets are based on atom optimised PGTO's generated by the group and contracted using a segmented scheme. The most commonly used basis sets in this series are the *X*ZVP sets. These are multiple split valence basis set of order *X*. The polarisation functions used in parts of the QZ sets are taken from the cc-PV*X*Z sets which are discussed above.

2.8.4 Atomic Natural Orbitals (ANO) Basis Sets.

These basis sets are generally contracted basis sets founded on atomic natural orbitals. The aim of these basis sets is to contract a large set of PGTO's into a small contracted basis set using correlated calculations. The method is based on combining PGTO's using the natural orbitals produced in a correlated calculation usually CISD. The natural orbitals are those which diagonalise the density matrix. The natural orbitals have eigenvalues called the orbital occupation numbers. The orbital occupation numbers are equivalent to the number of electrons present in the orbital. In correlated calculations, orbital occupation numbers range from zero to two depending on the contribution of each orbital to the overall wave function. ANO basis sets are constructed by using the orbital occupation numbers to determine the contraction coefficients of PGTO's. Contraction coefficients are determined by how each PGTO contributes to a CGTO in the calculation. Basis sets of differing size can be generated based on limits as to how small a orbital occupation number is considered when including orbitals in a CGTO. Good examples of ANO basis sets are those of Almlöf and Taylor [25].

2.8.5 Wachters basis sets

The Wachters basis sets [26] are a collection of primitive atom optimised basis sets for third row atoms from Potassium to Zinc. There is an accompanying set of contracted basis sets which are more widely used. An extension of the [8s 4p 3d] contracted basis set has

been made. The extension includes two diffuse p-functions and a diffuse d-function [27] along with a set of f-functions based on a three term fit to an STO [28] for polarisation. These sets called Wachters+f [29] are very appropriate for use with transition metal atoms.

Chapter 3

Active Space Splitting - The Chromium Dimer

3.1 Introduction

The proposal for investigation in this chapter is, whether a method can be developed in order to reduce the computational work required to calculate energies for a system using a multiconfigurational approach.

At the current time a multiconfigurational calculation is limited to an active space of relatively small size. That limit is in the tens of electrons in tens of orbitals range. The limitations are due to both computational time and storage, and are due to the fact that as the size of the active space increases the number of CSF's explodes. These integrals take more time to process and require more RAM and disk space to store. As an example, using the same Molpro [30] calculation scheme as outlined below for the Chromium dimer (Cr_2) the active space for the calculation was reduced from a 12 electron in 12 orbital (12 in 12) active space to a 10 in 11 active space. This was achieved by moving a b_{1u} orbital from the active space into the inactive space. This resulted in the following active space : $3a_g$ $1b_{3u}$ $1b_{2u}$ $1b_{1g}$ $2b_{1u}$ $1b_{2g}$ $1b_{3g}$ $1a_u$, with an inactive space of $5a_g$ $2b_{3u}$ $2b_{2u}$ $0b_{1g}$ $6b_{1u}$ $2b_{2g}$ $2b_{3g}$ $0a_u$. the small reduction in the active space produced a noticeable reduction in both calculation time and number of CSF's. Calculation time is reduced in the single

state CASSCF calculation from 166.76 seconds for the 12 in 12 space to 77.04 seconds in the 10 in 11 space whilst the number of CSF's decreases from 78848 to 12270. As can be seen in this example a small decrease in active space size results in a large decrease in computational work.

The method proposed here for reducing computational load is to sub-divide the calculation in to a number of smaller sub-calculations each with its own smaller active space. Each calculation would be centred on a different atom or group of atoms using localised orbitals. This method would work best where a system has a number of parts which could be easily separated. As an example most transition metal based molecules are complexes with a metal atom or group of atoms at the centre and a number of ligands surrounding it. The calculation on a simple single metal atom centred complex could easily be split to produce two sub-calculations. One calculation would treat the complex electronic states in the metal atom whilst another could treat the ligand area.

The practical implementation of the proposed method will require that the orbitals be localised, sorted and assigned to a specific atom or ligand before the separate multiconfiguration calculations can take place.

In order to test this method small systems with a well understood electronic makeups will be required. Once the systems are identified, a set of reliable results based on that system must be found in literature with which to compare. As this thesis will mostly be concerned with systems involving transition metal atoms the test system must contain a transition metal atom. Transition metal atoms are those in which at least one *d*-type orbital is at least partially filled in the valence shell. In order to make the best use of the test system,a system where the *d*-type orbitals are are easily accessed for study would be of most use.

The first test system that will be used in the initial part of this thesis is a variation on the Chromium dimer (Cr_2). Instead of the Chromium dimer at its equilibrium geometry, where the *d* orbitals are strongly interacting and thus deformed, a dimer is chosen with a longer bond length. The Chromium dimer is useful here, in that at bond lengths exceeding 2.2 Å a weak bond is formed between the 4*s* orbitals on each centre, whilst there is

virtually no interaction between the 3*d* orbitals. The bond length chosen for use is 4.4 atomic units (a_0) which is approximately 2.328 Å. This makes it a good test system for exploring weakly interacting transition metal complexes such as those in this thesis.

The results calculated here will be compared to those presented in a paper by Ghosh and Taylor [31]. The paper shows both graphic and numerical representations of the exchange coupling of the Chromium dimer at 2.328 Å for various quantum mechanical methods.

Whilst the Chromium dimer is a simple system in its own right a need for an even simpler test system may be required. For example if results from the Chromium dimer are not good matches for the cited results or the method does not give a full set of results. In that case a new test system will be investigated.

The investigation of the Chromium dimer will proceed first with a set of benchmarks on the system using the same conditions as in the cited work to allow for internal consistency in results. The benchmarks will be carried out using D_{2h} symmetry. Following the benchmarks an expended set of calculation using the new methodology will be carried out. These calculations require a set of localised orbitals for the Chromium dimer. To make this possible the two atoms have to be symmetrically non-equivalent. To produce symmetrically non-equivalent Chromium atoms the symmetry needs to be reduced to C_{2v}. The localised orbitals can then be divided up based upon which atom the orbital is localised to. Two active spaces, one centred on each Chromium atom are created and an energy calculation is carried out for each position on the spin ladder.

3.2 Methodology

This section details the basics of the programs used and which variables were used in each program to produce the results as described.

3.2.1 Benchmarks

For the initial tests on the Chromium system, benchmarks were made in order to test the methods as laid down on the Ghosh and Taylor [31]. The benchmarks required a reproduction of values for the Heisenberg exchange coupling constant (J) as presented for all appropriate base methods used in this thesis. J is derived from the Heisenberg spin Hamiltonian shown below for two weakly coupled spins $\mathbf{S}_1$ and $\mathbf{S}_2$.

$$\mathcal{H} = -2J\hat{S_1} \cdot \hat{S_2} \tag{3.1}$$

In equation (3.1) $\hat{S_1}$ and $\hat{S_2}$ are the spin operators for sites 1 and 2 J is Heisenberg exchange coupling constant and the factor -2 is conventional for dinuclear iron sites. This equation was used unmodified for different systems in the Ghosh and Taylor paper [31] therefore it will also be used unmodified here.

In order to produce values for J a plot of total energy verses the overall spin quantum number is required. More strictly the value required is the eigenvalue of $\hat{\mathrm{S}}^2$ rather than overall spin quantum number here S is the spin quantum number. The value $\mathrm{S}(\mathrm{S}+1)$ is calculated as the appropriate eigenvalue of $\hat{\mathrm{S}}^2$ to represent the overall spin quantum number whilst energy relative to the $\mathrm{S} = 5$ state is used to represent total energy. J can be read as half the negative of the gradient of this plot as established in equation (3.1).

In the full $\mathrm{D_{2h}}$ symmetry this system does not lend itself to treatment using single reference methods due to the large quantity of near degenerate electronic states that arise at all spin states save the $\mathrm{S} = 5$ state. The near degenerate states make it impossible to optimise to a single low energy solution with an appropriate configuration to produce each state in the spin ladder.

The methods used will therefore be limited to the multireference methods CASSCF, CASPT2 and ACPF.

3.2.2 Programs

Two different program suites were used in the benchmark calculations. The Molpro [30, 32, 33, 34] suite and the MOLCAS [35]. These two program suites were selected as each had different advanced functions which are required in future experiments. Molpro [30] was used for the ACPF calculations, whilst MOLCAS [35] was used for CASPT2 calculations. For each calculation a set of optimised CASSCF orbitals are required. These orbitals are processed to produce the ACPF or CASPT2 result, as such CASSCF results are presented for both suites.

In order to test the new method a program suite was required that had a two specialised functions, first a system for creating localised orbitals and secondly a way of specifying multiple active spaces using the localised orbitals. The suite selected for this was the Molpro [30, 32, 33, 34] suite as the MOLCAS [35] suite does not have all the functions required. As MOLCAS [35] was not used in the split active space calculations CASPT2 results will not be obtained in this section.

A number of specialist directives were used to obtain the important local orbitals and split active space. localisation was carried out using the `locali` directive which prints local orbitals to a temporary file `2141.2` These orbitals were read using the following set of commands `start,2141.2,type=local`. The commands specify the file holding the orbitals, in this case the temporary file `2141.2` the type of orbitals present, and to use them as the starting orbitals for the calculation. Finally the active spaces were constructed using the `restrict` directive which restricts certain electrons to certain orbital spaces. The restrict command takes the following form: `restrict,nmin,nmax,` $orb_1, orb_2, \ldots orb_n$;. Here `nmin` is the minimum number of electrons in the space and `nmax` is the maximum and $orb_1, orb_2, \ldots orb_n$ is a list of orbitals making up the space. In the case of these calculation a number of electrons were restricted to two spaces of orbitals representing the $4s$ and $3d$ orbitals present on each centre.

3.2.3 Program Set-Up

In both programs a correlation consistent ANO basis set was used. The basis set used is a ANO-CC basis set using basis functions up to and including *g*-type from unpublished work by B. J. Persson. See appendix D for full details.

Molpro

The Molpro [30, 32, 33, 34] calculations were set-up as a multi-part calculation, each part passing optimised orbitals to the next part.

For the benchmark calculations the calculation was set up as follows:

1. A closed shell Hartree-Fock SCF calculation in D_{2h} symmetry. This was performed on the $[Cr_2]^{12+}$ ion. For all calculations the orbital occupation numbers were $5a_g$ $2b_{3u}$ $2b_{2u}$ $0b_{1g}$ $5b_{1u}$ $2b_{2g}$ $2b_{3g}$ $0a_u$ for both α and β orbitals.
2. A Single State CASSCF calculation on the $S = 5$ state, using a 12 electron in 12 orbital (12 in 12) active space of the form : $3a_g$ $1b_{3u}$ $1b_{2u}$ $1b_{1g}$ $3b_{1u}$ $1b_{2g}$ $1b_{3g}$ $1a_u$, with an inactive space of $5a_g$ $2b_{3u}$ $2b_{2u}$ $0b_{1g}$ $5b_{1u}$ $2b_{2g}$ $2b_{3g}$ $0a_u$. In order to promote orbital optimisation in this system the first 15 iterations of the optimisation used uncoupled orbital and CI coefficient optimisation. This step was used to pre-condition and partially pre-optimise the CASSCF orbitals for the third stage.
3. A single state CASSCF calculation on the state of interest, using a 12 electron in 12 orbital (12 in 12) active space of the form : $3a_g$ $1b_{3u}$ $1b_{2u}$ $1b_{1g}$ $3b_{1u}$ $1b_{2g}$ $1b_{3g}$ $1a_u$, with an inactive space of $5a_g$ $2b_{3u}$ $2b_{2u}$ $0b_{1g}$ $5b_{1u}$ $2b_{2g}$ $2b_{3g}$ $0a_u$. In order to promote orbital optimisation in this system the first 15 iterations of the optimisation used uncoupled orbital and CI coefficient optimisation.
4. An ACPF calculation using the optimised CASSCF orbitals produced in the third stage.

The split active place calculations required two separate calculations to first produce and visualise the localised orbitals for viewing and then to run the follow up calculations using the split active space methodology. As the second set of calculations necessarily in-

clude the first set, only the work flow for the second set of calculations needs to be listed here. Anything up to and including localisation represent the first calculations performed. In all cases the a_1 state symmetry was used. The calculations are performed in C_{2v} symmetry in order to brake the plane of symmetry between the two Chromium atoms in order to allow for localisation.

1. A closed shell Hartree-Fock SCF calculation in C_{2v} symmetry. This was performed on the $S = 0$ state of the $[Cr_2]^{12+}$ ion. For all calculations the orbital occupation numbers were$10a_1$ $4b_1$ $4b_2$ $0a_2$ for both α and β orbitals.
2. A three state average CASSCF calculation was performed. The calculation used a 12 electron in 12 orbital (12 in 12) active space of the form: $6a_1$ $2b_1$ $2b_2$ $2a_2$, with an inactive space of $10a_1$ $4b_1$ $4b_2$ $0a_2$. This was performed on the $S = 1$ state of Cr_2. In order promote orbital optimisation in this system the first 15 iterations of the optimisation used uncoupled orbital and CI coefficient optimisation.
3. A single state CASSCF calculation was performed. The calculation used a 12 electron in 12 orbital (12 in 12) active space of the form: $6a_1$ $2b_1$ $2b_2$ $2a_2$, with an inactive space of $10a_1$ $4b_1$ $4b_2$ $0a_2$. This was performed on the state of interest for each state of the spin ladder in Cr_2. In order promote orbital optimisation in this system the first 15 iterations of the optimisation used uncoupled orbital and CI coefficient optimisation.
4. The orbitals produced in the previous step were localised and printed to an output file for visualisation and sorting.
5. A single state CASSCF calculation was performed using the same 12 in 12 active space used above and the localised orbitals produced in the previous stage. This was performed on the state of interest for each state of the spin ladder in Cr_2. In order to promote orbital optimisation in this system the first 15 iterations of the optimisation used uncoupled orbital and CI coefficient optimisation.
6. An ACPF calculation was performed using the localised orbitals from stage 4 . In order to use the localised orbitals a different orbital input string is required from that detailed for CASSCF. This string has the following format:

`orbit,2141.2,type=local.`

7. A single state CASSCF calculation was performed using the localised orbitals from stage 4. This required the orbitals to be read from a temporary file using the following commands `start,2141.2,type=local.` This step also used the split active spaces. These Active spaces were defined using the following command strings:

   `restrict,6,6,11.1,5.2,5.3,13.1,15.1,1.4;`

   `restrict,6,6,12.1,6.2,6.3,14.1,16.1,2.4;`

   These commands specify two 6 in 6 active spaces one restricted to the selected active orbitals in space A and the other the active orbitals on space B. As before in order promote orbital optimisation in this system the first 15 iterations of the optimisation used uncoupled orbital and CI coefficient optimisation.
8. An ACPF calculation was performed using the localised orbitals produced in a previous step and the same restricted active spaces detailed above. In order to use the localised orbitals a different orbital input string is required from that detailed for CASSCF. This string has the following format: `orbit,2141.2,type=local.`
9. The final orbitals produced were printed to an output file.

The local orbitals once produced require sorting to construct the two local active spaces. To do this the orbitals were loaded into an orbital visualisation program called MOLDEN [36]. Here the molecular orbitals are represented as maps of orbital amplitudes in three dimensions over a skeletal view of the molecule. The orbitals were identified by energy , shape and location and sorted to produce two active spaces that represented the 4*s* and 3*d* orbitals on each centre. The orbitals chosen were those labelled 11.1, 13.1, 15.1, 5.2, 5.3 and 1.4 for the lower atom (Space A) and 12.1, 14.1, 16.1, 6.2, 6.3 and 2.4 for the upper atom (Space B). The labels represent the orbitals numerically, the first number represents the order of the orbital within each symmetry and the second is the Molpro [30] symmetry number in C_{2v} symmetry. The Molpro [30] symmetry numbers for C_{2v} symmetry follow the relationship $1 = a_1$, $2 = b_1$, $3 = b_2$ and $4 = a_2$.

As an example the MOLDEN [36] orbital plots for the active spaces from the $S = 1$ state of Cr_2 are shown here. The plots were created using the space filling orbital function

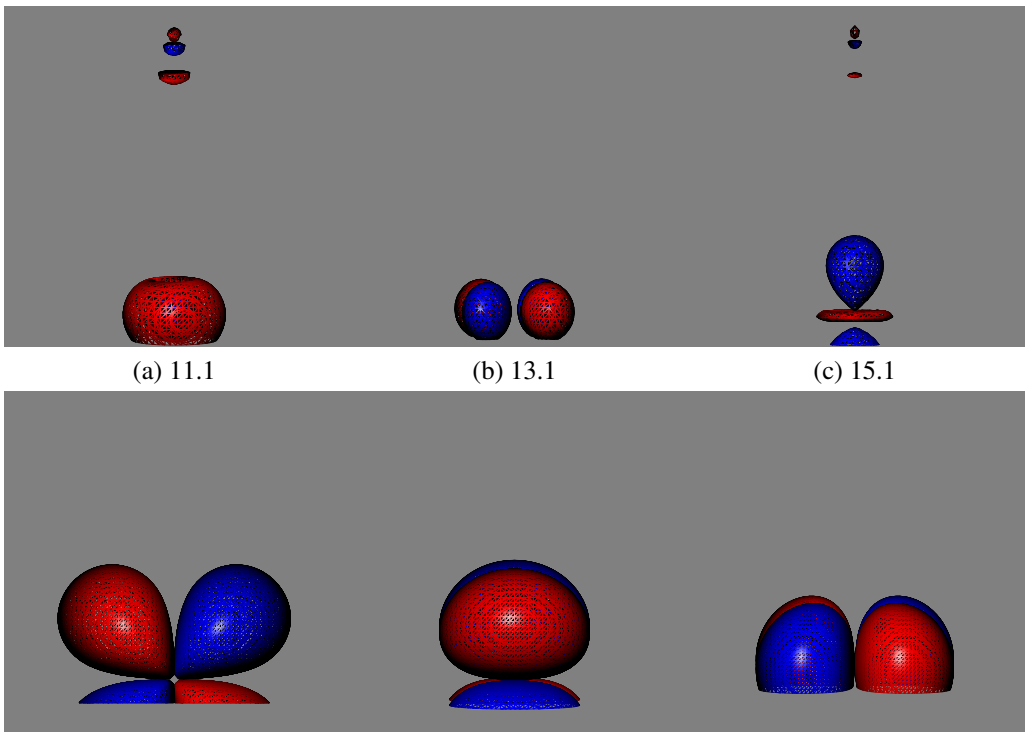

(a) 11.1 (b) 13.1 (c) 15.1

(d) 5.2 (e) 5.3 (f) 1.4

Figure 3.1: Localised orbitals for active space A in the S = 1 state of Cr_2

and a contour value of 0.07.

The localised orbitals that make up active space A are shown in figure 3.1, and the localised orbitals that make up active space B are shown in figure 3.2. The orbitals that make up each active space are nearly identical save that the polarities of lobes in the orbitals are reversed compared to each other.

In all spin states the orbitals were arranged in the same way with the even numbered orbitals on one atom and the odd numbered orbitals on the other. This made the sorting and selection of orbitals easy, as a different active space was not required for each state.

3.2.4 MOLCAS set-up

The MOLCAS [35] calculations were performed in C_{2v}, retaining the inter-molecular axis as the twofold rotation. This was done to complement other calculations later in this thesis. The construction of these calculations were more complex due to problems with finding a suitable set of starting orbitals for the CASSCF calculations. The orbitals finally used were generated using a sequence of separate pre-optimised CASPT2 orbitals generated from separate calculations. These orbitals natural orbitals obtained from the

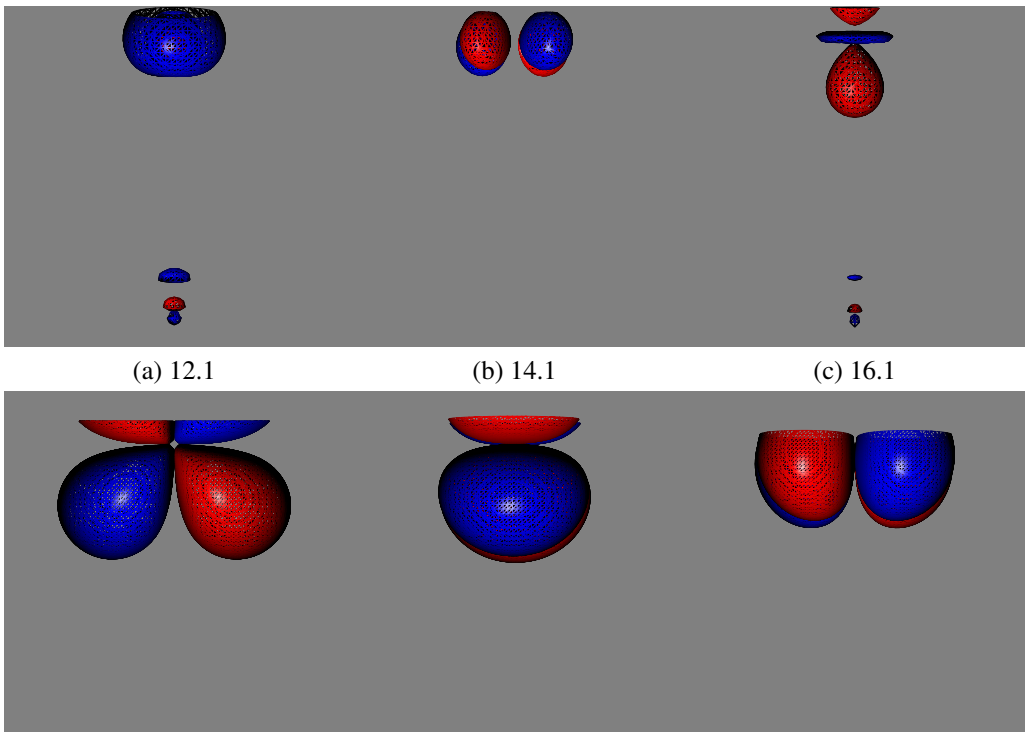

(a) 12.1 (b) 14.1 (c) 16.1

(d) 6.2 (e) 6.3 (f) 2.4

Figure 3.2: Localised orbitals for active space B in the S = 1 state of Cr_2

density matrix of the (normalized) wave function through first order. However, the active/active block of that density matrix is not computed exactly. An approximation has been designed in such a way that the trace is correct, and the natural occupation numbers of active orbitals are between zero and two.

The first set of orbitals common to all results were generated by a four part calculation on $[CrMn]^+$ an electronically identical system with a more defined broken symmetry. This calculation didn't fully optimise so the CASSCF and CASPT2 steps were repeated using the previous orbitals. The fully optimised orbitals produced from the $[CrMn]^+$ calculations were then used to produce optimised S = 0 Cr_2 orbitals. The optimised S = 0 orbitals were then used to produce the CASSCF and CASPT2 results for the S = 0, S = 2 and S = 5 states. For the S = 3 and S = 4 states the S = 0 orbitals produced a high energy solution so the S = 5 orbitals were used to produce results. The S = 1 state produced the same high energy state with both the S = 0 and S = 5 orbitals so the S = 2 orbitals were tried which produced the desired low energy solution.

The basic setup for the initial $[CrMn]^+$ optimisation was a four part calculation with each part passing optimised orbitals to the next part.

The first and second part of the calculation were Hartree-Fock SCF calculations on the S = 0 state using the following orbital occupations : $13a_1$ $5b_1$ $5b_2$ $1a_2$ for both α and β orbitals.

The third part was a CASSCF calculation using a 12 electron in 12 orbital (12 in 12) active space of the form : $6a_1$ $2b_1$ $2b_2$ $2a_2$, with an inactive space of $10a_1$ $4b_1$ $4b_2$ $0a_2$. This is equivalent to the active and inactive spaces used in the the Molpro [30] calculations. A level shift of 1.4 was used to aid in the convergence.

The final part was a CASPT2 calculation using the optimised CASSCF orbitals produced in the third part. An imaginary shift value of 0.1 was used to eliminate possible intruder states and aid convergence.

For all other optimisations the first two parts were excluded and replaced by the pre-optimised CASPT2 orbitals from a previous optimisation, only parts three and four were carried out using the same parameters as detailed above.

3.2.5 Additional Calculations

In order to fully analyse the data produced in the above calculations further data was required. Some of the data was produced in the calculations above whilst other data required new calculation, the methods for these calculations are listed here.

Additional calculations were required to look at how the the change to localised orbitals affected the energy of the resulting states in the spin ladder. The additional calculations were required to calculate ACPF energies using delocalised orbitals for comparison with those produced in the orbital optimisation step.

This calculation required a set of pre-optimised CASSCF type orbitals and a CASSCF wave function. The calculation was therefor constructed in the same manner as those used in the optimisation stage with the exception of the orbital localisation and subsequent restricted active space steps. These steps were replaced with a single ACPF calculation.

In order to investigate the differences between an ACPF calculation using a restricted active space and an ACPF calculation using the wave function output of a restricted CASSCF calculation, a set of calculations were produced using the same procedure out-

lined for the split active space calculations with the exception of the ACPF stage where a standard ACPF calculation was performed. Molpro [30] in the absence of any extra instructions carries out ACPF calculations using the data from the most recent appropriate calculation, in this case that is the split active space CASSCF calculation so no additional instructions were required.

3.3 Results

In this section the results of the calculations listed in the methodology section are presented. All results are rounded to six decimal places for ease of representation where necessary.

3.3.1 Raw Data

The raw calculated data which is used in construction of the graphs and tables shown in the analysis section is listed here. Where no usable date was produced n/a will be substituted. The results calculated using non-localised orbitals are represented by (nl).

Benchmark calculations

Table 3.1 shows the raw output energies for the tested states of Cr_2 at 4.4 a_0 in D_{2h} Symmetry. All values are shown in E_h, the atomic unit of energy.

Localised orbital and split active space calculations

This section contains the raw data concerning the localised orbital and Split active space calculation on tested states of Cr_2 at 4.4 a_0 in C_{2v} Symmetry. All values are shown in E_h, the atomic unit of energy.

S	0	1	2	3	4	5
Molpro [30, 33, 34] CASSCF Energy (E_h)	-2086.695236	-2086.693218	-2086.689269	-2086.683550	-2086.676245	-2086.667365
MOLCAS [35] CASSCF Energy (E_h)	-2086.593617	-2086.591377	-2086.586984	-2086.580611	-2086.572484	-2086.562660
Molpro [30] ACPF Energy (E_h)	-2086.945781	-2086.943476	-2086.938935	-2086.932279	-2086.923531	-2086.912028
MOLCAS [35] CASPT2 Energy (E_h)	-2086.833954	-2086.831540	-2086.827161	-2086.820108	-2086.809840	-2086.795007

Table 3.1: Molpro and MOLCAS state energies for Cr_2 at 4.4 a_0 in D_{2h} Symmetry

S	0	1	2	3	4	5
CASSCF energy using local orbitals (E_h)	n/a	n/a	n/a	n/a	n/a	-2086.667365
CASSCF energy using Split active space (E_h)	n/a	n/a	n/a	n/a	n/a	n/a
CASSCF energy using non-local orbitals (E_h)	-2086.695236	-2086.693218	-2086.689269	-2086.683550	-2086.676245	-2086.667365
ACPF energy using local orbitals (E_h)	-2086.945780	-2086.943475	-2086.938935	-2086.932279	-2086.923531	-2086.912015
ACPF energy using split active space (E_h)	-2086.903779	-2086.901734	-2086.898679	-2086.894826	-2086.890416	-2086.885859

Table 3.2: State energies for Cr_2 at 4.4 a_0 in C_{2v} Symmetry using localised orbitals and split active spaces

3.3.2 Benchmark Analysis

The data here is produced by manipulation of the raw data presented above.

Table 3.3 shows the energies for the tested states of Cr_2 at 4.4 a_0 as energies relative to the $S = 5$ state. All values have been converted to wave numbers (cm^{-1}) to reflect the data presented in the Ghosh and Taylor paper [31]. The conversion factor used was $1\,E_h$ is equivalent to $219474.63068\,cm^{-1}$.

The data from Table 3.3 was then plotted against $S(S+1)$ see figure 3.3. The value of J the exchange coupling for each method is half the negative of the gradients from the graph in figure 3.3 as shown in the bottom right of the graph.

The values of J are calculated using the best fit linear regression tool in Gnuplot.

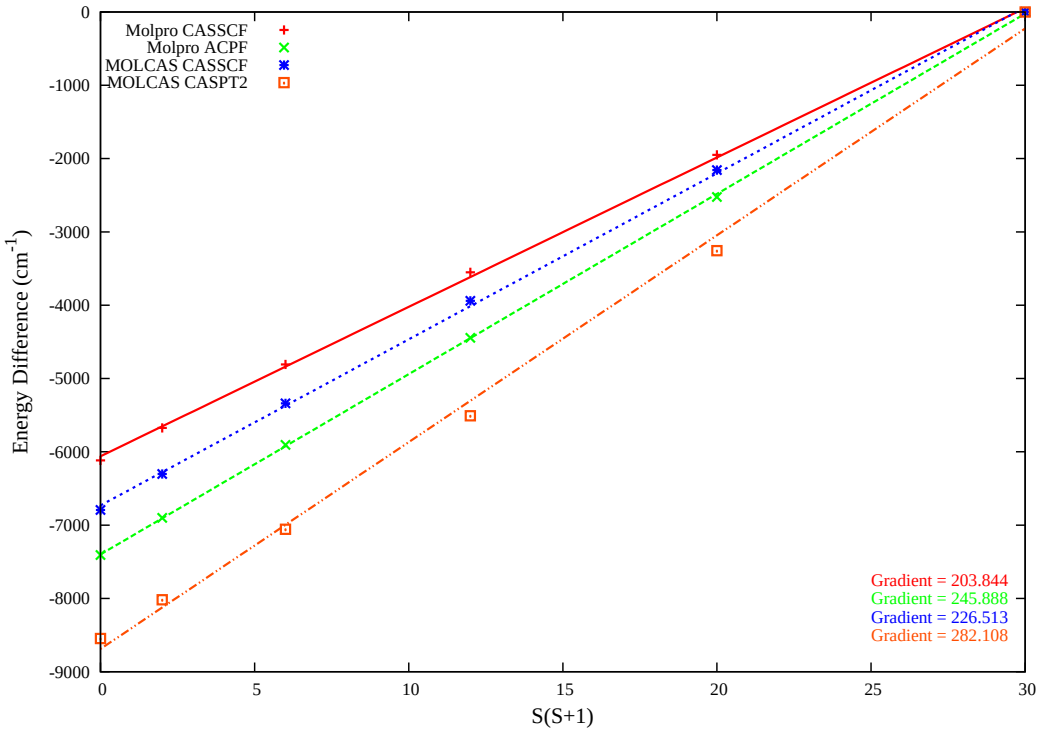

Figure 3.3: Energy of Cr_2 as a function of $S(S+1)$

As a comparison table 3.4 shows the J values calculated in these experiments compared with those in the Ghosh and Taylor paper [31].

S	0	1	2	3	4	5
Molpro [30, 33, 34] CASSCF	-6116.993778	-5674.159154	-4807.444470	-3552.187570	-1948.954820	0.000000
MOLCAS [35] CASSCF	-6794.180780	-6302.575539	-5338.391465	-3939.680324	-2156.173158	0
Molpro [30] ACPF	-7407.923346	-6901.971330	-5905.325547	-4444.599231	-2524.494566	0.000000
MOLCAS [35] CASPT2	-8547.965573	-8018.139548	-7057.009464	-5508.967104	-3255.372077	0

Table 3.3: Molpro and MOLCAS Cr_2 state energies (cm^{-1}) relative to the $S = 5$ state.

Method	Calculated J (cm^{-1})	J (cm^{-1}) from Paper
Molpro [30, 33, 34] CASSCF	-101.942	-108
MOLCAS [35] CASSCF	-113.266	-108
Molpro [30] ACPF	-122.944	-120
MOLCAS [35] CASPT2	-141.054	-168

Table 3.4: Molpro and MOLCAS J values for Cr_2 compared to appropriate paper values

3.3.3 Point Group Symmetry

The first thing to look at is how the changes to the point group symmetry and orbital type affect the energies of the various energy states. For this a direct energy comparison is made. The data used for the point group comparison is the D_{2h} data presented in chapter one from table 3.1, compared with data produced in the orbital sorting calculations as shown in table 3.2. All energies shown are in E_h except where noted and rounded to eight decimal places.

The table 3.5 shows how a change in the point group symmetry affects the calculation.

S	0	1	2	3	4	5
D_{2h}	-2086.69523575	-2086.69321805	-2086.68926901	-2086.68354964	-2086.6762448	-2086.66736469
C_{2v}	-2086.69523575	-2086.69321805	-2086.68926901	-2086.68354964	-2086.67624477	-2086.66736468
ΔE (cm^{-1})	0.00004649	0.00013274	0.00061363	0.00030696	-0.00012046	-0.00232542
% Error	0.00000000%	0.00000000%	0.00000001%	0.00000001%	0.00000000%	0.00000005%

Table 3.5: Comparison of D_{2h} and C_{2v} CASSCF state energies for Cr_2

3.3.4 Orbital Type

The other parameter which changes significantly in this process is the use of localised orbitals as against delocalised orbitals. Calculations have been produced using both localised and the usual delocalised orbitals. The data from these calculations are shown below using the same comparisons as used in comparing the two different spacial symmetries.

The table 3.6 shows how a change in the orbital type affects the energies of the states in the spin ladder. All energies shown are in E_h except where noted and rounded to eight decimal places

Finally tables 3.8 and 3.7 brings together all the changes used in this process using the standard 12 in 12 active space detailed above. All energies shown are in E_h except where noted and rounded to eight decimal places.

S	0	1	2	3	4	5
Delocalised Orbitals	-2086.69523575	-2086.69321805	-2086.68926901	-2086.68354964	-2086.67624477	-2086.66736468
Local Orbitals	n/a	n/a	n/a	n/a	n/a	-2086.66736468
ΔE (cm-1^{-1})	n/a	n/a	n/a	n/a	n/a	0.00047647
% Error	n/a	n/a	n/a	n/a	n/a	0.00000001%

Table 3.6: Comparison CASSCF state energies for Cr_2 using delocalised and localised orbitals

S	0	1	2	3	4	5
Delocalised Orbitals (D_{2h})	-2086.69523575	-2086.69321805	-2086.68926901	-2086.68354964	-2086.6762448	-2086.66736469
Local Orbitals (C_{2v})	n/a	n/a	n/a	n/a	n/a	-2086.66736468
ΔE (cm^{-1})	n/a	n/a	n/a	n/a	n/a	-0.001848897
% Error	n/a	n/a	n/a	n/a	n/a	-0.00000004%

Table 3.7: Comparison of CASSCF state energies for Cr_2 taking into account all changes

S	0	1	2	3	4	5
Delocalised Orbitals (D_{2h})	-2086.94578120	-2086.94347591	-2086.93893486	-2086.93227930	-2086.92353066	-2086.91202822
Local Orbitals (C_{2v})	-2086.94578041	-2086.94347549	-2086.93893511	-2086.93227908	-2086.92353063	-2086.91201493
ΔE (cm^{-1})	-0.173298989	-0.092294344	0.054999920	-0.047676691	-0.007366046	-2.916414222
% Error	-0.00000378%	-0.00000202%	0.00000120%	-0.00000104%	-0.00000016%	-0.00006367%

Table 3.8: Comparison of ACPF state energies for Cr_2 taking into account all changes

3.3.5 Split Active Spaces

The final stage in this experiment was to look at how sub-dividing the active space so that a separate space was used for each centre would affect the energy states in Cr_2. The result of these experiments are shown below with comments where appropriate.

Table 3.10 shows the energies for the tested states of Cr_2 at 4.4 a_0 as energies relative to the $S = 5$ state. All values have been converted to wave numbers (cm^{-1}) to reflect the data presented in the Ghosh and Taylor paper [31] and the data from chapter 3. The conversion factor used was $1\,E_h = 219474.63068\,cm^{-1}$.

The data from Table 3.10 was then plotted against $S(S+1)$ see figure 3.4. The value of the Heisenberg exchange coupling constant (J) for each method can be obtained from the graph in figure 3.4 as half the negative gradients of the best fit lines as shown in the bottom right of the graph. The values of J are calculated using the best fit linear regression tool in Gnuplot.

As a comparison table 3.4 shows the J values calculated in these experiments compared with those calculated in chapter 3 using Molpro [30, 32, 33, 34].

Method	Calculated J (cm^{-1})	J (cm^{-1}) from Chapter 3
Regular CASSCF	-101.942	-101.942
Spilt CASSCF	n/a	-101.942
Regular ACPF	-122.944	-122.944
Split ACPF	-64.823	-122.944

Table 3.9: J values for Cr_2 compared to appropriate Molpro results from chapter 3

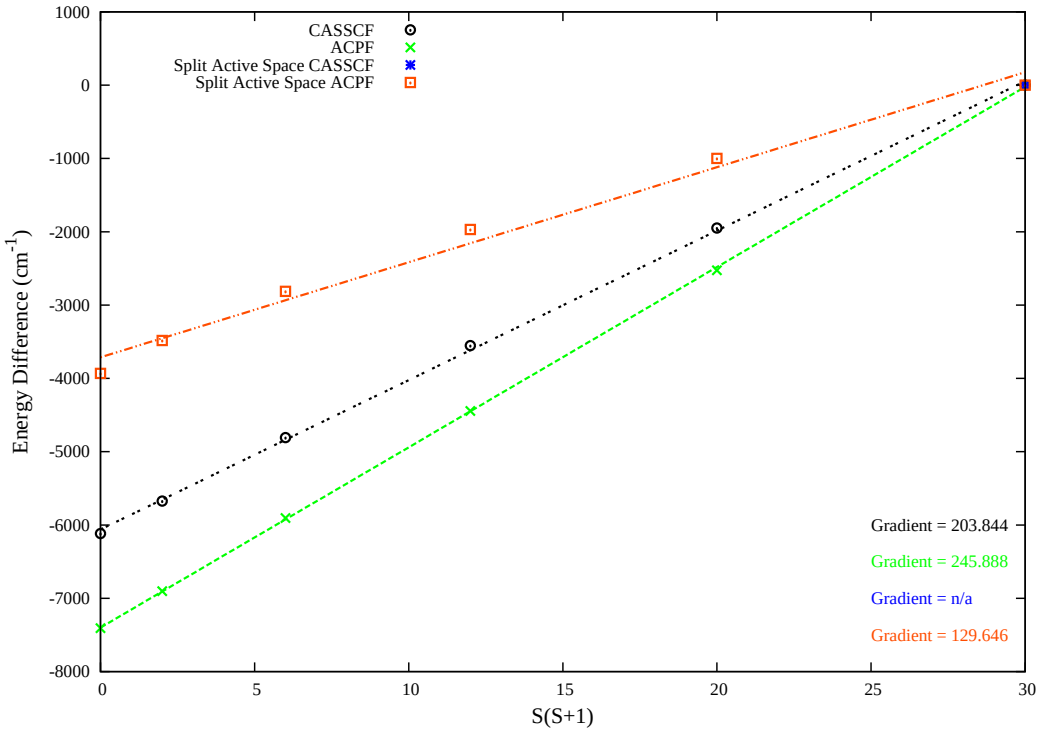

Figure 3.4: Energy of Cr_2 as a function of $S(S+1)$ using both split and regular active spaces

3.4 Analysis and Conclusions

3.4.1 Benchmark Calculations

It can be seen from table 3.4 that the results produced in the benchmarks are generally close to those presented in the Ghosh and Taylor paper [31]. Some methods fared better than others. Molpro [30, 33, 34] CASSCF produced a result over five cm^{-1} below the paper value whilst MOLCAS [35] CASSCF produced results over five cm^{-1} above the paper value. The CASPT2 result showed the greatest deviation at almost twenty seven cm^{-1} whilst ACPF gave the best result with an almost three cm^{-1} deviation.

Possible reasons for the differences include methodological differences in the preparation of calculations and the previous data the calculations used as starting points. A further possibility is differences in the programs used for these calculations and how they process the wavefunctions.

S	0	1	2	3	4	5
Regular CASSCF	-6116.993778	-5674.159154	-4807.444470	-3552.187570	-1948.954820	0.000000
Split CASSCF	n/a	n/a	n/a	n/a	n/a	n/a
Regular ACPF	-7407.923346	-6901.971330	-5905.325547	-4444.599231	-2524.494566	0.000000
Split ACPF -3932.921127	-3483.997359	-2813.649139	-1968.048753	-1000.018904	0.000000	

Table 3.10: Regular and split active space Cr_2 state energies (cm^{-1}) relative to the S = 5 state.

3.4.2 Changes between benchmark and testing

Several variables were changed between the benchmark calculations and the test calculations, these changes were required to accommodate the new active space design however these changes potentially effect the result. A measure of the change in the result can be calculated based on isolating each change and comparing it to the original data.

Point Group Symmetry

Table 3.5 shows how a change in the point group symmetry affects the calculations. As can be seen, the change in the point group does not significantly affect the CASSCF results with very small overall changes in energy, equivalent to millionths of a percent of total energy. With two exceptions the change in symmetry produces a slight lowering in energy which is unexpected. A slight raise in energy would be expected due to the reduction in the number of degrees of freedom due to symmetry available. The two exception are in the nineplet (S = 4) and elevenplet (S = 5) states where a small increase in the energy is present. Also of note is the fact that in S = 5 state the energy change is large. A possible reason for this is the S = 5 state has a large component of the wave function where all spins on a centre are aligned spin parallel in all five available *d*-orbitals which means more orbitals are in use emphasising the reduction in available degrees of freedom.

Orbital Type

Table 3.6 shows how a change in the orbital type affects the energies of the states in the spin ladder.

As can be seen in table 3.6 there was a major problem with the calculation of energies when using local orbitals were used in CASSCF calculations. The problem had to do with calculating the P-space to be used in these calculations. After using all the recommended solutions no further progress was made, as such no further information could be extracted from these calculations. No calculation using delocalised orbitals in C_{2v} symmetry were run as such no conclusion about the effect of localisation alone can be drawn. The one data point available however show little change due to localisation. This result is the S = 5

state however which has the least bonding interactions which would result in an almost localised appearance even using delocalised orbitals.

Finally Tables 3.7 and Table 3.8 show the overall effect of changing both point group symmetry and orbital type simultaneously. As before the lack of CASSCF results with local orbitals mean no conclusions can be draw in this case. There are however valid ACPF results that show that a change in both point group symmetry and orbital type produces a general rise in energy. This rise in energy is most significant in the S = 5 and S = 0 states where the most interaction between the *d*-orbitals take place. The only anomaly in the data is in the S = 2 state where a lowering of energy takes place.

3.4.3 Test Calculations

This experiment has been massively hampered by the failure of the CASSCF calculations using localised orbitals. These calculations have not rendered enough usable date to make any real conclusions, as such these comments will be restricted to the data produced at the ACPF level.

From table 3.9 it can be seen that the various changes in the set up has not affected the standard active space calculations, with a no change in the *J* value for the regular ACPF. However the change in the *J* value for the split ACPF is significant with the value just over half that of the standard calculation. This suggests that the use of the split active space technique has caused a reduction in the energy level splitting present in the spin ladder. A possible cause of this reduction in the splitting is a change in the number and variety of valid configurations available for creating the wave function. This may cause a small number of configurations to become more important whilst some lower energy configurations from the full active space may no longer be valid in the new split active spaces.

Overall this experiment has been a failure mostly due to a lack of usable data rather than a failure of the technique. This system has been exhausted as far as the technique is concerned without a useful conclusion, however the lack of usable data means that the technique has not been fully explored. In order to fully test this technique, further

data is required therefore it is suggested that a further system be tried. The new system should be similar to this system and preferably with a simpler electronic structure than the system tested here in order to promote easier understanding and to possibly simplify the calculation systems.

Chapter 4

Active Space Splitting: The Nitrogen Molecule

4.1 Introduction

After the failure of the Chromium dimer experiments a new system was required to further explore the split active space techniques outlined in chapter four. This new system needed to meet most of the same criteria as the original system, in that it needed to be small and well understood or easily testable in order that the results generated could be easily compared to known data. The system chosen was the Nitrogen molecule (N_2) at 4.5 a_0 which is approximately 2.381 Å. The experimental equilibrium bond length is 1.0977 Å: as the bond length moves further from this distance, interactions between the centres become increasingly weak. This system is set up to parallel the Chromium dimer system, with weakly interacting outer valence shells. In the case of the Chromium dimer the weak interactions involved the partially filled *d* orbitals. In (N_2) all weak interactions happen between the *p* orbitals which are normally involved in the formation of the triple bond. A large deviation from the equilibrium bond length is required as the *p* orbital interactions in N_2 are much stronger than the relatively weak interactions between the *d* orbitals in Cr_2.

As with the Chromium dimer calculations presented before, a spin ladder is produced

at each stage and a value for the Heisenberg exchange coupling constant (J) is calculated. Unlike for the Chromium dimer no previously published data has been found therefore a baseline set of calculations was also required.

As well as the initial investigation into the standard system an investigation into other active space splits will be undertaken

4.2 Methodology

This section details the basics of the programs used and which variables were used in each program to produce the results as described in the following sections.

4.2.1 Programs

The suite selected for these calculations was the Molpro [30, 32, 33, 34] suite used in the previous calculations. The calculations were constructed as before using the appropriate variables to produces localised orbitals and construct the appropriate restricted active spaces.

4.2.2 Basis Sets

For these calculations a TZVP basis set from the Ahlrichs [22, 23] group was used. This provides a triple zeta basis set with enhanced valence orbitals and polarisation functions. These additional functions are important for describing the long range effects studied in these calculations. This basis set provides basis functions up to and including the d-orbitals.

4.3 Baseline

In order to fully explore this system, a set of baseline results are required for comparison. These baseline results can be easily generated as a byproduct of the calculations required. In the orbital optimisation stage, a non-local orbital CASSCF calculation is

required before the localisation process so these results are already generated. An additional calculation is required to generate ACPF results but this does not significantly increase calculation time. These results will provide a suitable baseline from which to compare how the changes in orbital type and active space affect the spin ladder.

4.4 Orbital Optimisation and Sorting

In order to calculate the new active spaces the orbitals must be localised so that each orbital resides wholly on one atom. Once localised these orbitals can be visually sorted by type and atom in order to create the new local active spaces.

The orbital optimisation calculation was carried out on a C_{2v} geometry of the N_2 system. This calculation was carried out for each spin state on the spin ladder with each state having an overall a_1 state symmetry. The calculation used the following steps:

1. A closed shell Hartree-Fock SCF calculation in C_{2v} symmetry was performed on the $S = 0$ state of N_2. The Molpro [30] default a_1 symmetry occupation was used.
2. A single state CASSCF calculation was performed. The calculation used a 10 electron in 8 orbital (10 in 8) active space of the form : $4a_1\ 2b_1\ 2b_2\ 0a_2$, with an inactive space of $2a_1\ 0b_1\ 0b_2\ 0a_2$. This was performed on the state of interest for each state of the spin ladder in N_2. In order promote orbital optimisation in this system the first 15 iterations of the optimisation used uncoupled orbital and CI coefficient optimisation.
3. The orbitals produced in the previous step were localised and printed to an output file for visualisation and sorting.
4. An ACPF calculation was carried out using the non-local CASSCF orbitals generated in step two.
5. A single state CASSCF calculation was performed using the same 10 in 8 active space and the localised orbitals produced above. This was performed on the state of interest for each state of the spin ladder in N_2. In order promote orbital optimisation in this system the first 15 iterations of the optimisation used uncoupled orbital and

CI coefficient optimisation.

6. An ACPF calculation was performed using the same localised orbitals produced above. In order to use the localised orbitals a different orbital input string is required from that detailed for CASSCF, this string has the following format:
   `orbit,2141.2,type=local.`

The local orbitals once produced, require sorting to construct the two local active spaces to represent the 2*s* and 2*p* orbitals on each centre. This was carried out as detailed in chapter 3. The orbitals chosen were those labelled 3.1, 5.1, 1.2 and 1.3 and 1.4 for the lower atom (Space A) and 4.1, 6.1, 2.1 and 2.3 for the upper atom (Space B).

As an example the MOLDEN [36] orbital plots for the active spaces from the S = 1 state of N_2 are shown here. The plots were created using the space filling orbital function and a contour value of 0.07.

The localised orbitals that make up active space A are shown in figure 4.1, and the localised orbitals that make up active space B are shown in figure 4.2.The orbitals that make up each active space are identical save that the polarities of lobes in the orbitals are reversed compared to each other.

In all spin states the orbitals were arranged in the same way with the even-numbered orbitals on one atom an the odd-numbered orbitals on the other. This made the sorting and selection of orbitals easy as a different active space was not required for each state.

4.5 Split Active Space Calculations

Once the localised orbitals for the active spaces had been identified and sorted, the full calculations could be run. As the orbitals were not saved to a file that could be accessed for re-use the calculation had to be run in such a way that the orbitals required were generated as part of the calculation scheme. In order to keep the orbitals consistent it meant that the steps used to create the orbitals in the first place had to be repeated in the full calculations. As such the calculation followed the following steps:

1. Steps one and two of the orbital optimisation listed above were repeated in order to

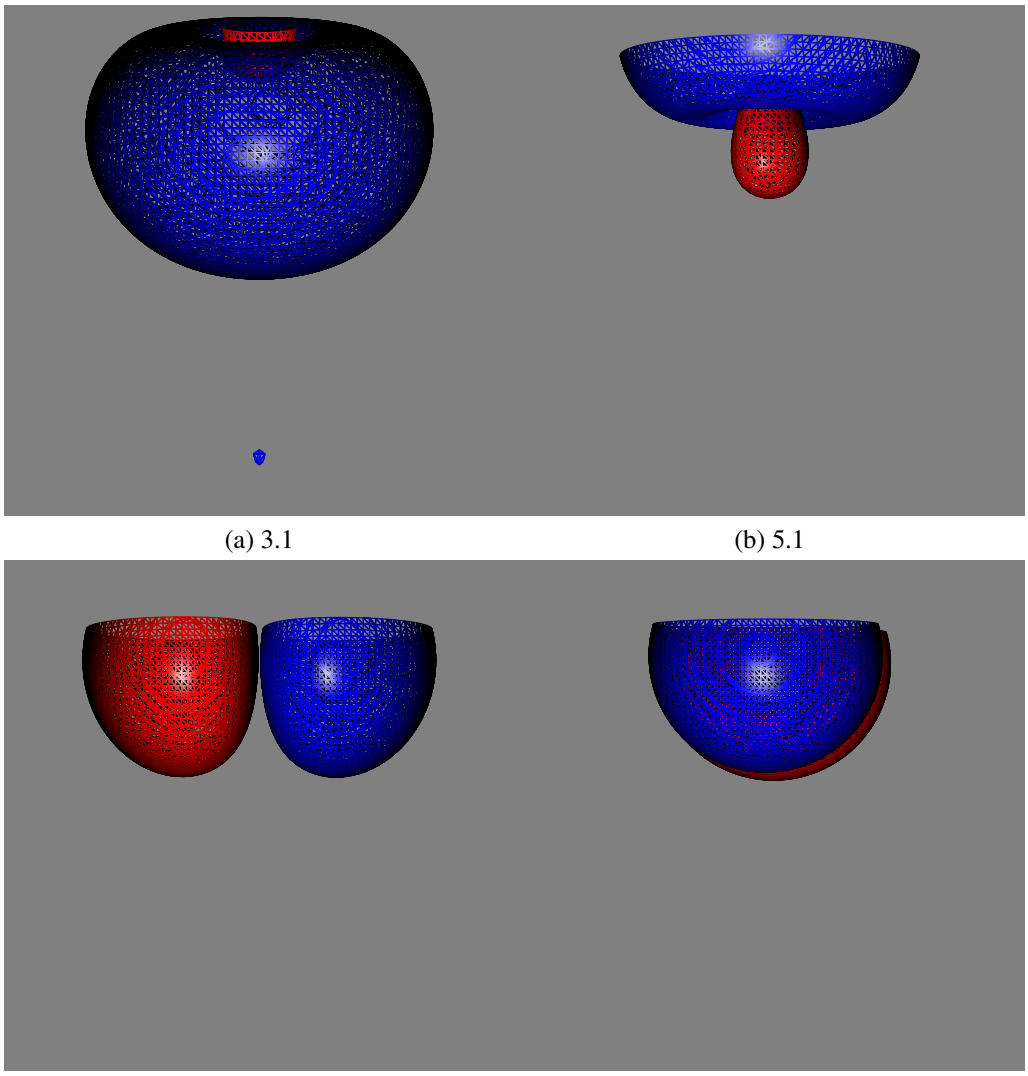

(a) 3.1 (b) 5.1

(c) 1.2 (d) 1.3

Figure 4.1: Localised orbitals for active space A in the S = 1 state of N_2

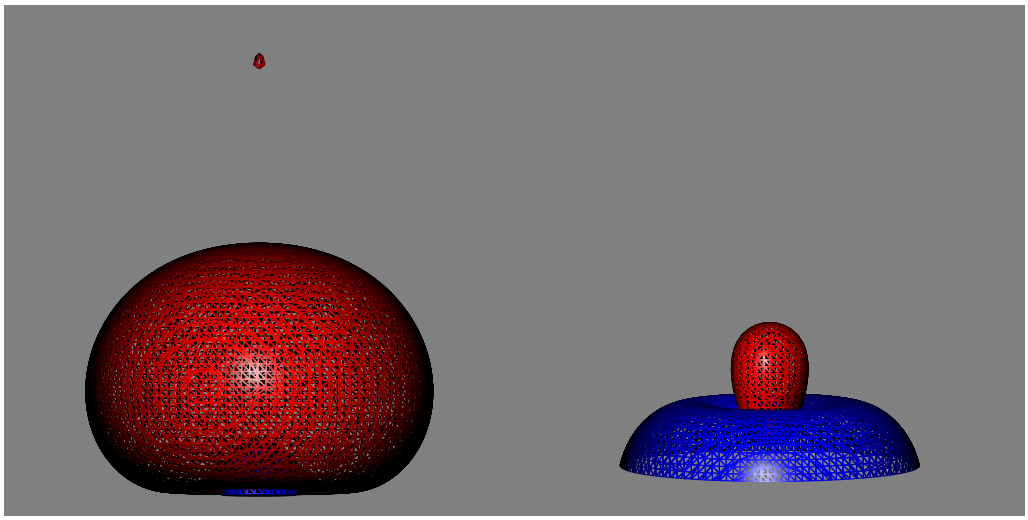

(a) 4.1 (b) 6.1

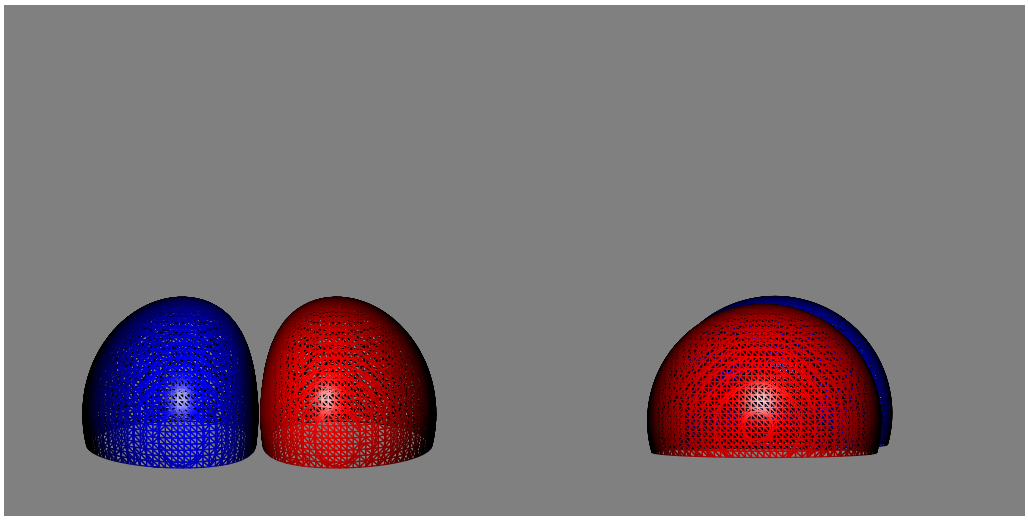

(c) 2.2 (d) 2.3

Figure 4.2: Localised orbitals for active space B in the S = 1 state of N_2

produce the pre-optimised non-local molecular orbitals.

2. The orbitals created in the first stage were localised using the `locali` command.
3. A single state CASSCF calculation was performed using the localised orbitals from the previous step. This required the orbitals to be read from a temporary file using the following commands `start,2140.2,type=local.` This step also used the split active spaces. These active spaces were defined using the following command strings `restrict,5,5,3.1,5.1,1.3,1.2;` and `restrict,5,5,4.1,6.1,2.2,2.3;` which specify two 5 in 4 active spaces one restricted to the selected active orbitals in space A and the other the active orbitals on space B. As before in order promote orbital optimisation in this system the first 15 iterations of the optimisation used uncoupled orbital and CI coefficient optimisation.
4. An ACPF calculation was performed using the optimised non-local orbitals produced in the previous stage. This will be shown as ACPF #.
5. An ACPF calculation was performed using the same restricted orbital spaces as above and the localised orbitals produced in stage two. In order to use the localised orbitals a different orbital input string is required from that detailed for CASSCF. This string has the following format:
   `orbit,2141.2,type=local.`
6. The final orbitals produced were printed to an output file.

4.6 Alternative Active Apace Splitting Schemes

Based on an idea from a post doctoral researcher in the group, Dr. G. Arantes, a set of calculations were devised to explore more complex active space splitting schemes. These calculations used multiple restricted active spaces to ensure certain orbitals were always occupied. This method was tested for various pairs of orbitals to see if locking certain configurations produced more accurate results for the different spin states in the N_2 test system.

As an extension of the split active space method, a test was also devised to see if

a limited mixing of orbitals from both atoms would help to smooth out the anomalies produced without reverting to a fully delocalised active space.

These methods will be detailed in the following sections with full results from the N_2 test system.

4.6.1 Calculations

As the N_2 test system has already been explored in this thesis, the basic set up for the calculations has already been carried out. The orbital sorting has already been done in previous calculations (section 4.4) so the active orbitals are already known. In the set up for these calculations a lot of the steps from previous calculations are still required due to the lack of saved orbitals.

4.6.2 Isolated Orbitals

In the first section of this experiment the restricted orbital method will be used to isolate orbitals of interest into their own active spaces with a set occupation. This method will help to establish whether a single orbital pair has a strong influence on the overall system.

In order to create these isolated orbitals the `restrict` key word is used to create two restricted spaces of one orbital with an electron in. The command takes the form `restrict,1,1,X;` where `X` is the orbital number in Molpro [30] notation. This command is equivalent to creating a one electron in one orbital restricted active space. The two restricted orbitals are selected so as to isolate pairs of orbitals one in each of the original restricted spaces with similar orbital characteristics which are most likely to form a bonding pair. For example the pair of orbitals labelled 5.1 and 6.1 have the same basic shape as seen in figures 4.1 and 4.2. These orbitals combined with spin paired electrons would form a σ or single bond, the same orbitals combined with spin parallel electrons would form an anti-bonding arrangement. The restriction of orbitals reduces their freedom to interact however by restricting linked pairs the combinations most likely to be important are still likely to be represented.

The orbital pairs of interest are 3.1/4.1, 5.1/6.1, 1.2/2.2 and 1.3/2.3. These orbital pairs

all share similar characteristics within the pair, which would suggest they would form a bonding or anti-bonding arrangement when combined with appropriate spin electrons.

In order to restrict the orbitals to fit the new active space scheme a change to the `restrict` directives for each space is required. The new split of the active spaces requires four `restrict` directives. Two containing four electrons and three orbitals (A and B) and two containing one electron and one orbital (C and D). For example the commands for the 3.1/4.1 orbital pair are

```
restrict,4,4,5.1,1.3,1.2; restrict,4,4,6.1,2.2,2.3;
restrict,1,1,3.1; restrict,1,1,4.1;
```

Table 4.1 shows the four orbital combinations used in this set of calculations.

Label	A	B	C	D
3.1/4.1	5.1,1.2,1.3	6.1,2.2,2.3	3.1	4.1
5.1/6.1	3.1,1.2,1.3	4.1,2.2,2.3	5.1	6.1
1.2/2.2	3.1,5.1,1.3	4.1,6.1,2.3	1.2	2.2
1.3/2.3	3.1,5.1,1.2	4.1,5.1,2.2	1.3	2.3

Table 4.1: The restricted spaces A,B,C and D for each investigated orbital pair

These calculations were carried out on a C_{2v} geometry of the N_2 system with each state having an overall a_1 state symmetry.

The Calculations followed the standard calculation scheme as detailed above in section 4.4 using the new modified active spaces.

In order to produce ACPF results for some of these calculations a further addition to the calculation was required. The 3.1/4.1 and 5.1/6.1 calculations would not produce a valid result for the ACPF using the scheme as presented above. This was due to a lack of overlapping CI vectors between the unrestricted CASSCF wave function used as a starting guess and the restricted ACPF wave function. To produce a result, the number of CI states used in constructing the wave function had to be increased using the `option,nstati=X;` where `X` is the number of states included. In most cases five states were needed to get a result, one case 3.1/4.1 S = 3 required six states and three cases failed to optimise. In two of the cases that failed to converge 5.1/6.1 S = 2 and 3.1/4.1 S = 2 as the number of

states increased the wave function failed to diagonalise due to the expansion set becoming singular. In the other case 5.1/6.1 S = 3 the additional CI states failed to converge resulting in no convergence of the overall wave function.

4.6.3 Cross Atom Active Spaces

In this section an exploration into whether allowing selected orbitals from both atoms to mix will help to smooth inconsistencies in the spin ladders as seen in the restricted active space experiments. In this experiment pairs of related orbitals one from each atom will be moved from their current active space to a new restricted active space in which the orbitals are free to interact with each other and up to two electrons. In order to create the the new cross atom restricted active space the `restrict` key word is used to create a new restricted space of two orbitals with between zero and two electrons in. The command takes the form `restrict,0,2,X,Y;` where `X` and `Y` are orbital numbers in Molpro [30] notation.

The orbital pairs of interest are 3.1/4.1, 5.1/6.1, 1.2/2.2 and 1.3/2.3. These orbital pairs all share similar characteristics within the pair, which would suggest they would form a bonding or anti-bonding arrangement when combined with appropriate spin electrons.

As the N_2 test system has already been explored in this thesis the initial set up for the calculations has been carried out in previous calculations. The orbital sorting has already been done in previous calculations (section 4.4) so the active orbitals are already known. In the set up for these calculations a lot of the steps from previous calculations are still required due to the lack of saved orbitals.

The calculation detailed below was carried out for each orbital pairing at each spin state in order to construct the spin ladders required for evaluation.

In order to restrict the orbitals to fit the new active space scheme a change to the `restrict` directives for each space is required. The new split of the active spaces requires three `restrict` directives. Two containing between four and five electrons and three orbitals (A and B) and one containing between zero and two electron and two orbitals (C). For example the commands for the 3.1/4.1 orbital pair are

`restrict,4,5,5.1,1.3,1.2; restrict,4,5,6.1,2.2,2.3; restrict,0,2,3.1,4.1;`

Table 4.2 shows the four orbital combinations used in this set of calculations.

Label	A	B	C
3.1/4.1	5.1,1.2,1.3	6.1,2.2,2.3	3.1,4.1
5.1/6.1	3.1,1.2,1.3	4.1,2.2,2.3	5.1,6.1
1.2/2.2	3.1,5.1,1.3	4.1,6.1,2.3	1.2,2.2
1.3/2.3	3.1,5.1,1.2	4.1,6.1,2.3	1.3,2.3

Table 4.2: The restricted spaces A,B and C for each investigated orbital pair

These calculations were carried out on a C_{2v} geometry of the N_2 system with each state having an overall a_1 state symmetry.

The Calculations followed the standard calculation scheme as detailed above in section 4.4 using the new modified active spaces.

In order to produce ACPF results for some of these calculations a further addition to the calculation was required. The 3.1/4.1 and 5.1/6.1 calculations would not produce a valid result for the ACPF using the scheme as presented above.This was due to a lack of overlapping CI vectors between the unrestricted CASSCF wave function used as a starting guess and the restricted ACPF wave function. To produce a result the number of CI states used in constructing the wave function had to be increased using the `option,nstati=X;` where `X` is the number of states included. In all cases five states were needed to get a result, save for the 5.1/6.1 $S = 3$ state where the additional CI states failed to converge resulting in no convergence of the overall wave function.

4.7 Results

In this section the results of the calculations listed in the methodology section are presented. All results are rounded to six decimal places for ease of representation where necessary.

4.7.1 Raw data

The raw calculated data which is used in construction of the graphs and tables shown in the analysis section is listed here. Where no usable date was produced n/a will be substituted. The results calculated using non-local orbitals are represented by (nl). The split ACPF# data was calculated using the data from a split CASSCF as detailed in additional calculations. Data marked with a * required CI state extension using `option,nstati=X;`.

S	0	1	2	3
Regular CASSCF (nl)	-108.799958	-108.797154	-108.791382	-108.782059
Regular CASSCF	-108.799958	-108.797154	-108.791382	-108.782059
Split CASSCF	-108.776023	-108.776815	-108.778595	-108.782059
Regular ACPF (nl)	-108.996492	-108.993625	-108.987539	-108.976788
Regular ACPF	-108.996492	-108.993625	-108.987539	-108.976788
Split ACPF	-108.993733	-108.990718	-108.984954	-108.976570
ACPF# (nl)	-108.996045	-108.993197	-108.987205	-108.976788

Table 4.3: Regular and split active space calculations on N_2 state energies (E_h)

S	0	1	2	3
CASSCF 3.1/4.1	-108.775862	-108.776655	-108.778428	-108.781843
CASSCF 5.1/6.1	-108.775862	-108.776655	-108.778428	-108.781843
CASSCF 1.2/2.2	-108.775970	-108.776764	-108.778544	-108.782009
CASSCF 1.3/2.3	-108.775970	-108.776764	-108.778544	-108.782009
ACPF 3.1/4.1	-108.946518*	-108.942925*	n/a	-108.924362*
ACPF 5.1/6.1	-108.943893*	-108.941246*	n/a	n/a
ACPF 1.2/2.2	-108.993448	-108.990477	-108.984817	-108.976564
ACPF 1.3/2.3	-108.993448	-108.990477	-108.984817	-108.976564

Table 4.4: State energies (E_h) for CASSCF and ACPF calculations using isolated orbitals

S	0	1	2	3
CASSCF 3.1/4.1	-108.795575	-108.793603	-108.789309	-108.781843
CASSCF 5.1/6.1	-108.795575	-108.793603	-108.789309	-108.781843
CASSCF 1.2/2.2	-108.777445	-108.778006	-108.779309	-108.782009
CASSCF 1.3/2.3	-108.777445	-108.778006	-108.779309	-108.782009
ACPF 3.1/4.1	-108.948273*	-108.944624*	-108.936965*	-108.924362*
ACPF 5.1/6.1	-108.944536*	-108.941780*	-108.936046*	n/a
ACPF 1.2/2.2	-108.993658	-108.990613	-108.984855	-108.976564
ACPF 1.3/2.3	-108.993658	-108.990613	-108.984855	-108.976564

Table 4.5: State energies (E_h) for CASSCF and ACPF calculations using cross atom restricted active spaces

4.7.2 Baseline

In order to analyse the data produced in the main experiments a baseline data set was needed. This data set is presented in table 4.3 by the rows labelled regular CASSCF (nl) and Regular ACPF (nl). This data can then be used to produce a graph from which the *J* value can be calculated. This process is shown in table 4.6 and figure 4.3. The *J* value can be obtained from the graph as half the negative of the calculated gradients produced using a linear regression from the best fit line produced by the Gnuplot program.

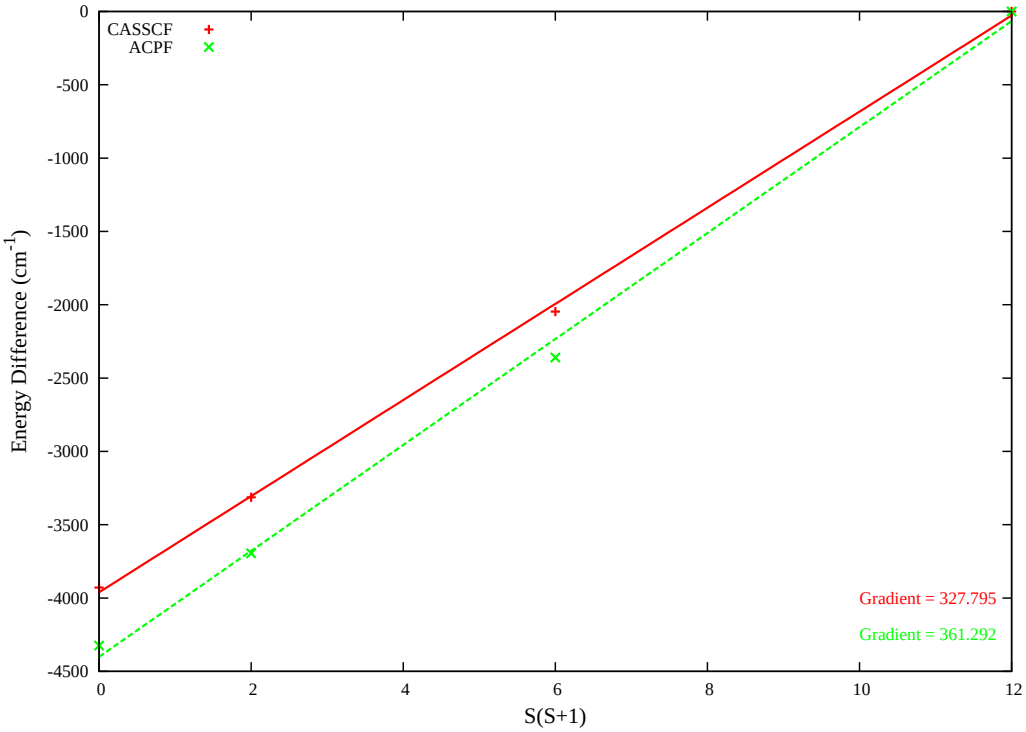

Figure 4.3: Baseline energies of N_2 as a function of $S(S+1)$

4.7.3 Orbital Type

In this process localised orbitals are required as against the delocalised orbitals used in the baseline calculations outlined above. Calculations have been produced using both localised and the usual delocalised orbitals. The data from these calculations are shown with a direct energy comparison. All energies shown are in E_h except where noted and rounded to nine decimal places. The two tables 4.7 and 4.8 show how a change in the orbital type affects the energies of the states in the spin ladder.

S	0	1	2	3
Regular CASSCF (nl)	-3928.386730	-3313.046609	-2046.309607	0.000000
Regular ACPF (nl)	-4324.531673	-3695.132993	-2359.542982	0.000000

Table 4.6: Baseline N_2 state energies (cm^{-1}) relative to the $S = 3$ state.

A comparison of table 3.8 from the previous chapter with tables 4.7 and 4.8 shows that the value of the energy change related to a move from delocalised orbitals to local orbitals is, approximately two orders of magnitude smaller in N_2 than in Cr_2. This large difference in the absolute energy difference although significant, is not so large when looked at as a percentage of the total energy of the system. In the Cr_2 calculations the energy difference was generally in the hundreds of thousandths of a percent range where as in the N_2 calculations they fall mostly in the high millionths of a percent, which equates to less than an order of magnitude.

Within the results from the N_2 calculations there are some interesting anomalies. In table 4.7 both the $S = 2$ and $S = 3$ show variation from the other two values with the state $S = 2$ showing a lower energy result for the local orbital value and the $S = 3$ showing an energy change approximately five times that of the other values. The lowering in the energy of the $S = 2$ state may be due to a favourable combination of orbitals produced in the localisation process, this is unusual but possible. The increase in energy in the $S = 3$ state is probably due to the an unfavourable combination of unpaired spins in the three *p*-orbitals on each centre.

In table 4.7 only the $S = 3$ state is unusual in that it shows a reduced energy as a result of localisation. This is probably due to a similar favourable interaction in orbitals as the $S = 2$ state in the CASSCF calculations.

Overall these changes in energy due to localisation are small compared to the overall energy of the states and should not excessively affect any trends revealed.

4.7.4 Split Active Spaces

The final stage in this experiment was to look at the how splitting the active space so that a separate space was used for each centre would affect the energy states in the N_2 dimer.

These results should hold the key to whether this technique can be successful in the current incarnation since the Cr_2 result were inconclusive. The result of the experiments are shown below with comments where appropriate.

S	0	1	2	3
Delocalised Orbitals	-108.799957743	-108.797154047	-108.791382368	-108.782058696
Local Orbitals	-108.799957747	-108.797154051	-108.791382368	-108.782058717
ΔE (cm^{-1})	0.000978637	0.000817981	-0.000074623	0.004695441

Table 4.7: Comparison CASSCF state energies for N_2 using delocalised and localised orbitals

S	0	1	2	3
Delocalised Orbitals	-108.996492392	-108.993624641	-108.987539245	-108.976788376
Local Orbitals	-108.996492400	-108.993624646	-108.987539255	-108.976788369
ΔE (cm^{-1})	0.001804081	0.001185820	0.002232496	-0.001631795

Table 4.8: Comparison ACPF state energies for N_2 using delocalised and localised orbitals

Table 4.9 shows the energies for the tested states of N_2 at 4.5 a_0 as energies relative to the $S = 3$ state. All values have been converted to wave numbers (cm^{-1}) to match previous results. The conversion factor used was $1\,E_h$ is equivalent to $219474.63068\,cm^{-1}$.

The data from Table 4.9 was then plotted against $S(S+1)$ see figure 4.4. The value of J the exchange coupling for each method can be read from the graph in figure 4.4 as half the negative of the gradients of the best fit lines as shown in the bottom right of the graph. The values of J are calculated using the best fit linear regression tool in Gnuplot. The final J values calculated at each stage are presented in table 4.10.

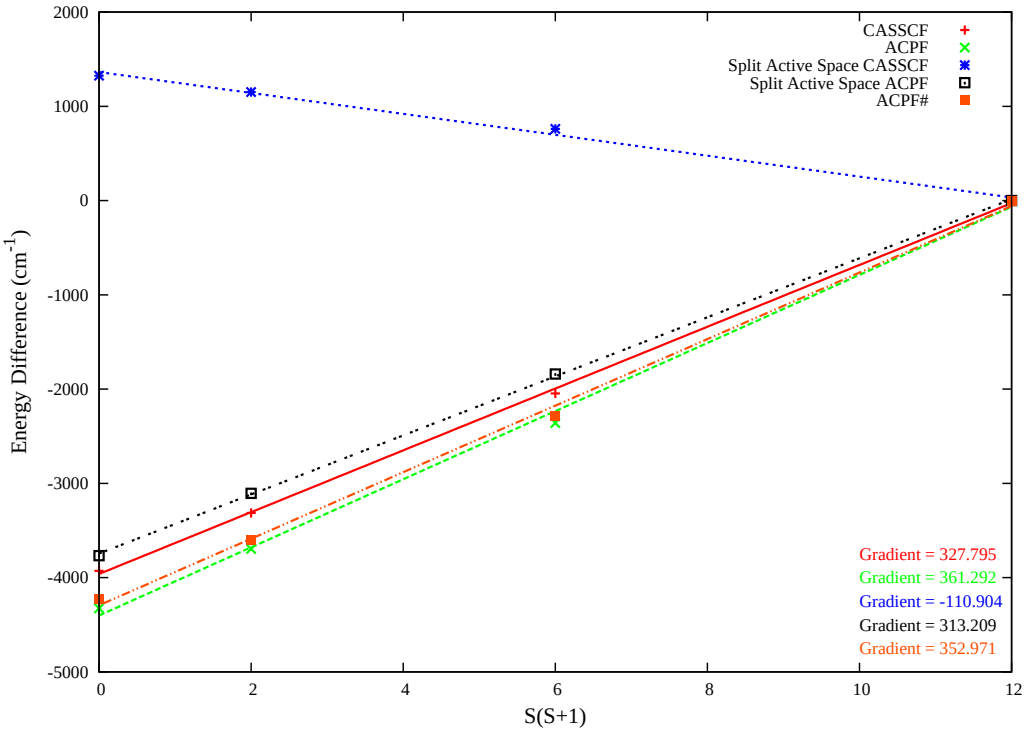

Figure 4.4: Energy of N_2 as a function of $S(S+1)$ using both split and regular active spaces

4.7.5 Isolated Orbitals

In these experiments an orbital was removed from the main restricted active space on each atom and isolated in its own restricted space with an electron forming four restricted active spaces as listed in table 4.1. These experiments were to investigate if a single pair of orbitals were causing the inconsistent results seen in chapter 3. A plot of relative energy versus $S(S+1)$ is used to investigate the relation between the calculated spin states. These

S	0	1	2	3
Regular CASSCF	-3928.383013	-3313.042731	-2046.304837	0.000000
Split CASSCF	1324.751587	1150.768154	760.128875	0.000000
Regular ACPF	-4324.535109	-3695.135810	-2359.546846	0.000000
Split ACPF	-3766.892784	-3105.050007	-1840.067820	0.000000
Split ACPF# (nl)	-4226.407751	-3601.221719	-2286.120137	0.000000

Table 4.9: Regular and split active space N_2 state energies (cm^{-1}) relative to the $S = 3$ state.

Method	Calculated J (cm^{-1})
Regular CASSCF (nl)	-163.898
Regular CASSCF	-163.898
Split CASSCF	55.452
Regular ACPF (nl)	-180.646
Regular ACPF	-180.646
Split ACPF	-156.605
ACPF# (nl)	-176.486

Table 4.10: J values for N_2 using Molpro ACPF and CASSCF

plots along with the raw data presented above will show if these new restricted spaces produce a more accurate representation of the spin ladder than the previous methods. In order to produce the plots the raw data must be converted to relative energies.

Table 4.11 shows the energies for the tested states of N_2 at 4.5 a_0 as energies relative to the $S = 3$ state except where results were unavailable in which case the highest available state was used. All values have been converted to wave numbers (cm^{-1}) to match previous results. The conversion factor used was $1E_h = 219474.63068 cm^{-1}$. Where data is unavailable the result is marked n/a.

The data from Table 4.11 was then plotted against $S(S+1)$ see figures 4.5 and 4.6. The value of the Heisenberg exchange coupling constant (J) for each method can be read from the graphs in figures 4.5 and 4.6 as half the negative of the gradients of the best fit lines as shown in the bottom right of the graph. The values of J are calculated using the best fit linear regression tool in Gnuplot.

S	0	1	2	3
CASSCF 3.1/4.1	1312.579703	1138.718949	749.585034	0.000000
CASSCF 5.1/6.1	1312.579703	1138.718949	749.585034	0.000000
CASSCF 1.2/2.2	1325.306354	1151.167103	760.291411	0.000000
CASSCF 1.3/2.3	1325.306354	1151.167103	760.291411	0.000000
ACPF 3.1/4.1	-4862.645462	-4074.034181	n/a	0.000000
ACPF 5.1/6.1	-580.974165	0.000000	n/a	n/a
ACPF 1.2/2.2	-3705.637229	-3053.676821	-1811.307798	0.000000
ACPF 1.3/2.3	-3705.634244	-3053.674143	-1811.307801	0.000000

Table 4.11: ACPF and CASSCF N_2 state energies (cm^{-1}) relative to the S = 3 state for isolated orbital calculations.

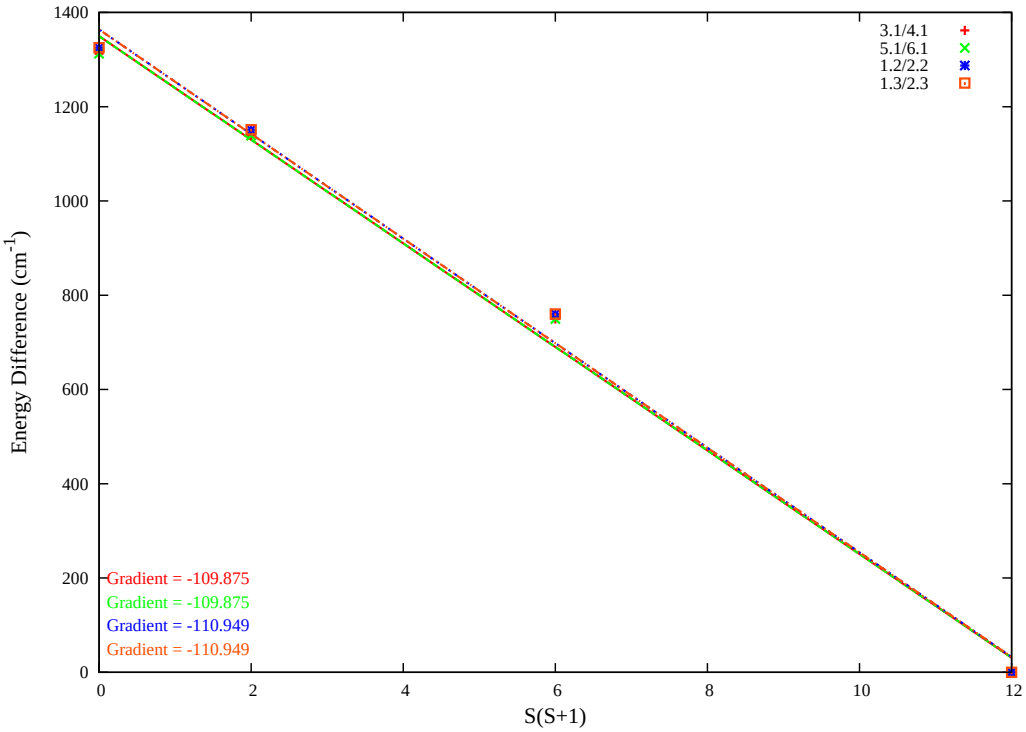

Figure 4.5: Plot of CASSCF energies of N_2 as a function of $S(S+1)$ using the isolated orbital method

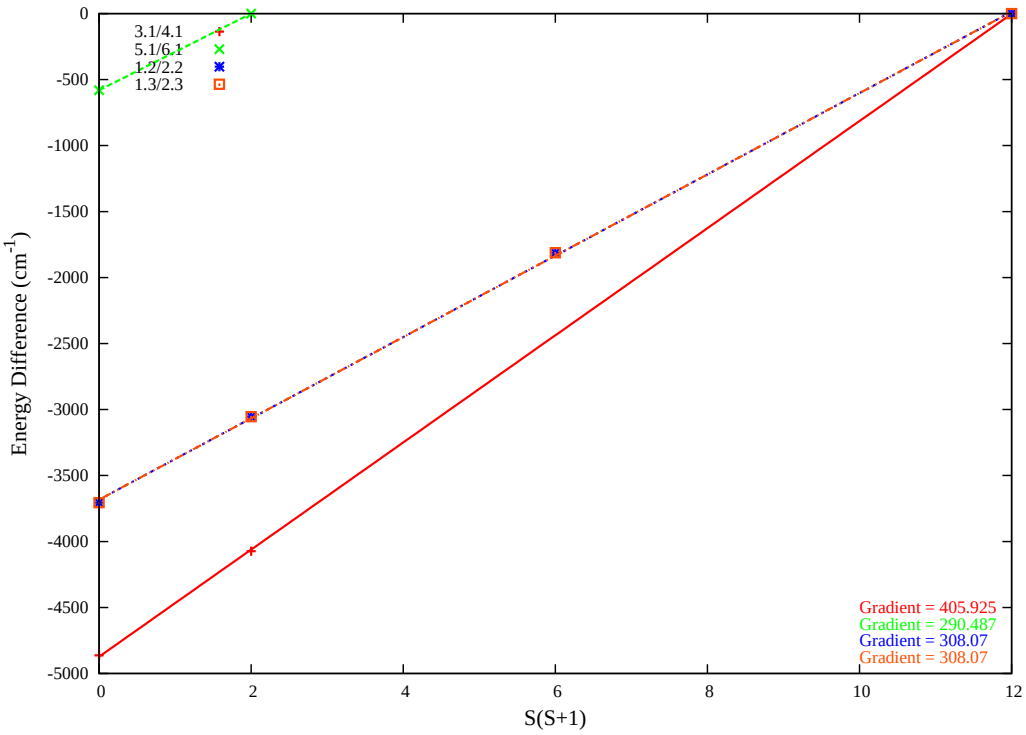

Figure 4.6: Plot of ACPF energies of N_2 as a function of $S(S+1)$ using the isolated orbital method

The final J values calculated at each stage are presented in table 4.12.

Method	Calculated J (cm^{-1})
Baseline CASSCF (l)	163.898
CASSCF 3.1/4.1	-54.938
CASSCF 5.1/6.1	-54.938
CASSCF 1.2/2.2	-55.475
CASSCF 1.3/2.3	-54.475
Baseline CASSCF (l)	180.664
ACPF 3.1/4.1	202.963
ACPF 5.1/6.1	145.244
ACPF 1.2/2.2	154.035
ACPF 1.3/2.3	154.035

Table 4.12: J values for N_2 using the isolated orbital method

As can been seen from the graph in figure 4.5 the isolation of the pairs of atoms in the CASSCF calculations has not produced any significant change to the overall distribution of points on the graph. The $S = 2$ point is still deviated from the best fit line and due to a high value for the $S = 3$ state the line still has a negative gradient where a positive gradient is expected. From the graph and the raw data it is obvious that the data set has split into two distinct groupings. One group contains the two experiments in which a_1 symmetry orbitals have been isolated and the other group here the b_1 or b_2 orbitals have been isolated. This can be explained by looking at the form of these orbitals and their eigenvalues which relates to the energy of the orbital. The forms of the local orbitals for this system can be seen in figures 4.1 and 4.2. The eigenvalues for the orbitals of the $S = 1$ state of N_2 are shown in table 4.13 below.

The two groups detailed above are split based on the type of bond the orbitals will form when combined and on orbital energy represented by the orbital eigenvalue. The 3.1/4.1 and 5.1/6.1 group contains a_1 symmetry orbitals which combine together to form two σ type bonds. The other group contains the b_1 and b_2 symmetry orbitals which combine to form a pair of π type bonds. From the eigenvalues in table 4.13 the b_1 and b_2 orbitals have the same eigenvalue and are therefore interchangeable, meaning that any configuration of

Orbital Number	eigenvalue
3.1	-0.5663
4.1	-0.5663
5.1	-0.5612
6.1	-0.5612
1.2	-0.1825
2.2	-0.1825
1.3	-0.1825
2.3	-0.1825

Table 4.13: Eigenvalues of the local orbitals in the S = 1 state of N_2

of these four orbitals will produce the same results. In the group containing the a_1 orbitals the 3.1/4.1 set and the 5.1/6.1 set have different eigenvalues, however this is not a problem as the eigenvalues are both lower than those of the b_1 and b_2 orbitals. This means that the a_1 orbitals will be occupied more often in the low energy configurations. This favourable occupation means that both sets of a_1 symmetry orbitals will be fully occupied in most configurations. Therefore isolating them as occupied does not affect their natural tendency to be occupied and thus the energy is the same no matter which a_1 pair is isolated.

This experiment has not greatly improved on the results of the split active space calculation in regards to a CASSCF treatment as this manipulation of the active space has not caused a large change in the the value of the S = 3 state relative to the other spin states.

Figure 4.6 shows a wider variation in the the gradient related to isolating pairs of orbitals in the ACPF calculations. Isolation of the 1.2/2.2 and 1.3/2.3 pairs which relate to the b_1 and b_2 symmetry orbitals has only a small change to the gradient compared to the basic split active space treatment. This change in gradient moves the *J* value further from the baseline value of -180.646 cm^{-1} for a system using local orbitals. The data of interest relates to the isolation of the 3.1/4.1 and 5.1/6.1 pairs, the isolation of these pairs has a significant effect on the value of *J*. The isolation of the 3.1/4.1 pair significantly increases the value of *J* bringing it above the baseline value but still closer than the basic split active space method. The isolation of the 5.1/6.1 pair significantly decreases the value of *J* compared to the baseline producing a worse result than the the standard split

active space method. The 5.1/6.1 results are of little diagnostic use however due to a lack of results for the $S = 2$ and $S = 3$ states. Although a result for the $S = 2$ state is missing in the 3.1/4.1 experiment, this data still provides some interesting results.

Table 4.14 shows a comparison of the raw results of the 3.1/4.1 isolated orbital ACPF calculations compared to the basic split active space results. All energies are in E_h unless stated and given to six decimal places. The first thing to note in this comparison is that the isolated orbital results are significantly higher in energy than the equivalent split active space results. This energy difference is similar in the 5.1/6.1 results but the 1.2/2.2 and 1.3/2.3 show very similar energies to those of the standard split active space results. This suggests that either the isolated orbitals or the additional CI states required to produce results in these calculations have a massive effect on the energy. The most likely culprit is the additional CI states as the results from CASSCF calculations shown using this method did not show these extreme energy changes. Also of note in this data is the significantly larger increase in energy seen in the $S = 3$ state, this increase to some extent is the reason for the decrease in the *J* value as the other values increased in proportion with each other.

Overall this experiment does not provide any valuable information compared to the other experiments presented before. The isolation of these orbitals does not greatly improve the results in either the CASSCF calculation of the ACPF calculations and in fact adversely affects convergence in some of the ACPF calculations.

4.7.6 Cross Atom Active Spaces

In these experiments selected orbitals from the split active spaces centred on each atom are moved to a third active space which contains orbitals from both atoms. This system is designed to see if using smaller basis sets a total delocalising of the active space can be avoided.

The experiment looks at four related orbital pairs split in to the third space as detailed in section 4.6.3. A plot of relative energy versus $S(S+1)$ is used to investigate the relationship between the calculated spin states. These plots along with the raw data presented

S	0	1	2	3
ACPF split	-108.993733	-108.990718	-108.984954	-108.976570
ACPF 3.1/4.1	-108.946518	-108.942925	n/a	-108.924362
ΔE (cm^{-1})	-10362.463001	-10489.231505	n/a	-11458.215679

Table 4.14: Comparison of baseline split ACPF and 3.1/4.1 orbital isolated ACPF energies

above will show if these new restricted spaces produce a more accurate representation of the spin ladder than the previous methods. In order to produce the plots the raw data must be converted to relative energies.

Table 4.16 shows the energies for the tested states of N_2 at 4.5 a_0 as energies relative to the $S = 3$ state except where results were unavailable in which case the highest available state was used. All values have been converted to wave numbers (cm^{-1}) to match previous results. The conversion factor used was $1E_h = 219474.63068 cm^{-1}$. Where data is unavailable the result is marked n/a.

The data from table 4.16 was then plotted against $S(S+1)$ see figures 4.7 and 4.8. The value of J the exchange coupling for each method can be read from the graphs in figures 4.7 and 4.8 as half the negative of the gradients of the best fit lines as shown in the bottom right of the graph. The values of J are calculated using the best fit linear regression tool in Gnuplot. The final J values calculated at each stage are presented in table 4.15.

Method	Calculated J (cm^{-1})
CASSCF 3.1/4.1	-126.035
CASSCF 5.1/6.1	-126.035
CASSCF 1.2/2.2	41.972
CASSCF 1.3/2.3	41.972
ACPF 3.1/4.1	-219.131
ACPF 5.1/6.1	-155.574
ACPF -1.2/2.2	155.889
ACPF 1.3/2.3	-155.889

Table 4.15: J values for N_2 using a cross atom active space

As with the isolated orbital experiments in the last section the CASSCF results show two distinct groups forming. The first group consists of the a_1 symmetry orbital experiments 3.1/4.1 and 5.1/6.1, the second consists of the b_1 and b_2 symmetry orbital experiments 1.2/2.2 and 1.3/1.4. The b_1 and b_2 orbital symmetry group shows a similar trend to the groups from the isolated orbital experiments and the basic split active space calculations. This plot has a negative gradient resulting form the energies of states decreasing as

S	0	1	2	3
CASSCF 3.1/4.1	-3013.864276	-2581.041476	-1638.617437	0.000000
CASSCF 5.1/6.1	-3013.864222	-2581.041443	-1638.616770	0.000000
CASSCF 1.2/2.2	1001.652541	878.466326	592.445508	0.000000
CASSCF 1.3/2.3	1001.652541	878.466326	592.445508	0.000000
ACPF 3.1/4.1	-5247.821579	-4446.990390	-2765.940103	0.000000
ACPF 5.1/6.1	-1863.412226	-1258.460888	0.000000	n/a
ACPF 1.2/2.2	-3751.776263	-3083.386827	-1819.795954	0.000000
ACPF 1.3/2.3	-3751.774764	-3083.386448	-1819.795767	0.000000

Table 4.16: ACPF and CASSCF N_2 state energies (cm^{-1}) relative to the S = 3 state using a cross atom active space

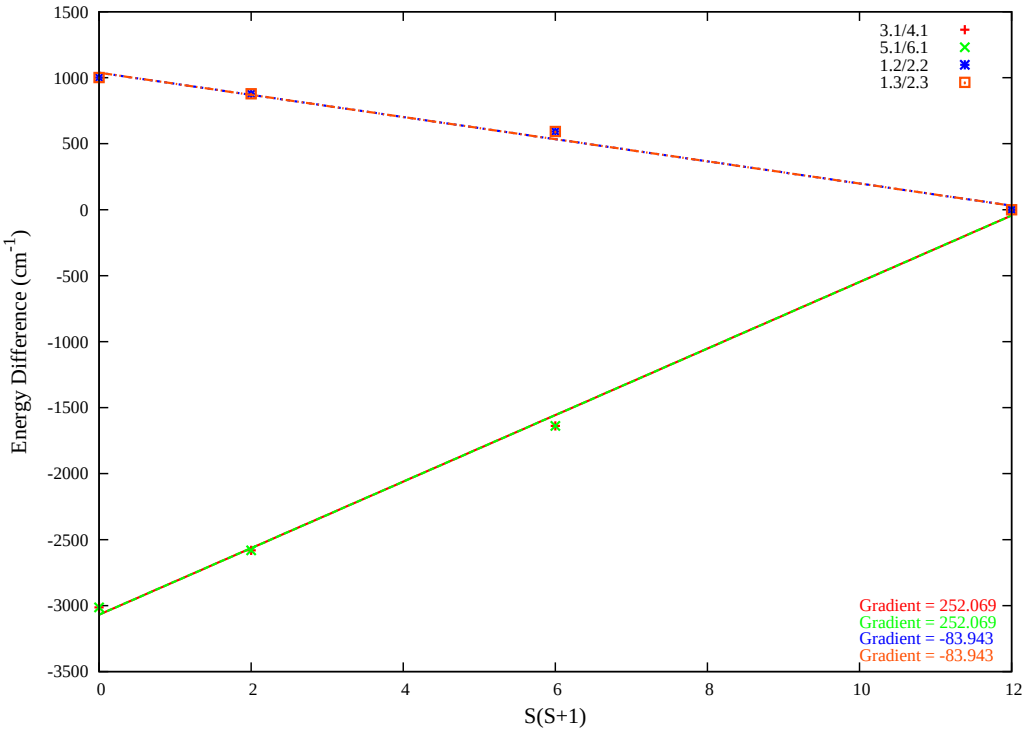

Figure 4.7: Plot of CASSCF energies of N_2 as a function of $S(S+1)$ using a cross atom active space

the spin state increases. This negative gradient is less extreme than those in the isolated orbital case due to a slightly higher $S = 3$ relative to the other states in the experiment.

Table 4.17 shows a comparison between the standard split active space state energies and the 1.2/2.2 cross atom active space states, the values shown are also valid for the 1.3/2.3 space. All energies are in E_h unless stated and given to six decimal places. As can be seen, the 1.2/2.2 states have a lower energy for all states except the $S = 3$ state where 1.2/2.2 energy is higher. This lowering of the energy is most likely due to the increased freedom provided by the less strict active space restrictions imposed in this experiment. The increase in energy in the $S = 3$ state may be due to a conflict between different states in the different active spaces, as the $S = 3$ requires all active orbitals to be occupied spin parallel.

The experiments using the a_1 symmetry orbitals show a better trend showing a positive gradient for the first time in these experiments using the CASSCF method. The gradient is not close to the baseline value using local orbitals. The gradient is however the best of any of the other tests so far.

Table 4.18 shows a comparison between the standard split active space state energies

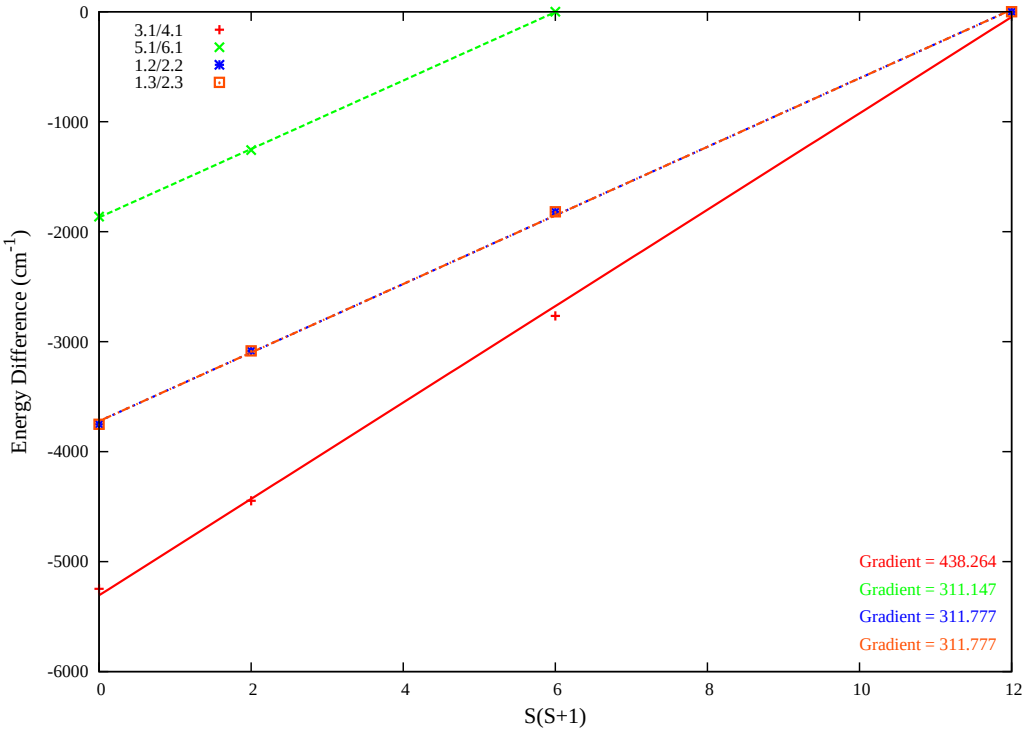

Figure 4.8: Plot of ACPF energies of N_2 as a function of $S(S+1)$ using a cross atom active space

and the 3.1/4.1 cross atom active space states, these values are also valid for the 5.1/6.1 space to six decimal places, there is slight variations between the two data sets but these are most likely computational noise. All energies are in E_h unless stated and given to six decimal places.

The ACPF calculations from this set of experiments show a cluster of J values with the b_1, b_2 and one of the a_1 symmetry calculations producing gradients just over -155 cm^{-1}. This gradient is close to the unmodified split active space results at -156.605 cm^{-1} but further from the baseline value using local orbitals at -180.646 cm^{-1}. The other a_1 symmetry results relating to the 3.1/4.1 cross atom active space shows a higher gradient which although higher than the baseline result, is slightly closer than either the basic split active space or the other cross atom active space experiments.

For both the a_1 symmetry orbital calculations a comparison of the energies between the basic split active space and the cross atom active space calculations show a significantly higher energy in the cross atom active space calculations. The values of these energy differences are similar to those seen in the ACPF calculations using isolated orbitals as shown in tables 4.19 and 4.20. All energies are in E_h unless stated and given to

six decimal places.

Overall the experiments using a cross atom active space show that allowing the a_1 symmetry orbitals to interact in their own cross atom active space provides improved gradients helping in the calculation of J, whilst at the same time giving a large increase in the energies of the states. Putting the b_1 or b_2 symmetry orbitals in a cross atom active space, results in little or no overall change in either the J value or the energy of the states.

S	0	1	2	3
CASSCF split	-108.776023	-108.776815	-108.778595	-108.782059
CASSCF 1.2/2.2	-108.777445	-108.778006	-108.779309	-108.782009
ΔE (cm^{-1})	312.100632	261.303414	156.684952	-10.998414

Table 4.17: Comparison of baseline split CASSCF and 1.2/2.2 orbital cross atom active space energies

S	0	1	2	3
CASSCF split	-108.776023	-108.776815	-108.778595	-108.782059
CASSCF 3.1/4.1	-108.795575	-108.793603	-108.789309	-108.781843
ΔE (cm^{-1})	4291.264128	3684.457894	2351.394576	-47.351736

Table 4.18: Comparison of baseline split CASSCF and 3.1/4.1 orbital cross atom active space energies

S	0	1	2	3
ACPF split	-108.996045	-108.993197	-108.987205	-108.976788
ACPF 3.1/4.1	-108.948273	-108.944624	-108.936965	-108.924362
ΔE (cm^{-1})	-10484.713314	-10660.358472	-11026.307176	-11506.127143

Table 4.19: Comparison of baseline split ACPF and 3.1/4.1 orbital cross atom active space energies

S	0	1	2	3
ACPF split	-108.996045	-108.993197	-108.987205	-108.976788
ACPF 5.1/6.1	-108.944536	-108.941780	-108.936046	n/a
ΔE (cm^{-1})	-11304.878656	-11284.643962	-11228.003268	n/a

Table 4.20: Comparison of baseline split ACPF and 5.1/6.1 orbital cross atom active space energies

4.8 Conclusions

Taking the values of the regular non-localised results from tables 4.3 and 4.10 as the baseline values for this experiment, the results from the split configuration systems show varying levels of correlation.

The actual energies of the states show a large deviation between the baseline values and the split active space values, this deviation is consistent over the states $S = 0$ to $S = 2$ however this trend breaks down at the $S = 3$ state. This is particularly noticeable at the CASSCF level where the energy for the $S = 3$ state is the same to six decimal places in all three data sets, whilst in the split active space calculations for the states $S = 0$ to $S = 2$ the energies increase considerably. This disparity results in a positive value for J in this experiment. At the ACPF level the variation in the $S = 3$ states are less pronounced producing results much closer to those expected. In fact the split active space value of J from the ACPF calculations whilst approximately twenty eight cm^{-1} higher than the baseline value is a lot closer than the same results in the Cr_2 system. The ACPF# values are very close to those calculated using a regular non-local CASSCF starting wave function and whilst these results are interesting, the fact that the wave function is un-partitioned when this process is carried out means that no time saving is included due to smaller active spaces. The ACPF calculation is at least as time consuming as the CASSCF calculations, therefore this lack of partitioning cancels out any advantage gained in the previous steps compared to a partitioned ACPF.

From these results the method has not worked with regard to the CASSCF method, but results are more promising when a split active space ACPF calculation is carried out on a localised CASSCF wave function. This method seems to produce a valid if higher energy wave function in ACPF calculations for most states. The method actually produced a very close match to the highest spin state wave function in N_2 and was closer in Cr_2 for the highest spin state than any other state

The experiments in the second part of this chapter deal with using extra segregation of orbitals into multiple active spaces in order to treat some of the problems experienced in simple split active space calculations.

The first method used two additional active spaces to isolate and selectively occupy orbitals of interest in order to see whether unfavourable interactions from these orbitals affected the overall wave function. These experiments showed very little change in the problems presented previously with failed results and increased complexity introduced due to incomplete CI spaces in the ACPF calculations. The increased number of CI states required in the optimisations almost certainly contributed to the large increases in energy seen in the calculations requiring this correction.

The second method used an additional active space in which two orbitals, one from each atom were allowed to interact. This set up was designed to see if a small amount of cross atom interaction would produce better results than a fully separated calculation. To some extent this experiment worked using the a_1 symmetry orbitals as the orbitals in the additional active space. The results produced in this experiment were more consistent with the baseline results achieved for the J values. This improvement in J came at the price of increased energies in the individual states. Overall this experiment produced a better trend in the relation of the spin states to each other but with a major sacrifice to the accuracy of the individual state energies.

Over these two chapters, an investigation was carried out in order to see if a method could be developed to allow a large complex multiconfigurational calculation to be successfully modified in order to decrease the time required to carry out the large active space calculations. This may also provide a method to move to much larger systems than are realistically feasible using the current computing power. The method suggested was to split the large active space in to a number of smaller active spaces localised on individual atoms. The experiments presented prove that a large amount of information is lost when the orbitals on different atoms are isolated from each other in the methods described. Even when some cross atom interaction is allowed the data still shows a significant error compared to a fully delocalised result.

The best results from the data shown in these chapters required a small single cross atom interaction and still resulted in significant rises in energy in the states involved. An increase in the size of the cross atom active space may improve this situation. The problem

with the cross atom active space approach is how to choose which orbitals to include in the cross atom space. This problem is relatively easy to solve via a trial and error system in the small diatomic systems tested here but will be increasingly difficult as more atoms and different atom types are included. As the number of atoms increases, so the number of interactions increase meaning that more cross atom spaces are required, also with more atoms the number of atoms in each cross atom space becomes important.

Are interactions between nearest neighbours enough or are longer range effects important? Can an orbital only be included in one space when it may interact with orbitals on more than one atom? What happens with delocalised orbitals ? None of these questions can be answered from the data provided and this makes a systematic approach to this method very difficult for larger systems.

The methods shown do not provide a good solution, as although calculation time for individual calculations may be reduced, the amount of extra calculations required to produce localised orbitals, sort those orbitals and create a split active space by hand significantly increases the time required to produce a result. With the added requirements to find a suitable cross atom active space and balance the CI states in an ACPF calculation, these calculations require a significant investment of time and interaction with the data at several stages which makes this approach unsuitable for mass adoption and automation.

Chapter 5

M(III)β-Diketoiminate Complexes (M= Fe, Co and Ni)

5.1 Introduction

This thesis focuses on the investigation of new ways to improve the methods used in the investigation of transition metals and their complexes.

The new OPTX exchange functional [37] is designed as a new variation of "pure" functional, a pure functional being a functional in which the exchange is not dependent on a part of the Hartree-Fock exchange. This new OPTX functional [37] has been combined with traditional correlation functionals including LYP [13] and PBE [38, 39] to create a new set of functionals such as OLYP [37] and OPBE [37]. These functionals have been successfully used in work by Ghosh and Condradie [40] to produce interesting result on the energy levels of a set of transition metal complexes. This chapter looks at these results and compares them to results produced using CASSCF, CASPT2 and CCSD(T). The aim is to see how well these new functionals can treat transition metal systems, an area where different DFT functionals have produced varying and often contradictory results.

The systems used by Ghosh and Condradie [40] were first row transition metal complexes of the form (β-Diketoiminato)M(NR) where M = Cr(III), Mn(III), Fe(III), Fe(IV), Co(III), Ni(III) and Cu(III) and R = alkyl or aryl. This chapter will concentrate on the

systems with M = Fe(III), Co(III) and Ni(III).

5.2 Ligand Choices

The main ligand used by Ghosh and Condradie [40] was the β-Diketoiminate nacnac. Where nacnac$^-$ is the anion of 2,4-bis(2,6-dimethylphenylimido)-pentane. The two imido ligands used were NPh and NMe. β-Diketoiminate ligands are often used for low oxidation state transition metal complexes, the most common being nacnac [41, 42], although in some cases additional functional groups are added to the base ligand [43, 44]. The nacnac ligand is useful in two ways, the large size often prevents more ligands attaching to the metal keeping the oxidation state of the metal low, and the trailing 2,6-dimethylphenyl groups are in a position where the delocalised electron density from the rings may help stabilise the metal-ligand bonds on the ligand opposite it.

A MOLCAS [35] CASSCF test calculation was carried out on an OLYP [37] optimised geometry from the Ghosh and Condradie paper [40], for the molecule (nacnac)Co^{III}(NPh). This molecule proved to be too large for the computing power available causing a failure due to a lack of memory. With this failure a smaller test system was required, two possible systems were constructed. First a minimal test system with all functional groups of the main ligand being replaced with Hydrogens, leading to system A $(CH(CHN)_2)M^{III}(NH)$. The second system returned the phenyl group on the imido ligand to help stabilise the metal-nitrogen double bond, leading to system B $(CH(CHN)_2)M^{III}(NPh)$.

Figure 5.1 shows graphical representations of the two test systems, drawn using chemtool [45] a chemical drawing package. The bond lengths and angles shown are not representative of those in the optimised geometries and are used only for ease of representation.

The smaller test systems unfortunately lose some of the advantages provided by the nacnac ligand. The lack of size is unimportant as there are no competing ligands in the calculations. The loss of the stabilising effects of the aromatic rings and methyl groups on the β-Diketoiminate may result in a less rigid structure and possible convergence issues.

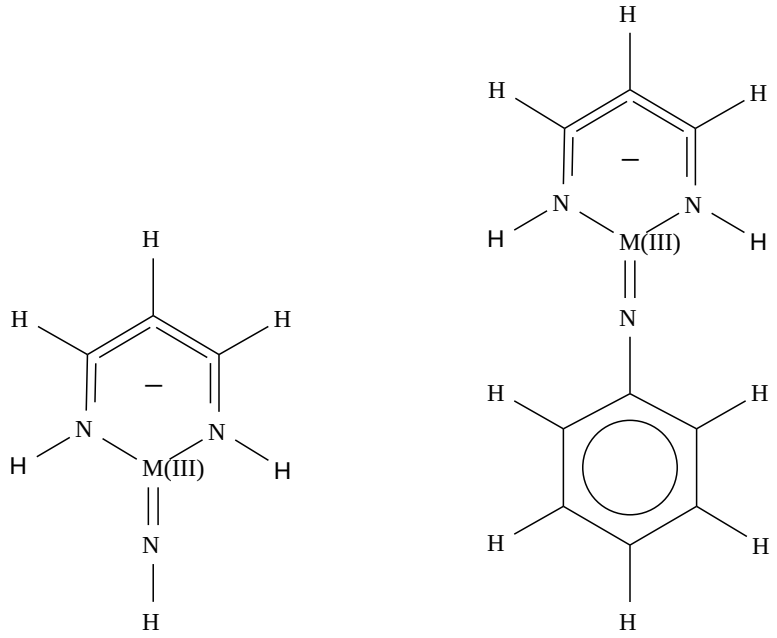

(a) $(CH(CHN)_2)M^{III}(NH)$ (b) $(CH(CHN)_2)M^{III}(NPh)$

Figure 5.1: Graphical representations of the two test systems

The loss of the aromatic rings may also cause problems for the stability of the metal-nitrogen bond especially in system A. System B may go some way to strengthening the metal-nitrogen bond thanks to electron donation from the phenyl group.

Geometries for both test systems were produced and energies calculated using a number of different techniques. The calculations will be detailed in the following sections.

5.3 Geometries and DFT Energies

The first step in any computational investigation of a system is to generate and optimise an appropriate geometry.

For system A a starting set of Cartesian coordinates were created by hand, the initial coordinates can be seen in table 5.1, all values are in a_0.

For system B the starting geometry was taken from the lowest energy Co(III) geometry of system A with the added phenyl group produced by repeating the top ring with the original metal atom at the position of the imide hydrogen, and all non-carbon atoms replaced by carbons, this results in the geometry shown in table 5.2.

From these initial coordinates a number of DFT geometry optimisations were performed to create individual metal specific geometries. Not only were separate geometries

created for each metal, but also for each spin state and C_{2v} orbital symmetry for which a valid configuration could be created. With the amount of geometries created they cannot all be displayed in the main text, therefore appendix A will contain all geometries of states referenced in this chapter. All geometries will be included as sets of Cartesian coordinates in a_0. Not having access to the OPTX functionals [37] discussed earlier, an alternative functional was needed for use in these geometry optimisations. The B3-LYP functional [12, 13] has become one of the most popular functional for use with transition metal systems, and therefore was chosen for these tests. A large basis set is always useful when carrying out an optimisation, therefore in these calculations the TZVP basis set [22] was chosen. The geometry optimisation was carried out using Turbomole [46, 47, 48, 49] version 5-7-1.

As there are so many calculations to detail an individual rundown of the parameters used in each calculation is unnecessary. Table 5.3 and table 5.4 show each metal, spin state and symmetry calculated with the orbital occupations used for systems A and B respectively.

With a full set of DFT geometries and energies the next step is the CASSCF, CASPT2 and CCSD(T) calculations.

Atom	X	Y	Z
M	0.00	0.00	0.00
N	0.00	0.00	1.75
N	1.52	0.00	-0.88
N	-1.52	0.00	-0.88
C	1.52	0.00	-2.35
C	-1.52	0.00	-2.35
C	0.00	0.00	-3.12
H	1.57	0.00	-0.20
H	-1.57	0.00	-0.20
H	1.57	0.00	-3.00
H	-1.57	0.00	-3.00
H	0.00	0.00	2.65
H	0.00	0.00	-4.02

Table 5.1: Initial coordinate set for system A

Atom	X	Y	Z
M	0.000000	0.000000	1.685137
N	0.000000	0.000000	4.931055
N	2.657282	0.000000	-0.856374
N	-2.657282	0.000000	-0.856374
C	0.000000	0.000000	6.852042
C	0.000000	0.000000	-4.567281
C	2.327530	0.000000	-3.329346
C	-2.327530	0.000000	-3.329346
C	2.657282	0.000000	11.856374
C	-2.657282	0.000000	11.856374
C	2.327530	0.000000	8.529346
C	-2.327530	0.000000	8.529346
C	0.000000	0.000000	14.277281
H	4.499721	0.000000	11.519619
H	-4.499721	0.000000	11.519619
H	4.011144	0.000000	7.327325
H	-4.011144	0.000000	7.327325
H	4.499721	0.000000	-0.341962
H	-4.499721	0.000000	-0.341962
H	4.011144	0.000000	-4.517325
H	-4.011144	0.000000	-4.517325
H	0.000000	0.000000	-6.609468
H	0.000000	0.000000	16.852014

Table 5.2: Initial coordinate set for system B

		α				β			
Metal	State	a_1	b_1	b_2	a_2	a_1	b_1	b_2	a_2
Fe(III)	$^2a_1$	19	10	5	2	18	10	5	2
	$^2a_2$	19	10	5	2	19	10	5	1
	$^4b_1$	19	10	6	2	18	10	5	1
	$^4b_2$	19	10	6	2	17	10	5	2
	$^6a_1$	19	11	6	2	17	10	5	1
Co(III)	$^1a_1$	19	10	5	2	19	10	5	2
	$^3b_1$	19	11	5	2	18	10	5	2
	$^3b_2$	19	10	6	2	18	10	5	2
	$^5a_1$	19	11	6	2	18	10	5	1
	$^5a_2$	19	11	6	2	17	10	5	2
Ni(III)	$^2b_1$	19	11	5	2	19	10	5	2
	$^2b_2$	19	10	6	2	19	10	5	2
	$^4a_1$	19	11	6	2	19	10	5	1
	$^4b_2$	19	11	6	2	19	9	5	2
	$^4a_2$	19	11	6	2	18	10	5	2

Table 5.3: Orbital occupations for System A

		α				β			
Metal	State	a_1	b_1	b_2	a_2	a_1	b_1	b_2	a_2
Fe(III)	$^2a_1$	29	17	7	3	28	17	7	3
	$^2a_2$	29	17	7	3	29	17	7	2
	$^4b_1$	29	17	8	3	28	17	7	2
	$^4b_2$	29	17	8	3	27	17	7	3
	$^6a_1$	29	18	8	3	27	17	7	2
Co(III)	$^1a_1$	29	17	7	3	29	17	7	3
	$^3b_1$	29	18	7	3	28	17	7	3
	$^3b_2$	29	17	8	3	28	17	7	3
	$^5a_1$	29	18	8	3	28	17	7	2
	$^5a_2$	29	18	8	3	27	17	7	3
Ni(III)	$^2b_1$	29	18	7	3	29	17	7	3
	$^2b_2$	29	17	8	3	29	17	7	3
	$^4a_1$	29	18	8	3	29	17	7	2
	$^4b_2$	29	18	8	3	29	16	7	3
	$^4a_2$	29	18	8	3	28	17	7	3

Table 5.4: Orbital occupations for System B

5.4 CASSCF, CASPT2 and CCSD(T) Calculations

Two separate program suites will be used in this chapter, the CASSCF and CASPT2 wave functions will be calculated using MOLCAS [35] as seen before and CCSD(T) wave functions will be calculated in Molpro [30, 32, 50, 51].

This section will give example procedures for how each type of calculation is carried out and details of where each system varies from this procedure.

Both systems A and B contain only the metal, carbon, hydrogen and nitrogen atoms, this means that other than the metal the basis sets do not need to change between each calculation. The use of two suites of programs will affect which basis sets are used between methods. In all cases the basis sets used were an ANO-CC basis set for the metal centre (this basis set is from unpublished work by B. J. Persson see appendix D),and aug-CC-PVDZ [20] basis sets for all other atoms.

The calculations were carried out for the following geometries in both systems:

- Fe(III): $^2a_1$, $^2a_2$, $^4b_1$, $^4b_2$ and $^6a_1$.
- Co(III): $^1a_1$, $^3b_1$, $^3b_2$, $^5a_1$ and $^5a_2$
- Ni(III): $^2b_1$, $^2b_2$, $^4a_1$, $^4b_2$ and $^4a_2$

Each CASPT2 calculation using MOLCAS [35] followed the same basic procedure with only the geometry, orbital numbers and active spaces changing. In order to get an idea of how the system changed with the size of the active space, two active spaces were used in system A a minimal one (min) and an extended one (ext). Only the extended active space was used for system B. The minimal active space consisted of either five, six or seven electrons for Fe(III), Co(III) or Ni(III) respectively in five orbitals. The space (min) had the following make up $2a_1$ $1b_1$ $1b_2$ $1a_2$. System A has the following inactive orbitals $17a_1$ $10b_1$ $5b_2$ $1a_2$. The larger set consisted of fifteen, sixteen or seventeen electrons for Fe(III), Co(III) or Ni(III) respectively in thirteen orbitals. The space (ext) had the following make up $2a_1$ $4b_1$ $4b_2$ $3a_2$. System A has the following inactive orbitals $17a_1$ $8b_1$ $3b_2$ $0a_2$ whilst System B has the following inactive orbitals $27a_1$ $15b_1$ $5b_2$ $1a_2$.

The procedure was as follows:

1. A closed shell Hartree-Fock SCF calculation in C_{2v} symmetry performed on an $S = 0$ state. See table 5.5
2. A single state CASSCF calculation was performed. The calculation used one of two active spaces (min) or (ext) as described above. The calculation was performed on the state to be investigated in each case.Level shifts were used as required to aid convergence.
3. A CASPT2 calculation was carried out using the optimised wave function from the previous step. A 0.1 imaginary level shift was used. This level shift is to deal with this fairly common situation, for excited states, that weakly coupled intruders cause spurious singularities. The level shift will introduce an imaginary shift in the energy denominators, thus avoiding singularities. the program will also correct the energy for the use of this shift.

	Occupation			
Metal/System	a_1	b_1	b_2	a_2
Fe/A	19	11	5	1
Co/A	19	10	5	2
Ni/A	19	10	5	2
Fe/B	29	17	7	3
Co/B	29	17	7	3
Ni/B	29	17	8	3

Table 5.5: Occupation numbers used in MOLCAS HF-SCF calculations

As with the CASPT2 calculations a basic procedure was followed in the calculation of the CCSD(T) energies. The procedure was as follows:

1. A CASSCF calculation was performed. The calculation used the active space equivalent to the restricted Hartree-Fock SCF occupations described in table 5.6 and 5.7. The calculation was performed on the state to be investigated in each case. This was used to produce a better starting point for the next step.
2. A restricted Hartree-Fock SCF calculation was performed on the state of interest using the orbital occupations described in table 5.6 and 5.7. Where necessary a

level shift between the closed and open-shell orbitals was used to aid convergence.

3. A restricted CCSD(T) calculation was performed using the optimised wave function from the previous step. Where necessary a pairs denominator shift was used to aid convergence.

All calculations were completed although certain calculations required the use of alternate orbital sets. In system A the Fe(III) $^2a_2$ (min) calculation used the CASPT2 orbitals from the $^2a_1$ (min) calculation to prime the CASSCF. In the (ext) calculations for system A both the Ni(III) $^2b_1$ and Fe(III) $^6a_1$ calculations used the CASPT2 orbitals from the equivalent (min) calculation to prime the CASSCF.

		α				β			
Metal	State	a_1	b_1	b_2	a_2	a_1	b_1	b_2	a_2
Fe(III)	$^2a_1$	19	10	5	2	18	10	5	2
	$^2a_2$	19	10	5	2	19	10	5	1
	$^4b_1$	19	10	6	2	18	10	5	2
	$^4b_2$	19	10	6	2	17	10	5	2
	$^6a_1$	19	10	6	2	17	10	5	2
Co(III)	$^1a_1$	19	10	5	2	19	10	5	2
	$^3b_1$	19	11	5	2	18	10	5	2
	$^3b_2$	19	10	6	2	18	10	5	2
	$^5a_1$	19	11	6	2	18	10	5	1
	$^5a_2$	19	11	6	2	17	10	5	2
Ni(III)	$^2b_1$	19	11	5	2	19	10	5	2
	$^2b_2$	19	10	6	2	19	10	5	2
	$^4a_1$	19	11	6	2	19	10	5	1
	$^4b_2$	19	11	6	2	19	9	5	2
	$^4a_2$	19	11	6	2	19	10	5	1

Table 5.6: Occupation numbers used in Molpro CCSD(T) calculations on system A

		α				β			
Metal	State	a_1	b_1	b_2	a_2	a_1	b_1	b_2	a_2
Fe(III)	$^2a_1$	29	17	7	3	28	17	7	3
	$^2a_2$	29	17	7	3	29	17	7	3
	$^4b_1$	29	17	8	3	27	17	7	3
	$^4b_2$	29	17	8	3	28	17	7	2
	$^6a_1$	29	18	8	3	27	17	7	2
Co(III)	$^1a_1$	29	17	7	3	29	17	7	3
	$^3b_1$	29	18	7	3	28	17	7	3
	$^3b_2$	29	17	8	3	28	17	7	3
	$^5a_1$	29	18	8	3	28	17	7	2
	$^5a_2$	29	18	8	3	27	17	7	3
Ni(III)	$^2b_1$	29	18	7	3	29	17	7	3
	$^2b_2$	29	17	8	3	29	17	7	3
	$^4a_1$	29	18	7	3	29	17	7	3
	$^4b_2$	29	18	8	3	29	16	7	3
	$^4a_2$	29	17	8	3	29	17	7	3

Table 5.7: Occupation numbers used in Molpro CCSD(T) calculations on system B

5.5 Results

This section will show the results derived from the calculations discussed above and compare them to those in reference [40]

5.5.1 Raw Data

The data shown here is the raw data as extracted from the calculations. This data will be analysed later in this section. All energies are listed in E_h and rounded to six decimal places for ease of presentation. Table 5.8 shows data from system A whilst table 5.9 shows data from system B.

		Methods					
Metal	State	DFT/B3-LYP	CASSCF(min)	CASSCF(ext)	CASPT2(min)	CASPT2(ext)	CCSD(T)
Fe(III)	$^2a_1$	-1545.748863	-1542.775883	-1542.969489	-1544.026389	-1544.198141	-1544.194923
	$^2a_2$	-1545.743671	-1542.781916	-1542.952328	-1544.049362	-1544.105269	-1544.189140
	$^4b_1$	-1545.757902	-1542.855388	-1542.931766	-1544.049349	-1544.053732	-1544.180305
	$^4b_2$	-1545.761945	-1542.839838	-1542.903616	-1544.052030	-1544.072621	-1544.193271
	$^6a_1$	-1545.749029	-1542.928709	-1542.985201	-1544.105407	-1544.106035	-1544.186708
Co(III)	$^1a_1$	-1664.801789	-1661.726910	-1661.927147	-1663.136491	-1663.153979	n/a
	$^3b_1$	-1664.803300	-1661.775598	-1661.974706	-1663.045462	-1663.158893	n/a
	$^3b_2$	-1664.813020	-1661.838152	-1661.953444	-1663.131374	-1663.148485	-1663.221104
	$^5a_1$	-1664.804083	-1661.503176	-1661.952998	-1662.800873	-1663.162572	n/a
	$^5a_2$	-1664.806982	-1661.893887	-1661.951028	-1663.139252	-1663.141891	n/a
Ni(III)	$^2b_1$	-1790.333241	-1787.203753	-1787.417017	-1788.697754	-1788.690093	-1788.750284
	$^2b_2$	-1790.359732	-1787.278609	-1787.355911	-1788.637137	-1788.716587	-1788.767549
	$^4b_2$	-1790.337197	-1786.956433	-1787.396902	-1788.334368	-1788.660058	-1788.734110
	$^4b_2$	-1790.333551	-1786.754020	-1787.379982	-1788.208128	-1788.653840	-1788.730687
	$^4a_2$	-1790.342673	-1787.347538	-1787.405900	-1788.661696	-1788.666318	-1788.736177

Table 5.8: Raw data from DFT, CASSCF, CASPT2 and CCSD(T) calculations on system A

		Methods			
Metal	State	DFT/B3-LYP	CASSCF(ext)	CASPT2(ext)	CCSD(T)
Fe(III)	$^2a_1$	-1776.747490	-1772.506403	-1774.399436	-1774.552763
	$^2a_2$	-1776.742774	-1772.305790	-1774.176166	-1774.546795
	$^4b_1$	-1776.753742	-1772.571702	-1774.419346	-1774.549161
	$^4b_2$	-1776.757347	-1772.161458	-1774.061437	-1774.543354
	$^6a_1$	-1776.746752	-1772.097854	-1773.997449	-1774.539623
Co(III)	$^1a_1$	-1895.803482	-1891.490456	-1893.435521	-1893.599801
	$^3b_1$	-1895.808023	-1891.533150	-1893.445853	-1893.571613
	$^3b_2$	-1895.810096	-1891.513622	-1893.463289	-1893.577955
	$^5a_1$	-1895.804471	-1891.199109	-1893.172735	-1893.461817
	$^5a_2$	-1895.807138	-1891.340620	-1893.295236	-1893.574843
Ni(III)	$^2b_1$	-2021.350013	-2016.874452	-2018.877467	-2019.113375
	$^2b_2$	-2021.361850	-2016.912952	-2018.961064	-2019.120529
	$^4a_1$	-2021.340680	-2016.754899	-2018.771496	-2018.989683
	$^4b_2$	-2021.332209	-2016.672180	-2018.711954	-2019.080183
	$^4a_2$	-2021.345982	-2016.800471	-2018.837860	-2019.097117

Table 5.9: Raw data from DFT, CASSCF, CASPT2 and CCSD(T) calculations on system B

5.5.2 Energy Level Diagrams

In order to understand how this data fits together and to make an easy comparison between it and the information from reference [40] energy level diagrams have been constructed. Tables 5.10 and 5.11 show the energies of each state relative to the lowest energy state for systems A and B respectively. Included are the OLYP [37] energy levels from the Ghosh and Condradie paper [40]. All energies have been converted to electron volts (eV) using the conversion factor $1\,E_h = 27.2114\,eV$ and rounded to three decimal places for comparison with the OLYP [37] data. The OLYP [37] data is only listed for each spin state with no symmetry so the same data will be shown in all symmetries of a state.

Each diagram below contains all the data for a single metal centre with the lines showing the energy in eV above the ground state, all states are labelled on the diagram. In the plots the active space is shown buy (E) for the expanded active space and (M) minimal active space. Figure 5.2 shows the data for Fe(III), figure 5.3 shows the data for Co(III) and figure 5.4 shows the Data for Ni(III) in system A. Figure 5.5 shows the data for Fe(III), figure 5.6 shows the data for Co(III) and figure 5.7 shows the Data for Ni(III) in system B.

		Methods						
Metal	State	DFT/B3-LYP	CASSCF (min)	CASSCF (ext)	CASPT2 (min)	CASPT2 (ext)	CCSD(T)	DFT/OLYP [40]
Fe(III)	$^2a_1$	0.356	4.159	0.428	2.150	0.000	0.000	0.290
	$^2a_2$	0.497	3.994	0.895	1.525	2.527	0.157	0.290
	$^4b_1$	0.110	1.995	1.454	1.525	3.930	0.398	0.000
	$^4b_2$	0.000	2.418	2.220	1.452	3.416	0.045	0.000
	$^6a_1$	0.351	0.000	0.000	0.000	2.506	0.224	0.530
Co(III)	$^1a_1$	0.306	4.544	1.294	0.075	0.234	n/a	0.000
	$^3b_1$	0.264	3.219	0.000	2.552	0.100	n/a	0.200
	$^3b_2$	0.000	1.517	0.579	0.214	0.383	0.000	0.200
	$^5a_1$	0.243	10.632	0.591	9.208	0.000	n/a	0.530
	$^5a_2$	0.164	0.000	0.644	0.000	0.563	n/a	0.530
Ni(III)	$^2b_1$	0.721	3.913	0.000	0.000	0.721	0.000	0.000
	$^2b_2$	0.000	1.876	1.663	1.649	0.000	1.003	0.000
	$^4a_1$	0.613	10.643	0.547	9.888	1.538	0.854	0.880
	$^4b_2$	0.712	16.150	1.007	13.323	1.707	0.910	0.880
	$^4a_2$	0.464	0.000	0.302	0.981	1.368	0.470	0.880

Table 5.10: Relative energies for system A including OLYP data from [40]

		Methods				
Metal	State	DFT/B3-LYP	CASSCF (ext)	CASPT2 (ext)	CCSD(T)	DFT/OLYP [40]
Fe(III)	$^2a_1$	0.268	1.777	0.542	0.000	0.290
	$^2a_2$	0.397	7.236	6.617	0.162	0.290
	$^4b_1$	0.098	0.000	0.000	0.098	0.000
	$^4b_2$	0.000	11.163	9.739	0.256	0.000
	$^6a_1$	0.288	12.894	11.480	0.358	0.530
Co(III)	$^1a_1$	0.180	1.162	0.756	0.000	0.000
	$^3b_1$	0.056	0.000	0.474	0.767	0.200
	$^3b_2$	0.000	0.531	0.000	0.594	0.200
	$^5a_1$	0.153	9.090	7.906	3.755	0.530
	$^5a_2$	0.080	5.239	4.573	0.679	0.530
Ni(III)	$^2b_1$	0.322	1.048	2.275	0.195	0.000
	$^2b_2$	0.000	0.000	0.000	0.000	0.000
	$^4a_1$	0.576	4.301	5.158	3.561	0.880
	$^4b_2$	0.807	6.552	6.779	1.098	0.880
	$^4a_2$	0.432	3.061	3.353	0.637	0.880

Table 5.11: Relative energies for system B including OLYP data from [40]

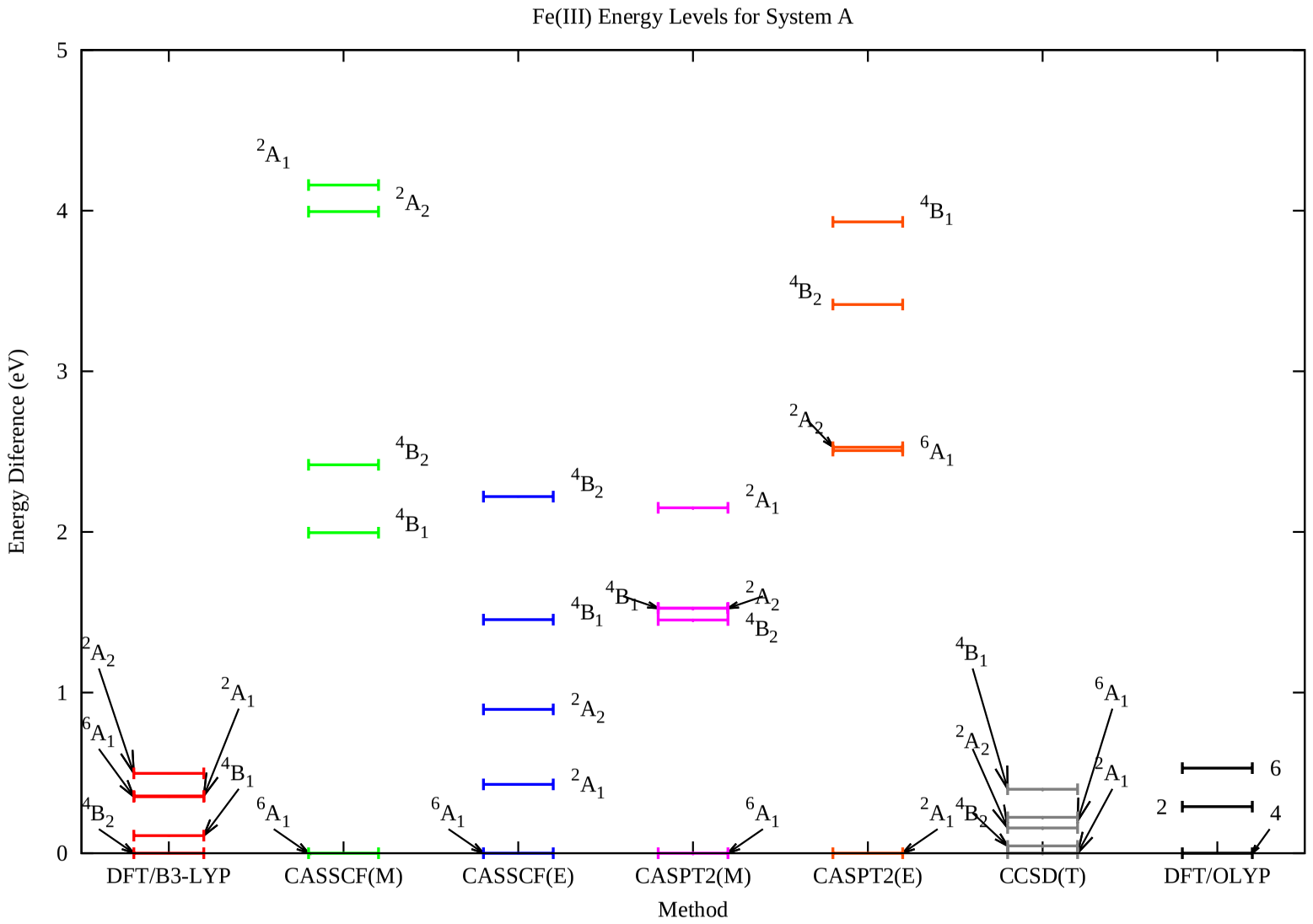

Figure 5.2: Relative energies (eV) for the Fe(III) analogue of system A

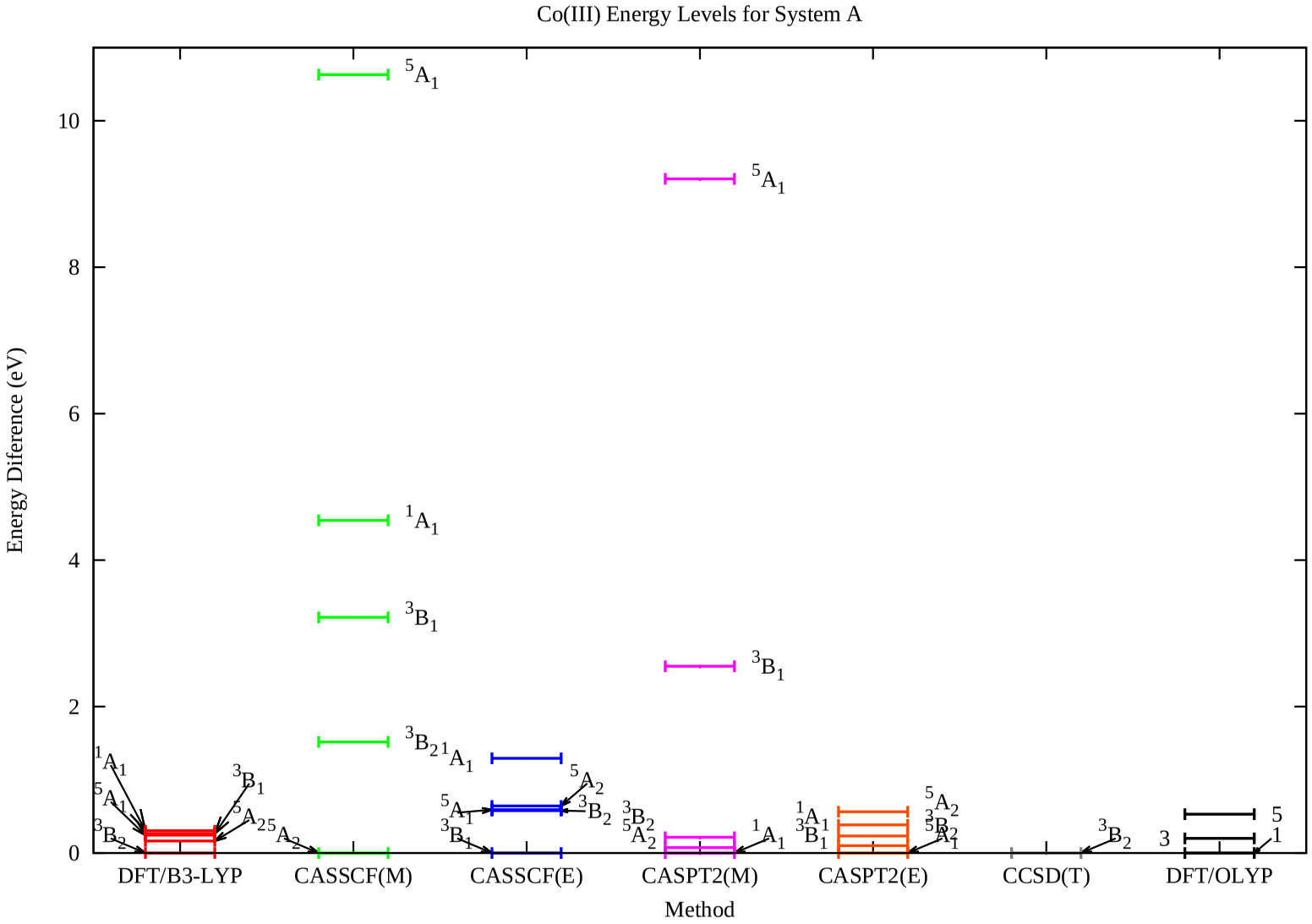

Figure 5.3: Relative energies (eV) for the Co(III) analogue of system A

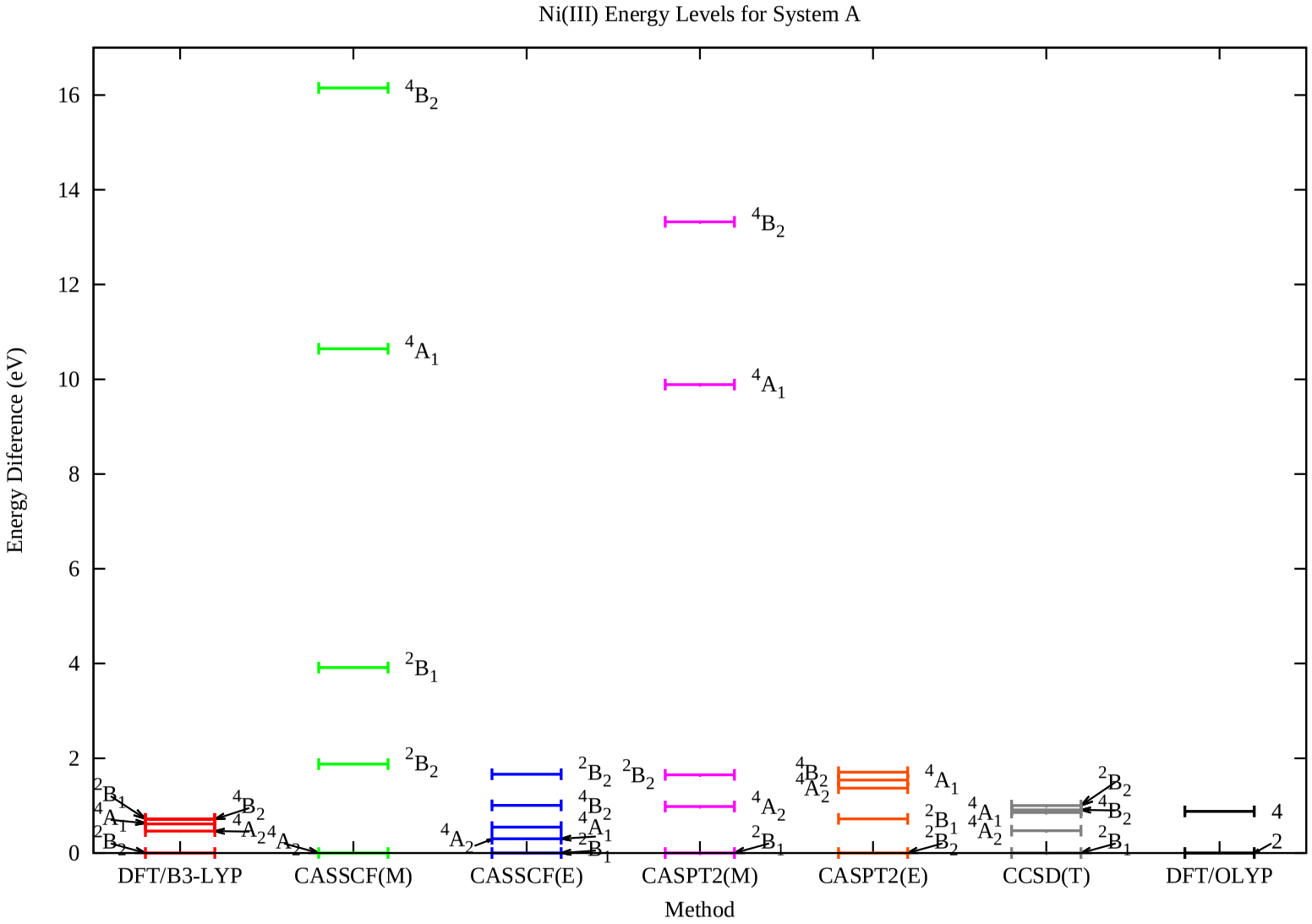

Figure 5.4: Relative energies (eV) for the Ni(III) analogue of system A

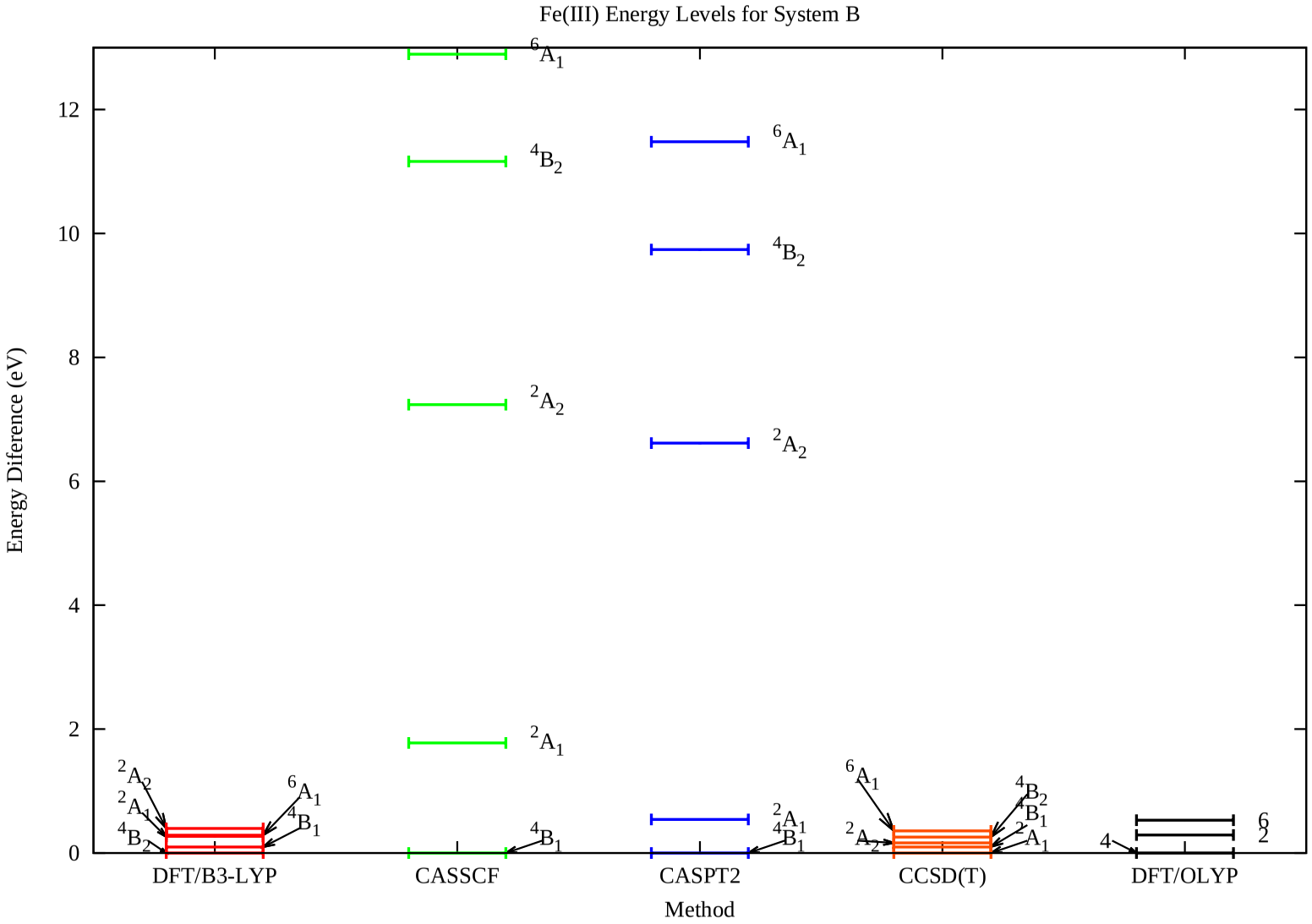

Figure 5.5: Relative energies (eV) for the Fe(III) analogue of system B

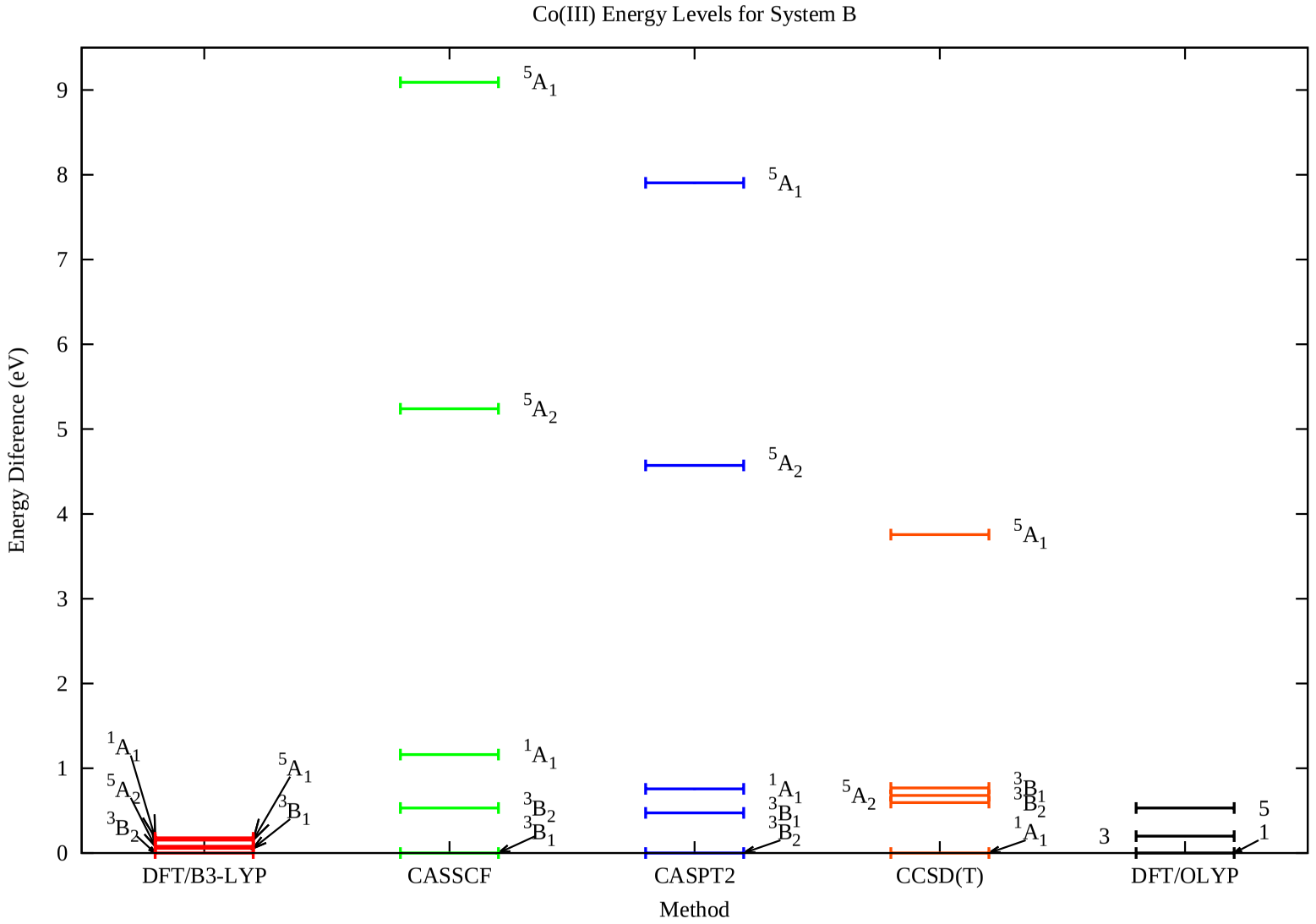

Figure 5.6: Relative energies (eV) for the Co(III) analogue of system B

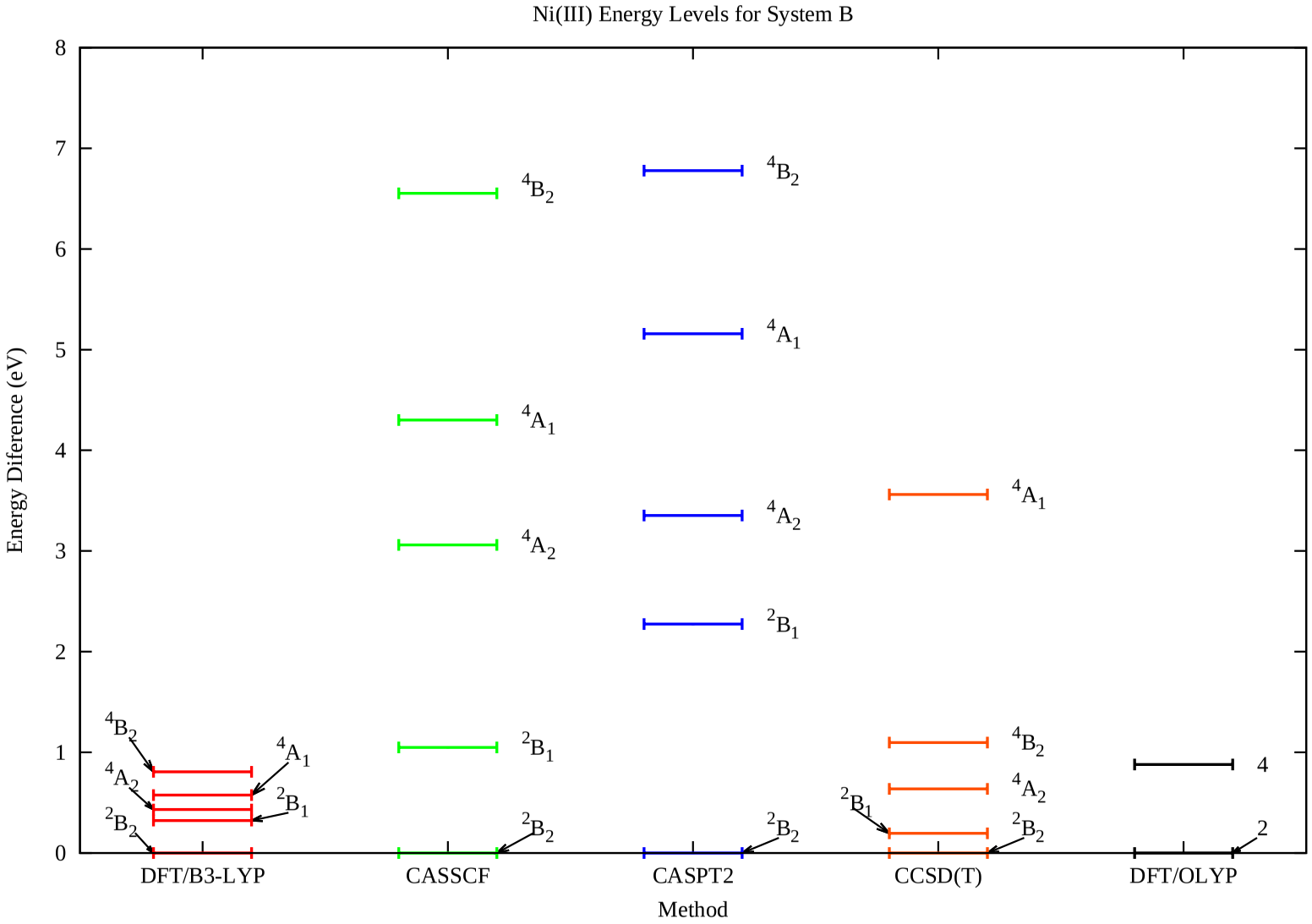

Figure 5.7: Relative energies (eV) for the Ni(III) analogue of system B

5.6 Analysis

The results presented above help in the understanding of how different methods, and even the different functionals, favour different spin states.

Traditionally DFT methods have tended to favour low spin states in metal based systems with hybrid functionals such as B3-LYP [12, 13] being less discriminatory than pure functionals. OLYP [37] being a pure functional was expected to follow the trend favouring the low spin option in each, case however as clearly stated in the paper Ghosh and Condradie [40] found that OLYP [37] predicted higher spin states where appropriate and in agreement with experimental evidence.

The results from above will be discussed on a metal by metal basis.

5.6.1 Fe(III)

The Fe(III) complexes are probably the most important of those tested here in relation to the data provided in the Ghosh and Condradie paper [40]. The OLYP [37] tests predicted an $S = \frac{3}{2}$ ground state in agreement with experiment [52] whilst other pure functionals predicted an $S = \frac{1}{2}$ ground state. The B3-LYP [12, 13] calculations in this chapter, like the hybrid functionals tested in the Ghosh and Condradie paper [40] also shows the $S = \frac{3}{2}$ ground state. The hybrid functionals in their paper show a different order of the $S = \frac{1}{2}$ and $S = \frac{5}{2}$ states to the OLYP [37] test, whilst this is also evident to some extent in both systems using B3-LYP [12, 13], here a $S = \frac{1}{2}$ state is also present which is on par with the $S = \frac{5}{2}$.

In system A the CASSCF calculations both predict a $S = \frac{5}{2}$ ground state, with a distant $S = \frac{3}{2}$ states in the minimal basis followed by the two $S = \frac{1}{2}$ states. The order of the exited states is reversed with an extended basis. The CASPT2 results show a large difference depending on the active space size with the min space following the minimal CASSCF result. The ext active space shows an $S = \frac{1}{2}$ ground state by a clear margin, followed by the $S = \frac{5}{2}$ state with all but the ground state massively higher in energy. The CCSD(T) results showed a $S = \frac{1}{2}$ ground state followed closely by a $S = \frac{3}{2}$ the other states are higher

in energy but do not show the same wide spacing as the CAS based methods.

In system B the CAS based methods predicted an S $= \frac{3}{2}$ ground state, followed by an S $= \frac{1}{2}$ state within 2 eV. The CCSD(T) again showed all states within a small range with an S $= \frac{1}{2}$ ground state.

Neither test system proves one way or the other the results in the paper. However on the larger B system broadly supports the proposed state ordering whilst the smaller A system disagrees. Of the two systems B is more like the system in the Ghosh and Condradie paper [40] and the results for this system agree on on two of the three non-DFT based calculations. The large difference in results from the paper and the systems presented here allows little concrete evidence either way but suggests that the smaller system may be a poor representation of the system presented in their paper. the relative success of the larger system may suggest that the loss of the aryl groups from the β-Diketoiminato ligand is the most likely problem as these may have changed how the metal orbitals interacted.

5.6.2 Co(III)

These complexes were much less of a test for OLYP [37] with all the pure functionals suggesting the low spin S $= 0$ solution as confirmed by experiment [41], whilst the hybrid functionals predicted higher spin solutions. The B3-LYP [12, 13] calculation on both systems shows an S $= 1$ solution.

In system A the min and ext active space CASSCF predict higher spin states, an S $= 2$ state for min and an S $= 1$ state for ext. The min CASPT2 calculations predict the low spin ground state with the ext calculation showing a high spin result. The CCSD(T) calculation was marred with a lack of data due to convergence errors.

In system B the CASSCF and CASPT2 calculations predicts an S $= 2$ ground state, whilst the CCSD(T) calculation predicts the S $= 0$ state. The CCSD(T) calculation predicts the first three states in the order as defined by the Ghosh and Condradie paper [40].

The Ghosh and Condradie paper [40] suggests that the older pure functionals produce larger energy gaps between the ground state and the S $= 2$ state than OLYP [37], however

the CCSD(T) calculations mirror the OLYP [37] calculations in energy spacing.

5.6.3 Ni(III)

These complexes showed little differentiation between functionals with all predicting an $S = \frac{1}{2}$ ground state, which is born out by the B3-LYP [12, 13] calculations from both systems as well as from experiment [43].

In system A only the min CASSCF failed to predict the correct ground state. Both the CASPT2 calculations and the CCSD(T) calculations showed good agreement with the OLYP [37] data on the energy gaps.

In system B all three non-DFT methods predicted an $S = \frac{1}{2}$ ground state in agreement with results for system A.

5.6.4 Orbitals

The Ghosh and Condradie paper [40] shows a set of orbital plots for the five molecular orbitals with large *d*-type contributions in the Ni(III) $S = \frac{1}{2}$ system. These orbitals consist of four of the five highest occupied molecular orbitals (HOMO, HOMO-1, HOMO-3 and HOMO-4) and the lowest unoccupied molecular orbital (LUMO).

Below are the Ghosh and Condradie plots [40] in figure 5.8 and the equivalent plots for system A from the Ni(III) $^2b_2$ ext CASSCF calculation in figure 5.9.

The orbital plots from the CASSCF calculation were produced in MOLDEN [36] using the space filling orbital function and a contour value of 0.02. The orbital labels are based on the ordering within an orbital symmetry, and not the energies within the overall system due to the way MOLCAS [35] arranges the orbitals in the MOLDEN output.

Whilst the two orbital sets are not identical between the DFT results and the CASSCF results, the plots do show similarities in most areas. An orbital in the DFT set has been matched with a similar orbital in the CASSCF set for each of the five primarily 3*d* based molecular orbitals. The ordering in each set is slightly different, but this may be due to the use of different state symmetries, or due to the fractional orbital occupations associated with the CASSCF method. These fractional orbital occupations are due to the mixing

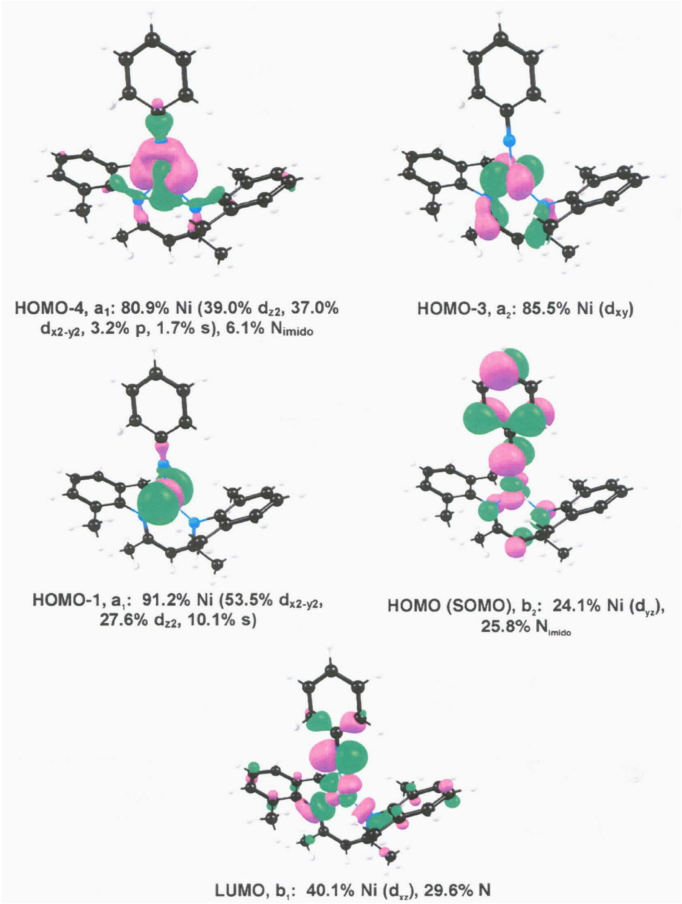

Figure 5.8: Plots of OLYP generated Ni(III) primarily 3*d* based molecular orbitals from [40]

of different occupations in the creation of the wave function. Overall both the HOMO and LUMO match in both systems, and as these are the most important orbitals for any additional chemistry, the match suggests a good result for both methods.

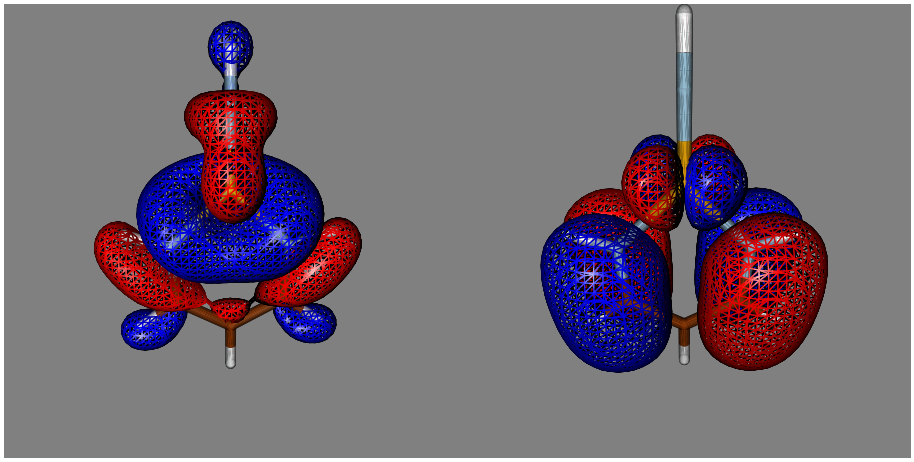

(a) a_1 HOMO (b) a_2 HOMO-1

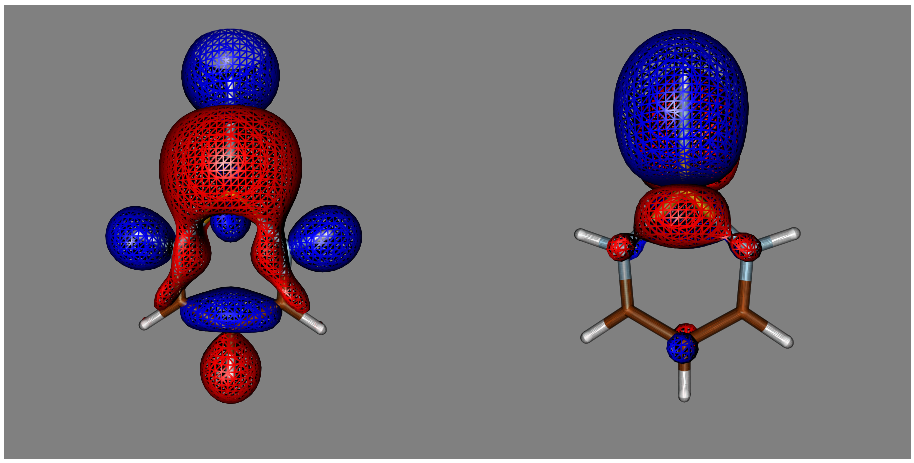

(c) a_1 HOMO-2 (d) b_2 HOMO

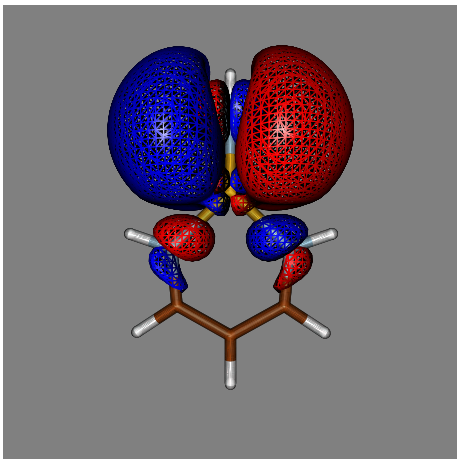

(e) b_1 LUMO

Figure 5.9: Plots of CASSCF(ext) generated Ni(III) primarily 3*d* based molecular orbitals for system A

5.7 Conclusions

The aim of these experiments was to test how well the DFT/OLYP [37] results presented in Ghosh and Condradie paper [40] compare to other calculation methods. The other methods used were CASSCF, CASPT2 and CCSD(T). All the methods try to improve on single configuration results. To do this DFT uses fitting functions, whilst CASSCF and CASPT2 use a large number of orbital configurations, and CCSD(T) uses a mathematical approach to improving the base calculations used towards a better representation of the wave function. Overall the best method based on the results here was CCSD(T) with almost all ground states and many of the excited states predicted in agreement with experiment, and the OLYP [37] results. CASSCF and CASPT2 often predicted the wrong ground state or excited state order, although with the larger ext active space the CASPT2 results for system A were more right than wrong.

When comparing the calculations it is important to remember that the results presented here were actually produced using model systems of the complexes used in the Ghosh and Condradie paper [40]. Of the two model systems B behaved most like the full complex with similar energetics predicted by several methods with all three metals. System A has neither the aryl or phenyl groups and seems to act differently to the full complex, while system B has the added phenyl group and the energetics showed fewer differences.

Overall the results from these tests are inconclusive, with no two methods agreeing on all states for one system let alone both. Of the two systems, B produced the better results which was unsurprising, however neither model consistently showed the same results as the full nacnac complexes.

DFT using the OLYP [37] functional seems to be a good choice for use as a fast method of producing data on new transition metal complexes compared to DFT with B3-LYP [12, 13] the current standard method. As always for large systems or systems with difficult low symmetry geometries, DFT is a reasonable choice due to its speed and the lack of a reliance on active spaces. With the OLYP [37] functional the results seem more likely to match those shown in experiments and to not suffer as extensively from the trends older functionals exhibit.

As an extension of this work a system could be designed with a less extensive functional group attached at various points on the β-Diketoiminate ligand, in order to test whether a functional group on either the nitrogen or secondary carbons would affect the results seen.

Chapter 6

A Possible Transition State of $[Cr^{II}(CN)_5]^{3-}$

6.1 Introduction

This chapter covers the possible discovery of a transition state in the interconversion of the square pyramidal and trigonal bipyramidal forms of the molecule $[Cr^{II}(CN)_5]^{3-}$. The $[Cr^{II}(CN)_5]^{3-}$ complex and its dimer $[Cr_2{}^{II}(CN)_9]^{5-}$ are interesting for a number of reasons. Most importantly is evidence from several sources [53, 54, 55, 56] both experimental and theory based, that the complex contains a high spin metal centre, which is unusual as cyanide is a famously high field ligand. High field ligands almost exclusively produce low spin complexes. This is due to high field ligands producing a large energy gap between different *d* orbitals in the metal which makes the disadvantage of pairing electrons in an orbital less than putting unpaired electrons in the higher energy *d* orbitals.

The papers listed above come to the conclusion that lack of coordinating solvent molecules in the preparation of the complex and a high ligand-ligand repulsion favours the high spin complex. The high spin complex has longer metal ligand bond lengths due to the presence of the unpaired electrons in anti-bonding (*d*) orbitals, this increased bond length appears to provide a great enough energy saving to justify the high spin solution.

6.2 Geometries and Transition State Search

As with all new systems the first step is to carry out a geometry optimisation, however in this case the optimisation threw up a few unexpected results.

The system as reported in the paper of Miller et al. [53] shows a number of geometries existing in the crystal structure. Two possible arrangements with an appropriately high symmetry could be constructed from the information available, a square pyramid and a trigonal bipyramid as shown in figure 6.1. The diagram was drawn using chemtool [45].

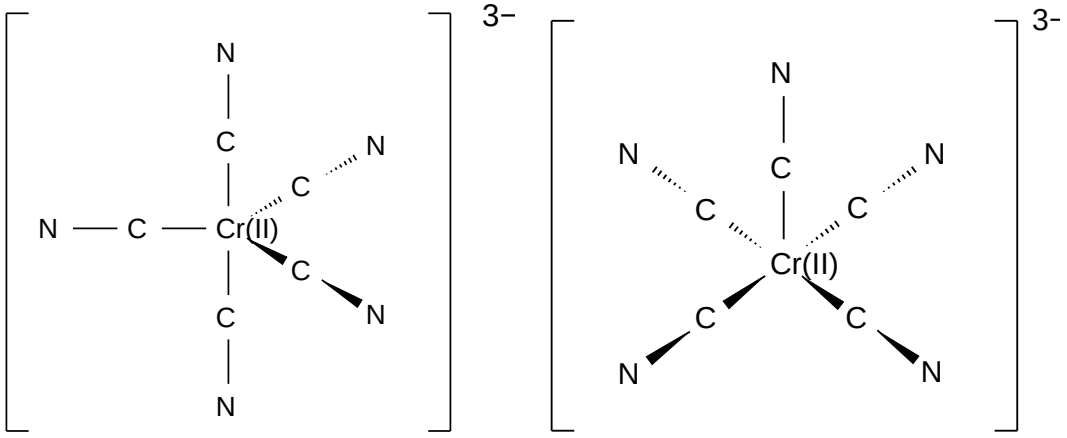

(a) Trigonal bipyramid (b) square pyramid

Figure 6.1: Graphical representations of the two high symmetry forms of $[Cr^{II}(CN)_5]^{3-}$

A set of Cartesian coordinates based on the average geometry parameters presented by Miller et al. [53] were created for each of the two possible arrangements as shown below. Table 6.1 shows the trigonal bipyramid and table 6.2 shows the square pyramid. All values are presented in Å.

Turbomole [46, 47, 48, 49] input geometries were created from the Cartesian coordinates in tables 6.1 and 6.2 using the x2t script which takes a xyz-format file in Å as an input. Using these geometries a set of geometry optimisations were prepared for the systems in C_{2v} symmetry as both the square pyramid and trigonal bipyramid can be represented in this symmetry. The optimisations covered the spin states and orbital occupations shown in table 6.3. The orbital occupations differ so dramatically between the two systems due to the lack of a common axis of symmetry.

All the geometries were optimised using DFT/B3-LYP [12, 13] and a TZVP basis

Atom	X	Y	Z
Cr	0.00000	0.00000	0.00000
N	0.00000	0.00000	3.31000
N	0.00000	0.00000	-3.31000
N	3.35000	0.00000	0.00000
N	-1.67500	2.90119	0.00000
N	-1.67500	-2.90119	0.00000
C	0.00000	0.00000	2.11000
C	0.00000	0.00000	-2.11000
C	2.15000	0.00000	0.00000
C	-1.07500	1.86195	0.00000
C	-1.07500	-1.86196	0.00000

Table 6.1: Initial coordinate set for trigonal bipyramid

Atom	X	Y	Z
Cr	0.00000	0.00000	0.00000
N	0.00000	0.00000	3.43000
N	2.31193	2.31193	-0.57651
N	-2.31193	-2.31193	-0.57651
N	-2.31193	2.31193	-0.57651
N	2.31193	-2.31193	-0.57651
C	0.00000	0.00000	2.23000
C	1.47629	1.47629	-0.36813
C	-1.47629	-1.47629	-0.36813
C	-1.47629	1.47629	-0.36813
C	1.47629	-1.47629	-0.36813

Table 6.2: Initial coordinate set for square base pyramid

		α				β			
Geometry	State	a_1	b_1	b_2	a_2	a_1	b_1	b_2	a_2
Trigonal bipyramid	$^1a_1$ (A)	22	11	10	3	22	11	10	3
	$^1a_1$ (B)	22	10	11	3	22	10	11	3
	$^1a_1$ (C)	22	11	11	2	22	11	11	2
	$^3b_1$ (A)	22	11	11	3	22	11	10	2
	$^3b_1$ (B)	23	11	10	3	22	10	10	3
	$^3b_2$ (A)	22	11	11	3	22	10	11	2
	$^3b_2$ (B)	23	10	11	3	22	10	10	3
	$^5a_1$	23	11	11	3	22	10	10	2
square pyramid	$^1a_1$ (A)	18	11	10	7	18	11	10	7
	$^1a_1$ (B)	18	10	11	7	18	10	11	7
	$^1a_1$ (C)	17	11	11	7	17	11	11	7
	$^3a_1$	19	10	10	8	17	10	10	8
	$^3a_2$	18	11	11	7	18	10	10	7
	$^5a_1$	19	11	11	7	17	10	10	7
	$^5a_2$	18	11	11	8	17	10	10	7

Table 6.3: Orbital occupations for geometry optimisations of $[Cr^{II}(CN)_5]^{3-}$

set [22] for all atoms. With the amount of geometries created they cannot all be displayed in the main text, therefore appendix B will contain all geometries of states referenced in this chapter. All geometries will be included as sets of Cartesian coordinates in a_0.

With the geometry optimisations complete, the $^5a_1$ state in the square pyramidal optimisations showed a single imaginary frequency which on inspection showed a mode which moved the geometry towards a trigonal bipyramid. States with one imaginary frequency are often transition states between two products. In this case the transition is between two geometries of a molecule. The mode of operation of this transition state is similar to a Berry pseudorotation [57, 58, 59] which describes the method by which a trigonal bipyramidal system appears to rotate by the movement of pairs of ligands. In the Berry pseudorotation [57, 58, 59] the axial ligand in the system swap with a pair of equatorial ligands via a square pyramidal transition state. Having found what appeared to be the transition state for the Berry pseudorotation [57, 58, 59] in this system, an attempt was made to confirm it. This consisted of optimising a distorted trigonal bipyramidal geometry shown in table 6.4 using a transition state finder in order to confirm the state from

Atom	X	Y	Z
Cr	0.0000000	0.0000000	0.0004698
N	3.2234432	0.0000000	-0.5679102
N	-3.2234432	0.0000000	-0.5679102
N	0.0000000	-2.8179758	-1.6302478
N	0.0000000	2.8179758	-1.6302478
N	0.0000000	0.0000000	3.2562703
C	2.0660676	0.0000000	-0.3638337
C	-2.0660676	0.0000000	-0.3638337
C	0.0000000	-1.8042380	-1.0440181
C	0.0000000	1.8042380	-1.0440181
C	0.0000000	0.0000000	2.0852339

Table 6.4: Initial coordinate set for transition state

the other direction.

The transition state finder in Turbomole [46, 47, 48, 49] is accessed by changing the job file to include `jobex -statpt` and including the following in the control file

```
$statpt itrvec=X
```

Where `X` is the number of imaginary frequencies to find.

The optimisation was again carried out using DFT/B3-LYP [12, 13] and a TZVP basis set [22] for all atoms. The occupation numbers were chosen as 23 a_1, 11 b_1, 11 b_2, 3 a_2, in the α space and 22 a_1, 10 b_1, 10 b_2, 2 a_2, in the β space. This is equivalent to the $^5a_1$ state in the square based pyramid, rotated to use the axis convention for the trigonal bipyramidal system.

The Cartesian coordinates for the optimised transition state can be seen in table B.16 which is in appendix B.

Figure 6.2 shows plots of the optimised geometries for the lowest energy $S = 2$ state of the trigonal bipyramid , the transition state and the lowest energy $S = 2$ state of the square pyramid the plots were generated using Gabedit's xyz-format plotting tool [60].

As can be seen from the diagrams the transition state is not really a square pyramidal geometry but more like a distorted trigonal bipyramid. This suggests that the mechanism

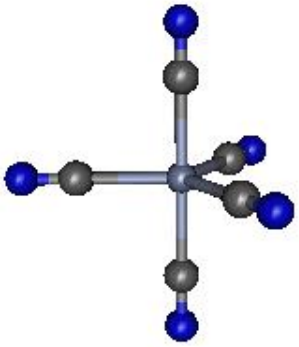

(a) Trigonal bipyramid

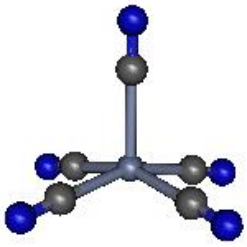

(b) square pyramid

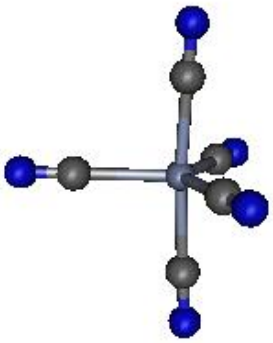

(c) Transition State

Figure 6.2: Plots of the optimised geometries for the lowest energy S = 2 states including the transition state.

is similar to a Berry pseudorotation [57, 58, 59] however the square pyramid is also a minimum on the energy surface. So the mechanism goes from the trigonal bipyramid to the transition state as an intermediate state then to the square pyramidal minimum and through a similar transition state to a different trigonal bipyramid. This mechanism will be further examined in the analysis section.

With the DFT calculations complete a further set of energies were produced using CASSCF, CASPT2 and CCSD(T) these are detailed in the next section. Some geometries were discarded due to high energies or imaginary frequencies.

6.3 CASSCF, CASPT2 and CCSD(T) Calculations

Two separate program suites will be used in this chapter, the CASSCF and CASPT2 wave functions will be calculated using MOLCAS [35] as seen before and CCSD(T) wave functions will be calculated in Molpro [30, 32, 50, 51].

This section will give example procedures for how each type of calculation is carried out.

The use of two suites of programs will affect which basis sets are used between methods. Where possible the same or similar basis sets have been used in both suites. In the MOLCAS [35] calculations the basis sets used for each atom are, an ANO-CC basis set for the chromium (this basis set is from unpublished work by B. J. Persson), and CC-PVDZ [20] basis sets for all other atoms. In Molpro [30], the basis sets used were an ANO-CC basis set for the metal centre (this basis set is from unpublished work by B. J. Persson), and CC-PVDZ [20] basis sets for all other atoms.

The calculations were carried out for the following geometries.

- In the trigonal bipyramid $^{1}a_1$ (A), $^{3}b_1$ (B), $^{3}b_2$ (A), and $^{5}a_1$.
- In the square pyramid $^{1}a_1$ (C), $^{3}a_1$, $^{3}a_2$, $^{5}a_1$ and $^{5}a_2$.
- The transition state.

Each CASPT2 calculation using MOLCAS [35] followed the same basic procedure with only the geometry, orbital numbers and active spaces changing. In order to get an

idea of how the system changed with the size of the active space, two active spaces were tested a minimal one (min) and a larger extended one (ext). For both systems the (min) space consisted of a four electron in five orbital space and had the following make up $2a_1$ $1b_1$ $1b_2$ $1a_2$. The trigonal bipyramid and transition states used the following inactive orbitals $22a_1$ $10b_1$ $10b_2$ $2a_2$ whilst the square pyramid states has the following inactive orbitals $17a_1$ $10b_1$ $10b_2$ $7a_2$. The space (ext) had different makeups dependent on the system shape. In the trigonal bipyramid and transition states ext was a fourteen electron in fourteen orbital active space and had the following make up $3a_1$ $4b_1$ $4b_2$ $3a_2$. The following inactive orbitals $20a_1$ $8b_1$ $8b_2$ $1a_2$ were used. In the square pyramid states ext was an eighteen electron in seventeen orbital active space and had the following make up $4a_1$ $4b_1$ $4b_2$ $3a_2$. The following inactive orbitals $16a_1$ $8b_1$ $8b_2$ $5a_2$ were used.

The procedure was as follows:

1. A closed shell Hartree-Fock SCF calculation in C_{2v} symmetry performed on an $S = 0$ state. See table 6.5
2. A single state CASSCF calculation was performed. The calculation used one of two active spaces (min) or (ext) as described above. The calculation was performed on the state to be investigated in each case. Level shifts were used as required to aid convergence.
3. A CASPT2 calculation was carried out using the optimised wave function from the previous step. A 0.1 imaginary level shift was used to smooth convergence.

In most cases the calculations were performed without problems, however in the case of the square pyramidal $^3a_2$ and $^5a_1$ states using the ext active space a set of CASPT2 orbitals were needed from the equivalent min active space calculation to prime the CASSCF.

As with the CASPT2 calculations a basic procedure was followed in the calculation of the CCSD(T) energies. The procedure was as follows:

1. A CASSCF calculation was performed. The calculation used the active space equivalent to the restricted Hartree-Fock SCF occupations described in table 6.3 for the

	Occupation			
System	a_1	b_1	b_2	a_2
Trigonal Bipyramid	22	11	10	3
Square Pyramid	18	10	11	7
Transition State	22	10	11	3

Table 6.5: Occupation numbers used in MOLCAS HF-SCF calculations

appropriate state. The calculation was performed on the state to be investigated in each case. This was used to produce a better starting point for the next step.

2. A restricted Hartree-Fock SCF calculation was performed on the state of interest using the orbital occupations described in table 6.3 for the appropriate state. Where necessary a level shift between the closed and open-shell orbitals was used to aid convergence.
3. A restricted CCSD(T) calculation was performed using the optimised wave function from the previous step. Where necessary a pairs denominator shift was used to aid convergence.

6.4 Results

This section will show the results derived from the calculations discussed above and further explore the proposed pseudorotation mechanism.

6.4.1 Raw Data

The data shown in table 6.6 is the raw data as extracted from the calculations. This data will be analysed later in this section. All energies are listed in E_h and rounded to six decimal places for ease of presentation.

		Methods					
Geometry	State	DFT/B3-LYP	CASSCF (min)	CASSCF (ext)	CASPT2 (min)	CASPT2 (ext)	CCSD(T)
Trigonal Bipyramid	$^{1}a_1$	-1508.406326	-1504.713855	-1504.261729	-1506.293471	-1505.643554	-1506.391219
	$^{3}b_1$	-1508.455971	-1504.771572	-1504.254633	-1506.328194	-1505.602210	-1506.428741
	$^{3}b_2$	-1508.455971	-1504.776261	-1504.295340	-1506.315885	-1505.585038	-1506.322237
	$^{5}a_1$	-1508.500134	-1504.865785	-1504.239288	-1506.397673	-1505.581771	-1506.486642
Square Pyramid	$^{1}a_1$	-1508.400928	-1504.720150	-1504.838460	-1506.286636	-1506.263958	-1506.384832
	$^{3}a_1$	-1508.300824	-1504.726937	-1504.841303	-1506.238878	-1506.213930	-1506.307212
	$^{2}a_2$	-1508.454683	-1504.775430	-1504.892910	-1504.892910	-1506.306971	-1506.432533
	$^{5}a_1$	-1508.456005	-1504.848020	-1504.930250	-1506.354038	-1506.348948	-1506.444261
	$^{5}a_2$	-1508.499951	-1504.866687	-1504.972508	-1506.398810	-1506.382881	-1506.487038
Transition State	$^{5}a_1$	-1508.499926	-1504.866358	-1504.282253	-1506.397535	-1505.582441	-1506.486639

Table 6.6: Raw data from DFT, CASSCF, CASPT2 and CCSD(T) calculations on $[Cr^{II}(CN)_5]^{3-}$

6.4.2 Analysis

From the evidence in the various calculation the complex definitely appears to be a high spin complex in both the trigonal bipyramidal and square pyramidal forms with an $S = 2$ ground state predicted for both forms. All calculation methods agreed on the ground state except the ext active space CASSCF and CASPT2 calculations where the trigonal bipyramid was predicted a $S = 1$ ground state in CASSCF and a $S = 0$ ground state in the CASPT2. All other methods also predicted a similar order of the excited states with a $S = 1$ state as the first excited state and a $S = 0$ as the second excited state at a significantly higher energy.

Table 6.7 shows the relative energies of each state to the $^5a_1$ state of the trigonal bipyramid system as a comparison between the different forms and states. All energies have been converted to electron volts (eV) using the conversion factor $1\,E_h = 27.2114\,eV$ and rounded to three decimal places for comparison.

As can be seen from table 6.7 in all cases where the $S = 2$ is the ground state the square pyramid is lower in energy than the trigonal bipyramid with the exception of DFT where the order is reversed.

6.4.3 Proposed Mechanism

As stated before the proposed mechanism containing the transition state found in this investigation is similar to a Berry pseudorotation [57, 58, 59], with a square pyramidal minimum at the centre.

Figure 6.3 shows a representation of the proposed mechanism for the pseudorotation with the two axial nitrogen's marked as N* throughout the process. The diagram was drawn using chemtool [45]. The graph in figure 6.4 shows a energy diagram of the pseudorotation based on the DFT/B3-LYP [12, 13] energies.

		Methods					
Geometry	State	DFT/B3-LYP	CASSCF (min)	CASSCF (ext)	CASPT2 (min)	CASPT2 (ext)	CCSD(T)
Trigonal Bipyramid	$^{1}a_1$	2.553	4.134	-0.611	2.835	-1.681	2.597
	$^{3}b_1$	1.202	2.564	-0.418	1.891	-0.556	1.576
	$^{3}b_2$	1.202	2.436	-1.525	2.226	-0.089	4.474
	$^{5}a_1$	0.000	0.000	0.000	0.000	0.000	0.000
Square Pyramid	$^{1}a_1$	2.700	3.963	-16.304	3.021	-18.563	2.770
	$^{3}a_1$	5.424	3.778	-16.382	4.321	-17.202	4.883
	$^{2}a_2$	1.237	2.459	-17.786	1.910	-19.734	1.472
	$^{5}a_1$	1.201	0.483	-18.802	1.187	-20.876	1.153
	$^{5}a_2$	0.005	-0.025	-19.952	-0.031	-21.799	-0.011
Transition State	$^{5}a_1$	0.006	-0.016	-1.169	0.004	-0.018	0.000

Table 6.7: energies relative to $^{5}a_1$ state of the trigonal bipyramid for calculations on $[Cr^{II}(CN)_5]^{3-}$

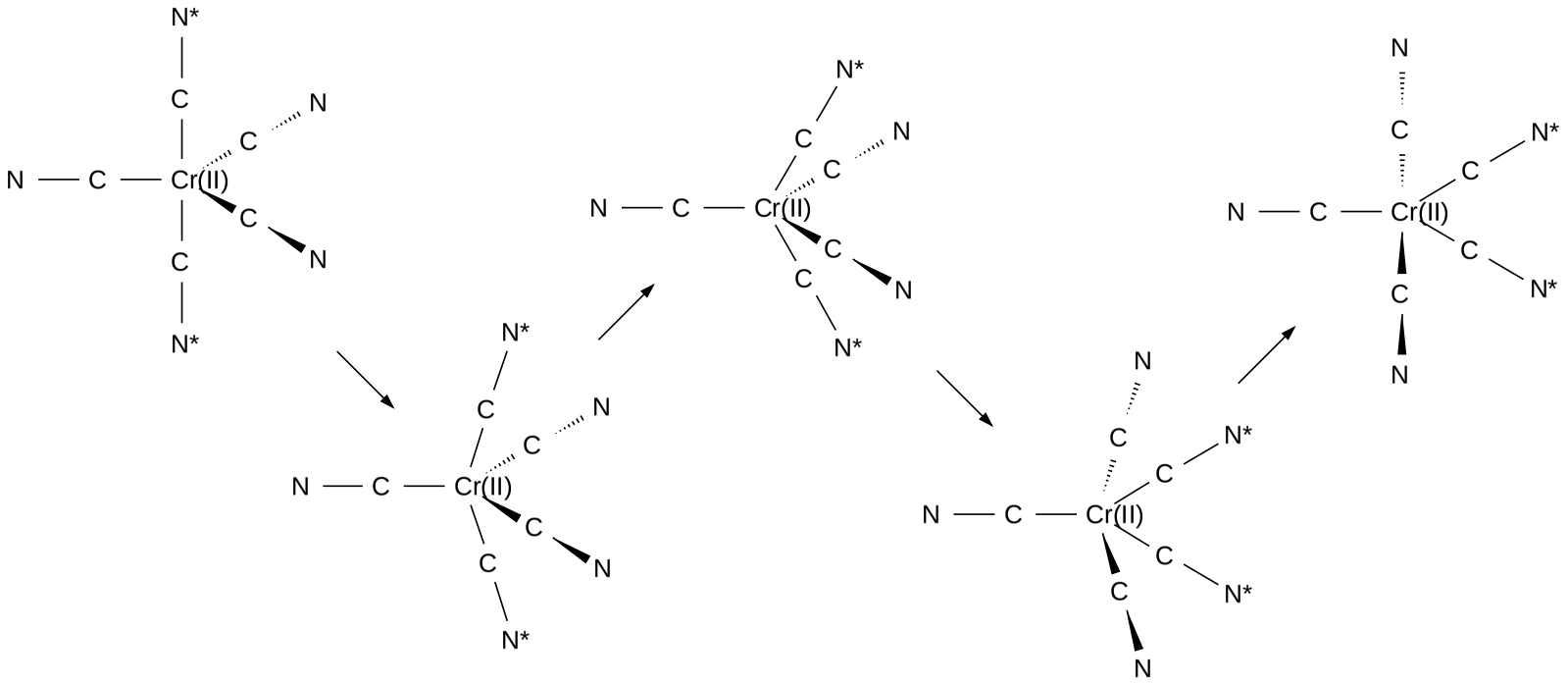

Figure 6.3: Proposed pseudorotation mechanism for $[Cr^{II}(CN)_5]^{3-}$

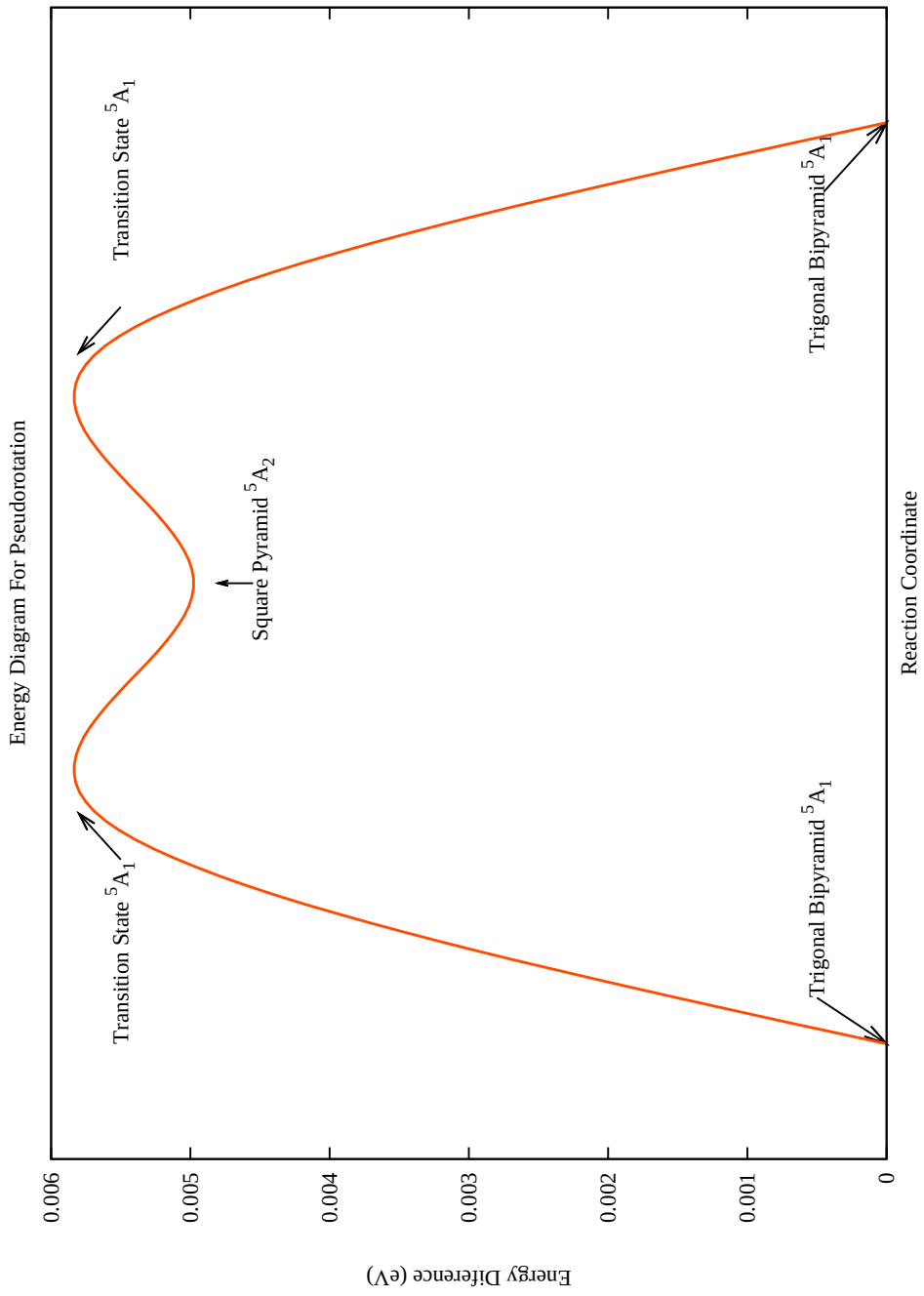

Figure 6.4: Energy diagram for $[Cr^{II}(CN)_5]^{3-}$ pseudorotation

6.5 Conclusions

The data presented in this chapter was initially going to be discarded as the method being tested failed to work sufficiently well to carry on with. Considering this much has been discovered about the $[Cr^{II}(CN)_5]^{3-}$. The use of transition state searching in Turbomole [46, 47, 48, 49] has resulted in a possible new transition state in the $[Cr^{II}(CN)_5]^{3-}$ system. This discovery may result in a new understanding of the pseudorotation mechanism in this system. With the low barriers to interconversion and pseudorotation this system is likely to be in constant flux at any but the lowest of temperatures. This may explain the scrambled geometries in crystal structure reported by by Miller et al. [53].

Overall this system has provided an interesting view of cyanide as a high field ligand, how the high spin tenancies can be overcome, the importance of pseudorotation in $M(L)_5$ systems, and the interesting world of transition states and how to find them.

Chapter 7

Creating Better Orbital Sets

7.1 Introduction

Throughout this thesis the construction of well optimised orbitals has been important to the production of a well behaved wave function and therefore accurate results. Often multiple calculations have needed to be strung together in order to produce a suitably well optimised set of orbitals with the appropriate qualities required for a particular calculation. In most cases a small number of precursor calculations have been required. Usually a Hartree-Fock calculation can be used to construct orbitals for a CASSCF whilst a CASSCF is needed for a CASPT2 or ACPF calculation. However in some cases the orbitals produced by the Hartree-Fock of CASSCF calculation are too far away from the optimal set of orbitals required to complete an optimisation or to produce a believable result. In these cases more complex calculations are required often consisting of multiple steps.

The states used in the precursor calculations are the closed shell $S = 0$ for the molecule in question in Hartree-Fock, or the the state to be used in future calculations in the case of CASSCF. This approach works most of the time as the orbital layout generally doesn't change significantly between states in the molecule or between linked methods of calculation. If the standard methods for constructing orbitals fail to give an appropriate result there are several ways to adapt the calculation to produce more suitable starting orbitals.

Firstly using well optimised orbitals constructed for a nearby state as the precursor orbitals rather than those from the ground state or a poorly optimised set from the same state may give a better result. Secondly using orbitals from the highest spin state available may help. The orbitals from the highest spin state are those most likely to contain orbitals missing from other optimised orbital sets due to having the largest number of occupied orbitals. Having the most occupied orbitals also means that more of the orbitals are better optimised. If neither of these manipulations of spin state work, then a more extreme approach may be required. Using orbitals from a similar calculation at the same level of theory is the most likely method for finding orbitals close enough to those required to produce a good result. Two types of calculation can be used to produce a set of usable orbitals, either the pre-optimised orbitals from a different spin state of the same system or orbitals optimised for a related system, which in most cases relies on changing the oxidation state or even the type of a metal atom.

Examples of the final method described above would include using a set of orbitals optimised for a Fe(III) system in a calculation on the equivalent Fe(IV) system, using a Ti(IV) system to produce orbitals representing an empty *d*-shell system or using a Zn(II) system to produce orbitals representing a totally full *d*-shell system. As a final alternative, orbitals optimised for a different geometry my be used, although if the geometries are too dissimilar orbital interactions may be changed. All these alternative methods are based on the supposition that, once a well optimised set of orbitals is produced, all subsequent calculations have a better chance of success.

These methods work well in many cases but sometimes the use of orbitals not designed for a particular system, even those from related systems results in poor compatibility, and at this point there is no good way to perform an accurate calculation. In order to solve this problem a set of orbitals with a close relation to those produced by a calculation on the appropriate system need to be constructed. This chapter describes one such approach to creating an appropriate set of orbitals. The description will include tests using two similar metal centred complexes.

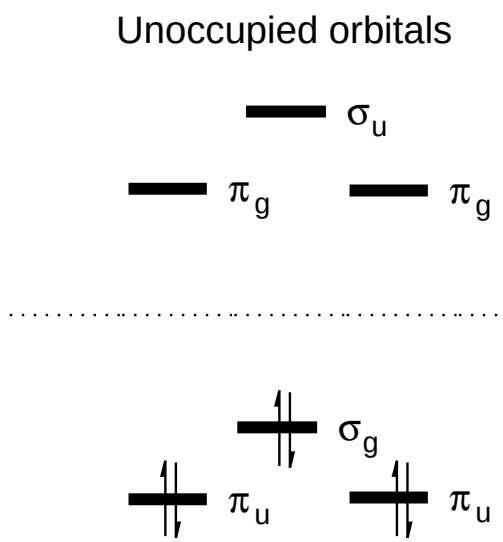

Figure 7.1: Representation of the valence orbitals of the N_2 molecule

7.2 Theory

In order to construct a better set of orbitals an understanding of what was wrong with the original set is needed.

The most common problem with an orbital set is that the unoccupied orbitals are poor approximations of the weakly occupied CASSCF active orbitals. The set of unoccupied orbitals make up part of the active space in a multiconfigurational calculation as well as the virtual orbitals. The best example of how the unoccupied orbitals are poorly optimised is in a closed shell Hartree-Fock SCF calculation. Here the unoccupied orbitals are optimised using a different potential to the occupied orbitals. The occupied orbitals see a potential of V^{N-1} where N is the number of electrons whilst the unoccupied orbitals see a potential of V^N which is equivalent to a view of an "anion" potential [61].

As an example figure 7.1 shows the the valence orbitals of the N_2 molecule. In the valence space only the σ_g and two π_u orbitals are occupied whilst the two π_g and the σ_u are unoccupied. In order to understand why the potentials are different imagine sitting on one of the electrons in the σ_g orbital. When you look out you see all the electrons except the one you are on this is equivalent to the $N-1$ electron potential. However if you sit in the empty σ_u orbital and look out you see all the electrons, this is equivalent to the N potential. The difference in the potentials results in a well optimised set of orbitals in the occupied space but a very poor representation of the orbitals in the unoccupied space. As stated in chapter 6 section 8 of Methods of Electronic Structure Theory [61, 62, 63] this

results in the unoccupied orbitals becoming very diffuse to the point that some orbitals have energies approaching zero. This blurs the line between the valence orbitals such as the π_g and σ_u orbitals in the example, and the higher virtual orbitals. This is not a problem in the closed shell Hartree-Fock SCF calculation. However when these orbitals are used to start a multireference calculation such as a CASSCF the unoccupied valence electrons are often included in the active space. If the unoccupied orbitals from the closed shell Hartree-Fock SCF calculation are too distorted then the CASSCF calculation will fail to converge due to a lack of appropriate orbitals in the active space. This is a particular problem for MOLCAS [35] as the CASSCF method used is a first order method which has a small radius of convergence. This small radius of convergence makes the method more sensitive to malformed orbitals as there is less scope for pulling in configurations using higher energy virtual orbitals which may have a better construction. A method was put in place to alleviate this problem in MOLCAS [35] using improved virtual orbitals (IVO's) [64]. The IVO's were created by changing the potential the unoccupied orbitals see from the standard V^N to the same V^{N-1} the occupied orbitals see. This change in the potential is created by removing $\frac{1}{N}$ of an electron from each occupied orbital when creating the potential. However changes to the MOLCAS [35] code have rendered this function inactive so other methods must be explored.

Other options for creating better unoccupied valence orbitals revolve around the introduction of correlation into the wave function. This improves the quality of the unoccupied valence orbitals by replacing them with the partially occupied orbitals produced by the inclusion of exited states in the wave function. A number of different orbital sets will produce good results, these include the orbitals from an open shell SCF calculation which occupies all valence orbitals, the orbitals from another CASSCF, MP2 natural orbital or CASPT2 natural orbitals.

In this chapter a method is proposed for the construction of a better orbital set. This is done by combining small subsets of CASPT2 orbitals to create a continuous set of orbitals for an entire system. This method allows for the division of problem parts of the system, and a better chance of a good set of virtual orbitals through the manipulation of different

orbital sets.

7.3 Proposal

In order to create a better set of orbitals for a calculation, an idea of which orbitals are causing problems is needed. In the systems in this thesis the orbitals most likely to cause a problem are the *d*-type orbitals associated with the transition metal atoms. These orbitals tend to be poorly optimised in calculations and can change drastically with small changes to the conditions set. In order to get accurate representations of *d*-type orbitals, large basis sets and high accuracy multiconfigurational calculations are required. This is one of the reasons that many scientists studying large systems with transition metal components have started using hybrid techniques. These use a high level multiconfigurational technique to calculate the interactions between the metal centre and the closest surrounding atoms and a faster DFT method to calculate the main body of the system.

The method proposed here is in some ways similar to the hybrid method mentioned above, in that the metal centre and the surrounding ligand system are treated separately in the calculation. The supposition is that by optimising the metal centre separate from the surrounding ligand, a more accurate representation of the pure metal centred *d*-type orbitals can be produced.

In order to produce a full set of orbitals using this method a number of different problems need to be addressed:

- Firstly a method of extracting orbitals from a calculation is needed.
- Secondly a way of making sure that the orbitals produced in each part of the calculation will interact correctly when combined.
- Thirdly a way to merge the orbitals produced and use them in a calculation.
- Finally a method for converting the newly combined orbital set, into an orthogonal set that can be used in MOLCAS [35].

The first problem is solved in the way that MOLCAS [35] handles orbitals. MOLCAS [35] prints human-readable orbitals to a set of temporary files in the working directory during a calculation, each set of orbitals is written to a specific file which can be copied back to a local directory using standard system commands. The second problem requires the orbitals produced in each set to interact correctly with each other. This means that each orbital must be optimised as if it were in the presence of all the other orbitals in the system. This problem is in some ways related to basis set superposition errors (BSSE) [65, 66]. BSSE is encountered when two or more fragments with large basis sets interact in a system. Due to the basis sets on each fragment being incomplete, the interaction of the basis sets from one fragment with the other results in a lowering of energy of both fragments. In order to correct this a counterpoise correction [65, 66, 67] is often used, this requires each fragment to be calculated in the full basis of the system and a correction made based on the energy difference. The solution to correcting the orbital interaction is similar to a counterpoise correction with each fragment calculated in the full basis for the system. In order to use the full basis with each fragment, nuclear and electronically charge-less "dummy" atoms are used to support basis functions as if the full system was present. The third problem requires a way to combine the two or more sets of orbitals together in such a way that there is a complete consistent set of orbitals, this is again partly solved by the way MOLCAS [35] handles orbitals. In a system where the atoms stay the same, the orbitals are arranged in the same order in the file produced, therefore all that is needed is a way of substituting the orbitals generated in one file into the other, for this a short program was produced in Python. The program was constructed to work with the formatted output file produced by the CASPT2 method of the MOLCAS [35] program and has not been tested on any other orbital sets produced by MOLCAS [35] or any other program, although the program could be adapted to accept other formats. The final problem requires a method for producing an orthogonal orbital set from the collection of orbitals in the new set. MOLCAS [35] automatically orthogonalises the orbital set at the start of each calculation using a Gram-Schmidt method. This means that as long as there are enough orbitals available and that the overlap of orbitals is

not too great orthogonalisation is managed by MOLCAS [35]. However as will be seen later in the next chapter a poor choice of virtual orbitals can lead to a failed orthogonalisation due to large amounts of linear dependence resulting from excessive orbital overlap. A simple way to avoid this problem would be to include all the virtual orbitals from the separate units, however restrictions in MOLCAS [35] prevent the use of more orbitals than were present in the original calculation. The only course of action is therefore trial and error in the construction of the virtual space. The easiest method and the one used here is to take all the virtual orbitals from one calculation and hope that a large enough selection is available to meet the MOLCAS [35] criteria. If this method were to fail the next best method would require an attempt to explicitly construct a set of virtual orbitals from multiple calculations.

A discussion of the program and the problems associated with its production and use will follow after the next section. A full copy of the code can be found in appendix C.

7.4 Orbital Creation

In order to produce the sets of orbitals needed to create the combined orbital set for use in experiments, the system in question must be broken down into discrete units which can be optimised separately. Each unit then needs to be optimised to the level of theory required in the final calculation in the cases seen in this thesis the CASPT2 level is used. The individual units are constructed by isolating parts of the system, and replacing the surrounding atoms with chargeless dummies carrying appropriate basis sets. In the experiments tested so far the systems used have been transition metal centred ligand systems. The test systems have a single transition metal-centre surrounded by one or more large organic ligands, this type of system is most easily split into one unit comprising the transition metal centre and one comprising the ligands. Due to the requirement to keep the symmetry of the orbitals consistent, splitting the ligands in multi-ligand systems into separate units is usually impossible.

Once the system is broken down into separate units, a calculation must be produced

to optimise each unit, therefore an idea of how the electrons are divided within the system and a strategy for distributing the electrons within the bonds between units is needed. The method used in the systems investigated in this thesis was to optimise the metal centre in an oxidation state that gives as large a number of important orbitals occupied as possible. The optimisation was done in the highest spin state resulting in the most partly filled orbitals, and thus the most orbitals requiring tight optimisation. For example the $S = \frac{5}{2}$ state of Fe(III) gives five partially full *d*-type orbitals. In the ligand unit the system was constructed as if the electrons used to form the metal-ligand bonds were present as negative charges.

Once all the parameters are known, the calculations are carried out using the following method. Here the system is optimised to the CASPT2 level and the orbitals extracted:

1. The full system geometry is optimised or a known good geometry is found.
2. The geometry is entered for the full system into the MOLCAS [35] input for each unit with an appropriate basis set.
3. For each unit the parts that are to be dummy atoms have a `Charge 0` directive added to their geometry, as shown below for an Oxygen atom.

   ```
   Basis Set O.CC-PVDZ...3s2p1d.  O1 X.XXX Y.YYY Z.ZZZ Charge 0 End of
   basis
   ```

4. A closed shell Hartree-Fock SCF calculation is carried for each unit, using the symmetry of the whole system and the orbital occupations of only the unit of interest.
5. A CASSCF calculation is carried out on each unit using a minimal active space of the most important orbitals in each unit and the highest spin available.
6. A CASPT2 calculation is carried out on each unit and the orbitals linked to an appropriate file using a system call as shown below.

   ```
   ln -fs $HomeDir/X.PT2Orb PT2ORB
   ```

   where `$HomeDir` is a link to the directory, the job was run in and `PT2ORB` is the internal MOLCAS [35] temp file containing the CASPT2 orbitals.

Once the orbital sets have been created, the appropriate orbitals must be selected from

each set and combined to form a new orbital set. This can be done by locating the appropriate orbitals from each symmetry in the output file, and noting their index which matches those in the orbital files. The orbitals are arranged by occupation number and it is reasonably easy to find the orbitals required for the inactive and active portions of each unit. Once the active and inactive portions are chosen a number of virtual orbitals need to be provided to fill the orbital set. This is done by adding the the number of active and inactive orbitals used in all units together for each symmetry, and subtracting this value from the total number of orbitals in each symmetry, as shown in the orbital file. The right number of orbitals can then be provided from the end of one of the files.

The orbitals are combined using the program described in the next section and can be included in further calculations as any other compatible orbital set. As an example to use a constructed PT2Orb file in a CASSCF leading to a CASPT2 the following input file snippet would be used:

```
cp $HomeDir/start.Orb $WorkDir/INPORB MOLCAS run rasscf <<"!"
>>$output 2>>$errlog &RASSCF &END

#INPORB 1.0 INFO * CASPT2 0 4 91 72 63 51 91 72 63 51
```

Here the first two lines show the file and section headers respectively, the third line shows the orbital type, the fourth line contains the number of spatial symmetries as the second character here 4, and the fifth and sixth lines show the total number of orbitals and basis functions respectively.

The #ORB section consists of orbital blocks for each orbital in each symmetry. It is sorted by symmetry and then by orbital occupation. The first three lines of the #ORB section are shown below for reference. Values have been trimmed to three decimal places.

```
#ORB * ORBITAL A B 0.999E+000.244E-02-.199E-050.319E-04
```

Above the first line is the section header, the second line shows the orbital labels (A, B) which are spatial symmetry and orbital number respectively, and the third line is the first of a number of lines showing the values used to construct the orbital within the program.

The #OCC section contains a list of the occupation number for each orbital in the order the orbitals are labelled in the #ORB section. The first three lines are shown below, values have been trimmed to three decimal places:

```
#OCC * OCCUPATION NUMBERS 0.200E+010.200E+010.199E+010.199E+01
```

Above the first line is the section header, the second line shows the data type and the third line shows the first line of occupation numbers.

In order to create the new orbital file the constituent orbital files need to be divided up so that each of the sections is stored separately and can be accessed for the construction of the new file.

7.4.1 The Code

The program consists of a number of parts, the pre-processing of the files, three enclosed subroutines and two main file processing loops.

In the description of the programs functions, the line numbers refer to those in the transcription of the code presented in appendix C, some lines have been split over multiple printed lines for ease of reading, where this is done only the first printed line is labelled.

The initial file processing is carried out in lines 7 through 23, here the output file (output) is created from the final argument used to run the program, a list of input files (Lin) is created from the arguments set when running the program. The first input file is opened and processed to extract important data. A temporary file is opened and the file header #INFO section and the #ORB header from the first input file are written to it. From the first input file a number of pieces of data are extracted including, the header and #INFO blocks (St), the #OCC block (Sb), the number of spatial symmetries (sym) and a list of all the orbitals in each symmetry (Lon). Line 24 sets a variable list of orbital types for later use (Lty) inactive, active and virtual.

The three subroutines are created, chop starts on line 26 , orblist starts on line 75 and imp starts on line 107.

The subroutine chop is designed to take six inputs A through F and produces a raw string of orbital blocks (S). Input A is the number of the spatial symmetry to be used,

input B is the list of text lines from an input file, input C is the orbital type either inactive, active or virtual, input D is the current working file name, input E is a list containing the selection of orbitals for each symmetry to be included, produced interactively, and input F is the a list of possible files for use in this procedure. The subroutine works by searching through the file specified in D for key strings and storing their indexes. These strings match those of the first and last orbitals defined for each symmetry and each orbital type from E. With these indexes the the subroutine creates a list of lines between the first and last orbital from the input list (B), and condenses them into a raw string text block (S).The subroutine requires some complexity due to the formatting of the orbital header lines of the orbital file and the formatting of the interactive input list(E). The header line of each orbital has an irregular number of spaces between the characters defining symmetry and orbital number, this spacing depends on the orbital number. This irregularity is corrected for in the loops between lines 42 and 58. The interactive input list (E) contains all the orbital spacing's for a certain orbital symmetry for all input files, therefore for this subroutine to process the right data, only the start and finish orbital for the specific orbital type and input file is needed. The if statements between lines 29 and 41 determine the orbital type (C) and then selects the correct starting orbital (x) and end orbital (y) for the current input file(D). As a final problem, once the subroutine has the index of the first line of the starting orbital (V), it needs to find the index of the end point of the last orbital (W), this is generally the beginning of the next orbital. If however there are no more orbitals in the symmetry it will be the first orbital in the next symmetry and if there are no more symmetries then it is the start of the #OCC section, this is handled in the if statements in lines 60 to 66.

The subroutine orblist is designed to take three inputs A, B and C and output a list of indices of orbital headers (Lorb). Input A is the number of the current symmetry, input B is the number of orbital symmetries available and input C is a list of text lines. This subroutine searches through the list of text lines finding the index of the start of each orbital block and saving them to a list (Lorb). In order to do this it searches the header text from the #INFO section in lines 78 to 80, to calculate the number of orbitals in the

current symmetry (e). The subroutine then loops through each orbital header searching for its index and adding it to the output list.

The subroutine imp takes one input A and outputs a list containing the orbitals to be taken for each input for a certain symmetry (L). A is the symmetry for the required orbitals. Imp is the interactive subroutine for this program, it writes questions to the standard output and accepts data from standard input. In lines 108 to 110 the subroutine asks for input in a standard format. This data is then parsed in lines 111 to 113 to form a standard list (L) containing only the data needed without formatting.

From lines 117 to 136 the first main loop of the program is set out. This first main loop cycles through each symmetry calling imp for that symmetry it then loops through each orbital type in each input file. The nested loops open each input file, extracts it to a list of lines (Lf), runs chop to remove the appropriate orbitals of the right symmetry and type.The orbitals are outputted to a temp file and the loop cycles to the next input file, orbital type or symmetry until all required orbitals have been written to the temp file. The end section of the orbital file specification (Sb) is then copied to the temp file. In lines 134-136 the temp file is copied to a list of lines (Ltemp) for processing and the temp file removed.

From line 138 to line 161 the final loop is run. This loop takes the list from the previous loop (Ltemp) and renames the orbital header lines so that the orbitals run in order with no duplicates. The loop runs over each orbital symmetry calling orblist, sorts the orbital header indexes and then loops over all orbital indices rewriting the orbital numbers to a continuous sequence. Lines 159-161 takes the resulting list of lines (L2) joins them to create a continuous string (S2) and writes that string to the output file.

The code has been tested and works so long as the program is called with at least one input and output file, and the orbital details are entered correctly.

This code is still a little rough and could do with some error handling and a proper input standard. When used correctly the result is a correctly formatted, usable orbital file, which conforms to the specification supplied for input to the program.

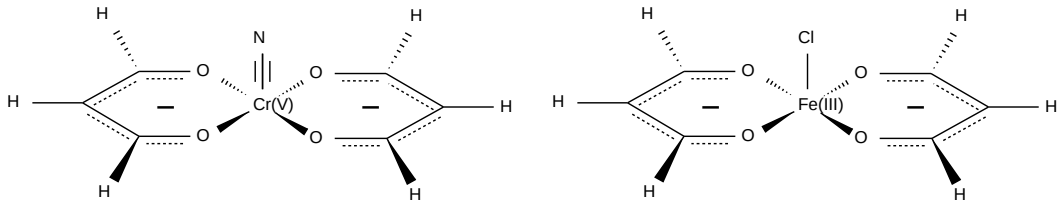

(a) $[Cr^{V}N(CH(CHO)_2)_2]$ (b) $[Cr^{III}Cl(CH(CHO)_2)_2]$

Figure 7.2: Graphical representations of the two test systems

7.5 Introduction To The Test Systems

Two test systems will be presented here to be optimised using the new orbital creation method. The main test system is $[Cr^{V}N(CH(CHO)_2)_2]$ a system that had already been examined during work on this thesis. The work was abandoned as originally the system failed to optimise correctly, even using alternative orbital optimisation methods which made it a good test for the new method. First a simplified test was needed to make sure the method would work in a practical setting. The main system contains a metal atom with an unusual oxidation state and an unusual triple bonded nitrogen ligand, which makes the optimisation difficult. In order to make the initial test system easier to optimise the system was simplified. By replacing the metal and nitrogen ligand, with a Fe(III) centre and a chloride ion this combined with the other ligands from the main system should produce a stable neutral molecule $[Fe^{III}Cl(CH(CHO)_2)_2]$. Figure 7.2 shows graphical representations of the two test systems, drawn using chemtool [45] a chemical drawing package. The bond lengths and angles shown are not representative of those in the optimised geometries and are used only for ease of representation.

In each of the test systems the bidentate ligand $CH(CHO)_2$ is a modified version of the popular acetylacetonate or acac ligand where hydrogen's have replaced the terminal methyl groups. This substitution is used to cut down the number of atoms and thus basis functions required in the calculation, and to allow for the use of higher symmetries.

7.6 Preliminary Test System: $[Fe^{III}Cl(CH(CHO)_2)_2]$

This section details the calculations carried out to test the new orbital creation methods using the preliminary test system $[Fe^{III}Cl(CH(CHO)_2)_2]$. The calculations are split into

four distinct parts. First an initial optimised geometry is produced, second a baseline data set must be produced, thirdly the new set of orbitals must be created, and finally a set of calculations must be performed using the new orbitals. Each of these steps will be detailed below.

7.6.1 Initial Optimisation

The geometry of the test system $[Fe^{III}Cl(CH(CHO)_2)_2]$ was optimised using Turbomole version 5-7-1 [46, 47, 48, 49]. The optimisation was carried out using the DFT method with a B3-LYP functional [12, 13] and a TZVP basis set [22] for all atoms.

The optimisation was carried out on the highest spin state of the molecule, in this case the $S = \frac{5}{2}$. The first optimisation failed to converge to a satisfactory result: although the geometry was a stationary point, on calculating the vibrational frequencies using Turbomole [46, 47, 48, 49] there were three imaginary frequencies. In an attempt to rectify this, a new set of orbitals were created in the hopes that they would be closer to those of the minimum of the system. The orbitals were constructed by substituting the Iron (III) centre for a Scandium (III) centre which has no occupied *d*-type orbitals.

The starting geometry used in these calculations is the same as the optimised geometry produced in the $[Cr^{V}N(CH(CHO)_2)_2]$ calculations, these will be discussed in the next section. In order to carry out the calculation on the Iron (III) system, a number of steps were required as described below.

1. A geometry optimisation was carried out on the system using a Sc(III) centre rather than a Fe(III) centre.The calculation used a TZVP basis set [22], B3-LYP functional [12, 13], and the $[Cr^{V}N(CH(CHO)_2)_2]$ geometry. The calculation was on a $S = 0$ a_1 state in C_{2v} symmetry with the following occupation numbers, $21a_1$ $15b_1$ $12b_2$ $8a_2$ for both α and β orbitals.
2. The α and β orbital sets from the Sc(III) calculation were copied to a new folder.
3. A new calculation was set up for the optimisation of the Fe(III) system using the same basis set, functional and geometry as before, with the Sc(III) centre replaced with a Fe(III) centre. The optimisation was set up for a $S = \frac{5}{2}$ a_1 state with occupa-

Atom	X	Y	Z
Fe	0.000000	0.000000	-0.232698
O	-2.562608	2.589608	0.844889
O	-2.562608	-2.589608	0.844889
O	2.562608	-2.589608	0.844889
O	2.562608	2.589608	0.844889
Cl	0.000000	0.000000	-4.406413
C	-4.883137	2.299455	1.362525
C	-4.883137	-2.299455	1.362525
C	4.883137	-2.299455	1.362525
C	4.883137	2.299455	1.362525
C	6.142518	0.000000	1.617841
C	-6.142518	0.000000	1.617841
H	-5.959594	4.045394	1.645809
H	-5.959594	-4.045394	1.645809
H	5.959594	-4.045394	1.645809
H	5.959594	4.045394	1.645809
H	8.132690	0.000000	2.075451
H	-8.132690	0.000000	2.075451

Table 7.1: Optimised geometry of $[Fe^{III}Cl(CH(CHO)_2)_2]$

tion numbers $23a_1$ $16b_1$ $13b_2$ $9a_2$ for the α orbitals and $21a_1$ $15b_1$ $12b_2$ $8a_2$ for the β orbitals.

4. The α and β orbitals from the Sc(III) calculation are copied over the α and β orbitals calculated by Define, the Turbomole [46, 47, 48, 49] input creation tool.

The Cartesian coordinates of the final geometry produced is shown in table 7.1. All values are in a_0 and presented to six decimal places.

7.6.2 Baseline Calculations

Using the DFT geometry, it was possible to move on to the next step of the calculation which was to produce a set of values using the standard calculation methods available in the MOLCAS [35] program suite. Three test calculations were prepared with slight differences in order to test how the new orbital creation method fared in different situations.

Both the first and second test use the same nine electron in nine orbital active space, but differ in the distribution of orbitals in the inactive space whilst the third test uses a larger thirteen electron in thirteen orbital active space. The first two tests compare how well the new orbitals adapt to a using a different electronic configuration from the one used to create them. Test three looks at how well the virtual orbitals are optimised, as the new orbitals in the larger active space will be pulled from the virtual orbitals.

Table 7.2 shows the orbital configurations used in the three test systems A, B, and C.

		Active Space				Inactive Space			
Test	Active e^-	a_1	b_1	b_2	a_2	a_1	b_1	b_2	a_2
A	9	3	2	2	2	21	15	10	8
B	9	3	2	2	2	20	14	12	8
C	13	5	4	2	2	19	13	12	8

Table 7.2: Test active space configurations for $[Fe^{III}Cl(CH(CHO)_2)_2]$

The three test setups use the same basis sets and basic method. The basis sets used for each atom are, an ANO-CC basis set for the Iron centre (this basis set is from unpublished work by B. J. Persson), aug-CC-PVDZ [68] basis set for chlorine, and CC-PVDZ [20] basis sets for all other atoms. The general method for each calculation is set out as follows:

1. A closed shell Hartree-Fock SCF calculation in C_{2v} symmetry performed on the $S = 0$ state . For test A the orbital occupation numbers were $22a_1\ 16b_1\ 12b_2\ 8a_2$ for both α and β orbitals and for tests B and C the orbital occupation numbers were $21a_1\ 16b_1\ 13b_2\ 8a_2$ for both α and β orbitals.
2. A single state CASSCF calculation was performed. The calculation used the active spaces as described in table 7.2 and was performed on the a_1 symmetry $S = \frac{5}{2}$ state in each case. A level shift of 1.45 was required to aid convergence.
3. A CASPT2 calculation was carried out using the optimised wave function from the previous step. The calculation used a set of frozen orbitals to reduce compute time and a 0.1 imaginary level shift to accelerate convergence. The frozen orbitals used were $8a_1\ 4b_1\ 3b_2\ 2a_2$.

The results of these calculations along with those from the constructed orbital set will be detailed in the results section.

7.6.3 Orbital Construction and Testing

In order to construct the new orbital set, a calculation is needed to produce orbital sets for each separate sub-unit. These orbital sets can then be combined to produce the new orbital set. There are many ways this system can be split in order to isolate different parts of the molecule but in order to maintain the symmetry of the system and keep as many bond as possible intact, only three splits seem reasonable. The three splits considered were:

1. A three way split with the Fe(III) centre in one unit, the Cl^- ion in another unit and the two $(CH(CHO)_2)^-$ ions in a third unit.
2. A two way split with the Fe(III) centre and the Cl^- ion in one unit and the two $(CH(CHO)_2)^-$ ions in another unit.
3. A two way split with the Fe(III) centre in one unit and both the two $(CH(CHO)_2)^-$ ions and the Cl^- ion in another unit.

For maximum flexibility the first option would be preferable. However as this is the first test of this system, and as the problem in the main test system is most likely the optimisation of metal centre orbitals the third option was chosen. This option has the advantage of singling out the metal centre from the ligands, whilst not making the orbital construction too difficult and time consuming.

Using the split from option three, two calculations are required, one calculating the orbitals for the metal centre in isolation from the ligands, and one to calculate the ligand orbitals in isolation from the metal centre. As described in section 7.4, this can be done by modifying the geometry input to set the nuclear charge of the atom or atoms not present in the calculation to zero and not including their electron configurations.

The calculation on each unit follows the same basic format as detailed below, any differences in the setup between the units are listed where necessary. All basis sets used are as specified in the baseline calculations.

1. For each unit a closed shell Hartree-Fock SCF calculation in C_{2v} symmetry was performed on the S = 0 state. For the Fe(III) centre the orbital occupation numbers were $7a_1$ $3b_1$ $2b_2$ $0a_2$ for both α and β orbitals, and for the ligands the orbital occupation numbers were $16a_1$ $13b_1$ $10b_2$ $8a_2$ for both α and β orbitals.
2. For each unit a single state CASSCF calculation was performed. For the Fe(III) centre the calculation was carried out on the $S = \frac{5}{2}$ a_1 state using a five electron in five orbital active space of the form $2a_1$ $1b_1$ $1b_2$ $1a_2$ with the following inactive orbitals $5a_1$ $2b_1$ $2b_2$ $0a_2$. For the ligands, the calculation was carried out on the S = 2 a_1 state using a four electron in four orbital active space of the form $1a_1$ $1b_1$ $1b_2$ $1a_2$ with the following inactive orbitals $15a_1$ $12b_1$ $10b_2$ $8a_2$. In both cases a 1.45 level shift was used to aid convergence.
3. For each unit a CASPT2 calculation was carried out using the optimised wave function from the previous step. The calculation used a set of frozen orbitals to reduce compute time and a 0.1 imaginary level shift to accelerate convergence. The frozen orbitals used were $2a_1$ $0b_1$ $0b_2$ $0a_2$ for the Fe(III) centre and $5a_1$ $3b_1$ $3b_2$ $2a_2$ for the ligands. The CASPT2 orbitals are copied to an appropriate file in the calculations home directory for processing.

Once the calculations have been performed the orbital sets from the two units are ready for compiling into a new set. To compile a new set, parts of each set need to be divided off from the different CASPT2 orbital files. The code discussed in section 7.4.1 is designed to do this once the right orbitals have been selected. For this system, the orbital set was constructed based on the sum of the active space configurations of the unit CASSCF calculations, this sum also gives rise to the active space configuration in test A. The virtual orbitals are taken from the metal orbital set and selected to fill the full quota of orbitals as defined at the top of the CASPT2 orbital file. Table 7.3 shows how this file is constructed from the orbital files using the ordered orbital numbering in the file, each range represents all orbitals from a file included in that range.

	Number of orbitals of symmetry			
File/Orbital use	a_1	b_1	b_2	a_2
Fe(III)/Inactive	1-5	1-2	1-2	0
Ligand/Inactive	1-15	1-12	1-10	1-8
Fe(III)/Active	6-7	3	3	1
Ligand/Active	16	13	11	9
Fe(III)/Virtual	24-91	17-72	15-63	11-51
Ligand/Virtual	0	0	0	0

Table 7.3: constructed orbital set for $[Fe^{III}Cl(CH(CHO)_2)_2]$ listed by file and orbital use.

The new orbital set was created as specified in table 7.3, and saved to a new directory for use in the next set of calculations.

With the new orbital set created, the final stage is to repeat the test cases detailed in section 7.6.2 using the new orbital set. In order to do this the calculation method needs to be modified slightly. The closed shell Hartree-Fock SCF calculation is no longer necessary, as the CASSCF calculation is now primed with the new CASPT2 orbital set. This is done using the following system call `cp $HomeDir/X.Orb $WorkDir/INPORB` which copies the orbital set `X.Orb` from the calculation home directory to the MOLCAS [35] temporary file `INPORB` . `INPORB` is the MOLCAS [35] orbital set used as the starting orbitals for the CASSCF calculations. With these modifications the calculations are carried out using the same steps as listed in the baseline tests.

7.6.4 Results and Conclusions

Table 7.4 shows the raw CASSCF and CASPT2 energies for both the baseline, closed shell Hartree-Fock SCF based calculations and the constructed orbital calculations for each test case. Included are the CASPT2 reference weights which gives an indication of how close to the reference CASSCF wave function the CASPT2 solution is. All energies are in E_h and rounded to six decimal places for display.

Table 7.5 shows the orbital occupations for the dominant configuration contributing to the CASSCF solution used in each test. In the table *u* stands for a single electron spin

Calculation	CASSCF Energy	CASPT2 Energy	Reference Weight
Baseline A	-2251.798013	-2254.001264	0.44586
Constructed A	-2251.806965	-2253.860490	0.52818
Baseline B	-2251.956697	-2254.261354	0.58497
Constructed B	-2252.349959	-2254.579668	0.28453
Baseline C	-2252.010297	-2254.319616	0.59295
Constructed C	-2252.386248	-2254.694928	0.40481

Table 7.4: Raw data from baseline and constructed orbitals set calculations on $[Fe^{III}Cl(CH(CHO)_2)_2]$.

	Orbital symmetry				
calculation	a_1	b_1	b_2	a_2	Weight
Baseline A	*u*,*d*,*u*	2,0	*u*,*u*	*u*,*u*	0.30674
Constructed A	*u*,*u*,2	*u*,0	2,*u*	*u*,0	0.27134
Baseline B	*u*,*u*,0	2,*u*	*u*,2	*u*,0	0.26133
Constructed B	2,2,*u*	*u*,*u*	*u*,*u*	0,0	0.43651
Baseline C	2,*u*,*u*,0,0	2,2,*u*,0	2,*u*	*u*,0	0.97905
Constructed C	2,2,*u*,*u*,0	2,2,*u*,0	*u*,0	*u*,0	0.77106

Table 7.5: Dominant orbital configuration in the CASSCF for all tests

up or with a spin projection quantum number of $+\frac{1}{2}$ whilst *d* stands for a single electron spin down or with a spin projection quantum number of $-\frac{1}{2}$.

As can be seen from the results in two out of the three tests the constructed orbital set gives a better result than the same calculation using a SCF staring orbital set. In the case of test A whilst the CASSCF result gave a lower energy using the constructed orbitals, the CASPT2 shows a large difference in energy in favour if the SCF orbital set. Looking at the reference weights for systems A and B whilst the values for system A are relatively close and around 0.5 the value for the constructed orbital set in system B is a lot lower at around 0.28. A low reference weight tends to suggest a poor result so although the energy is lower than the baseline in this case the result is questionable. A look at the dominant configurations for both test A and B shows an unusual dominant configuration in the baseline calculations for both tests. Test A shows a set of electrons spin paired across two orbital in the a_1 space which is an unusual occurrence. Test B

shows the filled b_2 orbital in the second position which is usually of a higher energy. These unusual dominant orbital configurations may suggest that the wave functions were not fully converged or converged to less than optimal wave functions using SCF orbitals. The weight of these dominant configurations is relatively low in both cases, this may help the CASPT2 converge to a better solution as other minor configurations may become more important. With a more normal configuration and a higher weight the constructed orbital calculation in test B shows a significantly lower CASSCF and CASPT2 energy. These lower energies may also be due to the overall active space configuration in tests B and C being more in line with the optimum configuration for the system. Test C shows a large improvement in all energies and a sensible configuration in both the SCF and constructed orbital set calculations, although each calculation has a different dominant configuration. Part of the energy improvement can be attributed to the larger active space which increases the degree of freedom in the system and usually results in lower energies overall, but the larger weighted dominant configurations of a sensible makeup may also have played a part.

Based on these tests, the constructed orbital sets have proven to be as good if not better, as a starting guess for this system as a preliminary optimised closed shell Hartree-Fock SCF orbital set. The two approaches produced different results in each of the tests. With better results in both tests B and C, where the active spaces were different than the active space the orbitals were constructed for, these orbitals have shown they work outside the limits of their construction, highlighting the need for a well thought out active space in CASSCF calculations.

7.7 Main Test System: $[Cr^{V}N(CH(CHO)_2)_2]$

The main test system $[Cr^{V}N(CH(CHO)_2)_2]$ was to be investigated in detail in this thesis, due to the interesting triple bonded nitrogen ligand (nitrido). The nitrido ligand is interesting in that it is one of the most strongly electron-donating ligands available. This is due to the three electrons available for donation and the strength of the nitrogen triple bond.

The strength of its electron-donation can produce unusual oxidation states in metals such as Fe(VI) [69] which was also of interest. After several failed attempts to produce an optimised geometry or wave function, work on these systems halted. When the constructed orbital set method was attempted, these nitrido complexes seemed like a good test. As chromium compounds of this sort appear more in literature than the Fe(VI) systems, the chromium test system was chosen. There is evidence for several Cr(V) complexes with multidentate ligands [70, 71, 72, 73] including macrocycles [74] (large multidentate ligands that fully surround a metal centre) available in literature. This includes the synthesis of a functionalised analogue of the test system [75].

7.7.1 Method

After the success of the preliminary test system, an attempt was made to again produce useful results for $[Cr^{V}N(CH(CHO)_2)_2]$. A DFT/B3-LYP [12, 13] optimised geometry with all real frequencies was produced in Turbomole [46, 47, 48, 49] version 5-7-1 using a SVP [23] basis set for all atoms.Table 7.6 shows the set of Cartesian coordinates of the optimised geometry of $[Cr^{V}N(CH(CHO)_2)_2]$ used in all subsequent calculations on this system. The data is shown to six decimal places and with all distances in a_0.

As attempts to calculate CASSCF and CASPT2 wave functions for this system with conventional orbital sets had already failed, no baseline calculations can be produced. The next step in the testing of this system is therefore to produce the separate units that will be used in constructing the new orbital set. As in the preliminary system the complex was split into a metal unit and a ligand unit. For each unit a set of CASPT2 orbitals were produced using the method detailed below. The basis sets used for each atom are, an ANO-CC basis set for the chromium centre (this basis set is from unpublished work by B. J. Persson), an aug-CC-PVDZ [21] basis set for Nitrogen, and CC-PVDZ [20] basis sets for all other atoms.

1. For each unit a closed shell Hartree-Fock SCF calculation in C_{2v} symmetry was performed on the $S = 0$ state. For the Cr(V) centre the orbital occupation num-

Atom	X	Y	Z
Cr	0.000000	0.000000	-0.563579
O	-2.524343	2.604544	0.3244380
O	-2.524343	-2.604544	0.324438
O	2.524343	-2.604544	0.324438
O	2.524343	2.604544	0.324438
N	0.000000	0.000000	-3.416683
C	-4.873340	2.305233	0.665571
C	-4.873340	-2.305233	0.665571
C	4.873340	-2.305233	0.665571
C	4.873340	2.305233	0.665571
C	6.171219	0.000000	0.764802
C	-6.171219	0.000000	0.764802
H	-5.968156	4.063535	0.957105
H	-5.968156	-4.063535	0.957105
H	5.968156	-4.063535	0.957105
H	5.968156	4.063535	0.957105
H	8.206854	0.000000	1.085731
H	-8.206854	0.000000	1.085731

Table 7.6: Optimised geometry of $[Cr^{V}N(CH(CHO)_2)_2]$

bers were $4a_1$ $1b_1$ $1b_2$ $1a_2$ for both α and β orbitals and for the ligands the orbital occupation numbers were $15a_1$ $13b_1$ $10b_2$ $7a_2$ for both α and β orbitals.

2. For each unit a single state CASSCF calculation was performed. For the CrV centre the calculation was carried out on the $S = \frac{5}{2}$ a_1 state using a five electron in five orbital active space of the form $2a_1$ $1b_1$ $1b_2$ $1a_2$ with the following inactive orbitals $5a_1$ $2b_1$ $2b_2$ $0a_2$. For the ligands the calculation was carried out on the $S = 2$ a_1 state using a four electron in four orbital active space of the form $1a_1$ $1b_1$ $1b_2$ $1a_2$ with the following inactive orbitals $15a_1$ $9b_1$ $11b_2$ $6a_2$. In both cases a 1.45 level shift was used to aid convergence.
3. For each unit a CASPT2 calculation was carried out using the optimised wave function from the previous step. The calculation used a set of frozen orbitals to reduce compute time and a 0.1 imaginary level shift to accelerate convergence. The frozen orbitals used were $2a_1$ $0b_1$ $0b_2$ $0a_2$ for the Cr(V) centre and $6a_1$ $2b_1$ $2b_2$ $1a_2$ for the ligands. The CASPT2 orbitals are copied to an appropriate file in the calculations home directory for processing.

Once the two sets of orbitals had been optimised the orbitals from each set were combined to form a new orbital set using the Python code detailed in section 7.4.1.

The new orbital set is constructed as detailed in table 7.7. Individual segments of the orbital files are arranged using the ordered orbital numbering in each file. The ranges in the table represent all orbitals included in that segment of the file.

	Number of orbitals of symmetry			
File/Orbital use	a_1	b_1	b_2	a_2
Cr(V)/Inactive	1-5	1-2	1-2	0
Ligand/Inactive	1-15	1-9	1-11	1-6
Cr(V)/Active	6-7	3	3	1
Ligand/Active	16	10	12	7
Cr(V)/Virtual	24-89	14-71	16-62	9-51
Ligand/Virtual	0	0	0	0

Table 7.7: constructed orbital set for [Cr*V*N(CH(CHO)$_2$)$_2$] listed by file and orbital use.

Once the new orbital set was constructed, the calculation on the full system could be carried out. The closed shell Hartree-Fock SCF calculation is no longer necessary as the CASSCF calculation is now primed with the new CASPT2 orbital set in the same was as described for the preliminary tests. The calculation is then carried out using the same steps as listed in the baseline tests for both the $^2a_1$ and $^6a_1$ states. The CASSCF calculations used a 9 electron in 10 orbital active space of the following make up $3a_1$ $3b_1$ $3b_2$ $1a_2$ with the following inactive orbitals $18a_1$ $12b_1$ $10b_2$ $8a_2$ and a 1.45 level shift to aid convergence. The CASPT2 calculation used frozen orbitals of the form $8a_1$ $2b_1$ $2b_2$ $1a_2$ to reduce the time and an imaginary level shift of 0.1 to accelerate convergence.

With the constructed orbital set as defined the CASSCF convergence was poor and failed due to a large numbers of deleted orbitals in the virtual space leading to a linear dependence in the orbital optimisation probably as a result of a failed orthogonalisation. In order to solve this problem the calculations were repeated with a new orbital set constructed with virtual orbitals from the ligand file. This orbital set has the same makeup as the first set except that the virtual orbitals have been taken from the ligand orbital set. This change in the virtual orbitals finally produced a set of usable results which are reported below.

7.7.2 Results and Conclusions

Table 7.8 shows the raw CASSCF and CASPT2 energies for the constructed orbital calculations on each state in the test system, also included are the CASPT2 reference weights which gives an indication of how close to the reference CASSCF wave function the CASPT2 solution is. All energies are in E_h and rounded to six decimal places for display.

Table 7.9 shows the orbital occupations for the dominant configuration contributing to the CASSCF solution used in each state. In the table *u* stands for a single electron spin up or with a spin quantum number of $+\frac{1}{2}$ whilst *d* stands for a single electron spin down or with a spin quantum number of $-\frac{1}{2}$.

Calculation	CASSCF Energy	CASPT2 Energy	Reference Weight
$S = \frac{1}{2}$ a_1	-1628.041562	-1630.197684	0.60375
$S = \frac{5}{2}$ a_1	-1627.640636	-1629.952704	0.46258

Table 7.8: Raw data from $S = \frac{1}{2}$ and $S = \frac{5}{2}$ a_1 constructed orbitals set calculations on $[Cr^{V}N(CH(CHO)_2)_2]$.

	Orbital Symmetry				
Calculation	a_1	b_1	b_2	a_2	Weight
$S = \frac{1}{2}$ a_1	2,*u*,0	2,2,0	2,2,0	0	0.78141
$S = \frac{5}{2}$ a_1	*u*,*u*,0	*u*,2,0	2,*u*,0	*u*	0.92227

Table 7.9: Dominant orbital configuration in the CASSCF for all tests

In this case with no other computational evidence to verify the results of these calculations, the only information to comment on is the results themselves. The two calculations both show energies in the same range although the $S = \frac{1}{2}$ state CASSCF is quite a bit lower in energy than the $S = \frac{5}{2}$ state, this is not too unusual as a $S = \frac{5}{2}$ state is usually a much less stable spin state, as it has five unpaired electrons. The differences in the CASPT2 energies are smaller but still significant and in line with those from the CASSCF calculations. Both CASPT2 calculations have a decent reference weight suggesting the wave function created using the constructed orbitals had a significant correlation with the final CASPT2 wave function, the $S = \frac{1}{2}$ reference weight especially suggests a very good correlation. Looking at the CASSCF dominant configurations, the $S = \frac{1}{2}$ state has a reasonable configuration within the expected ordering with a decent weight, however the $S = \frac{5}{2}$ configuration has an unusual electron ordering in the b_2 space with an unpaired electron in the first position, and paired electrons in the second. The fact that this configuration is so dominant with a weight that converts to over ninety percent of all configurations may have to do with the smaller reference weight in the CASPT2 calculation and the large gap in the CASSCF energies.

7.8 Overall Conclusions

Over the two test systems shown in this chapter the new orbital construction method has consistently shown better results compared to a traditional orbital system using a closed shell Hartree-Fock SCF calculation. In the first system, in two out of the three tests the energies produced using the constructed orbitals were lower than those of the baseline, and in the other test other factors contributed to the poor results. In the second system after some trouble with virtual orbitals which could always be a weakness for this method, a result was produced where no other method had worked. These successes suggest that this method should be applicable in any situation where traditional means of creating an orbital set have failed.

With more time this method could be further tested and the range of applications increased. Interesting ideas for further testing, include further subdividing of the molecule to produce smaller, more tightly optimised orbital sets, and work on systems where a metal is not the centre of the molecule or the main target of the method.

Chapter 8

Conclusions

The aim of this thesis was to investigate new procedures to aid in the calculation of large transition metal systems and investigations have been carried out into two new procedures and a number of transition metal systems.

The first new method used active spaces centred on atoms rather than the standard delocalised active spaces used in most calculations. This method ultimately proved inconsistent in its results and ultimately would be unusable in its current form. Even if the inconsistency in the results could be improved the level of human interaction required to properly construct the local active spaces make it a poor fit for the type of automated computation that is needed for most circumstances.

The second method looked at ways of improving and controlling starting orbitals for multiconfigurational calculations. The method produced new orbital sets by combining sets from small subunits of the full system. The method allowed control over the construction of the new orbital set, using a custom script also detailed. This method was more successful and with work on integration of the calculations and the script a level of automation could be achieved. The method allowed calculation of a system that had failed to work using other methods suggesting that the new orbital set created was better suited to the system.

As well as the new methods a set of related complexes were investigated. An in depth comparison between results from the DFT functional OLYP [37] and those from

CASSCF, CASPT2 and CCSD(T) calculations was made. This investigation has provided some calibration of the OLYP functional as used in large transition metal systems.

Finally an investigation was carried out on the system $[Cr^{II}(CN)_5]^{3-}$ leading to a new transition state. Through optimisation of this result a transition state was confirmed and a mechanism was suggested.

In meeting the aim of this thesis a new process has been implemented and another shown to be troublesome. As a part of this thesis a number of interesting systems have been investigated and the results provide new insights into the world of transition metal chemistry.

Appendix A

DFT Geometries

This appendix contains sets of Cartesian coordinates for all systems used in chapter 5. All values are in a_0 and rounded to six decimal places.

A.1 Fe(III)

A.1.1 System A

Atom	X	Y	Z
Fe	0.000000	0.000000	1.740985
N	0.000000	0.000000	4.888567
N	2.562347	0.000000	-0.807142
N	-2.562347	0.000000	-0.807142
C	2.308264	0.000000	-3.294597
C	-2.308264	0.000000	-3.294597
C	0.000000	0.000000	-4.558815
H	4.389872	0.000000	-0.236699
H	-4.389872	0.000000	-0.236699
H	4.022192	0.000000	-4.434696
H	-4.022192	0.000000	-4.434696
H	0.000000	0.000000	6.820869
H	0.000000	0.000000	-6.600874

Table A.1: Cartesian coordinates for system A Fe(III) $^2A_1$.

Atom	X	Y	Z
Fe	0.000000	0.000000	1.775203
N	0.000000	0.000000	4.929436
N	2.550541	0.000000	-0.843808
N	-2.550541	0.000000	-0.843808
C	2.302415	0.000000	-3.327215
C	-2.302415	0.000000	-3.327215
C	0.000000	0.000000	-4.601825
H	4.380766	0.000000	-0.280334
H	-4.380766	0.000000	-0.280334
H	4.018189	0.000000	-4.467764
H	-4.018189	0.000000	-4.467764
H	0.000000	0.000000	6.861907
H	0.000000	0.000000	-6.643494

Table A.2: Cartesian coordinates for system A Fe(III) $^2A_2$.

Atom	X	Y	Z
Fe	0.000000	0.000000	1.738748
N	0.000000	0.000000	4.976021
N	2.691175	0.000000	-0.834861
N	-2.691175	0.000000	-0.834861
C	2.338338	0.000000	-3.310334
C	-2.338338	0.000000	-3.310334
C	0.000000	0.000000	-4.532400
H	4.537748	0.000000	-0.335151
H	-4.537748	0.000000	-0.335151
H	4.010274	0.000000	-4.513806
H	-4.010274	0.000000	-4.513806
H	0.000000	0.000000	6.889571
H	0.000000	0.000000	-6.575112

Table A.3: Cartesian coordinates for system A Fe(III) $^4B_1$.

Atom	X	Y	Z
Fe	0.000000	0.000000	1.761220
N	0.000000	0.000000	5.015225
N	2.703466	0.000000	-0.864700
N	-2.703466	0.000000	-0.864700
C	2.337980	0.000000	-3.332853
C	-2.337980	0.000000	-3.332853
C	0.000000	0.000000	-4.556240
H	4.554407	0.000000	-0.380373
H	-4.554407	0.000000	-0.380373
H	4.004760	0.000000	-4.546182
H	-4.004760	0.000000	-4.546182
H	0.000000	0.000000	6.928383
H	0.000000	0.000000	-6.598565

Table A.4: Cartesian coordinates for system A Fe(III) $^4B_2$.

Atom	X	Y	Z
Fe	0.000000	0.000000	1.770814
N	0.000000	0.000000	5.054035
N	2.810173	0.000000	-0.890327
N	-2.810173	0.000000	-0.890327
C	2.362456	0.000000	-3.347964
C	-2.362456	0.000000	-3.347964
C	0.000000	0.000000	-4.533112
H	4.678787	0.000000	-0.478723
H	-4.678787	0.000000	-0.478723
H	3.991442	0.000000	-4.613245
H	-3.991442	0.000000	-4.613245
H	0.000000	0.000000	6.963068
H	0.000000	0.000000	-6.576593

Table A.5: Cartesian coordinates for system A Fe(III) $^6A_1$.

Atom	X	Y	Z
Fe	0.000000	0.000000	-1.887334
N	0.000000	0.000000	1.337819
N	2.566430	0.000000	-4.440871
N	-2.566430	0.000000	-4.440871
C	0.000000	0.000000	3.880825
C	0.000000	0.000000	-8.191919
C	2.308994	0.000000	-6.927720
C	-2.308994	0.000000	-6.927720
C	2.286044	0.000000	7.873642
C	-2.286044	0.000000	7.873642
C	2.300665	0.000000	5.259369
C	-2.300665	0.000000	5.259369
C	0.000000	0.000000	9.194405
H	4.056883	0.000000	8.902902
H	-4.056883	0.000000	8.902902
H	4.055529	0.000000	4.206559
H	-4.055529	0.000000	4.206559
H	4.396329	0.000000	-3.878947
H	-4.396329	0.000000	-3.878947
H	4.021578	0.000000	-8.070756
H	-4.021578	0.000000	-8.070756
H	0.000000	0.000000	-10.233918
H	0.000000	0.000000	11.241374

Table A.6: Cartesian coordinates for system B Fe(III) $^2A_1$.

A.1.2 System B

Atom	X	Y	Z
Fe	0.000000	0.000000	-1.865463
N	0.000000	0.000000	1.361034
N	2.558354	0.000000	-4.488976
N	-2.558354	0.000000	-4.488976
C	0.000000	0.000000	3.903047
C	0.000000	0.000000	-8.244467
C	2.303779	0.000000	-6.970703
C	-2.303779	0.000000	-6.970703
C	2.286329	0.000000	7.895949
C	-2.286329	0.000000	7.895949
C	2.300608	0.000000	5.281829
C	-2.300608	0.000000	5.281829
C	0.000000	0.000000	9.216540
H	4.056966	0.000000	8.925600
H	-4.056966	0.000000	8.925600
H	4.054530	0.000000	4.227436
H	-4.054530	0.000000	4.227436
H	4.390925	0.000000	-3.934022
H	-4.390925	0.000000	-3.934022
H	4.017527	0.000000	-8.115455
H	-4.017527	0.000000	-8.115455
H	0.000000	0.000000	-10.286049
H	0.000000	0.000000	11.263535

Table A.7: Cartesian coordinates for system B Fe(III) $^2A_2$.

Atom	X	Y	Z
Fe	0.000000	0.000000	-1.899800
N	0.000000	0.000000	1.384244
N	2.698522	0.000000	-4.512985
N	-2.698522	0.000000	-4.512985
C	0.000000	0.000000	3.926399
C	0.000000	0.000000	-8.207543
C	2.336330	0.000000	-6.983125
C	-2.336330	0.000000	-6.983125
C	2.266838	0.000000	7.926314
C	-2.266838	0.000000	7.926314
C	2.293048	0.000000	5.307356
C	-2.293048	0.000000	5.307356
C	0.000000	0.000000	9.268216
H	4.050436	0.000000	8.935776
H	-4.050436	0.000000	8.935776
H	4.063870	0.000000	4.281643
H	-4.063870	0.000000	4.281643
H	4.549291	0.000000	-4.026887
H	-4.549291	0.000000	-4.026887
H	4.005519	0.000000	-8.191768
H	-4.005519	0.000000	-8.191768
H	0.000000	0.000000	-10.249583
H	0.000000	0.000000	11.313869

Table A.8: Cartesian coordinates for system B Fe(III) $^4B_1$.

Atom	X	Y	Z
Fe	0.000000	0.000000	-1.908375
N	0.000000	0.000000	1.358360
N	2.688338	0.000000	-4.471043
N	-2.688338	0.000000	-4.471043
C	0.000000	0.000000	3.902330
C	0.000000	0.000000	-8.169980
C	2.337176	0.000000	-6.947376
C	-2.337176	0.000000	-6.947376
C	2.267776	0.000000	7.901940
C	-2.267776	0.000000	7.901940
C	2.292985	0.000000	5.283244
C	-2.292985	0.000000	5.283244
C	0.000000	0.000000	9.242848
H	4.050799	0.000000	8.912333
H	-4.050799	0.000000	8.912333
H	4.063111	0.000000	4.256185
H	-4.063111	0.000000	4.256185
H	4.535124	0.000000	-3.971078
H	-4.535124	0.000000	-3.971078
H	4.010770	0.000000	-8.147474
H	-4.010770	0.000000	-8.147474
H	0.000000	0.000000	-10.212383
H	0.000000	0.000000	11.288519

Table A.9: Cartesian coordinates for system B Fe(III) $^4B_2$.

Atom	X	Y	Z
Fe	0.000000	0.000000	-1.920177
N	0.000000	0.000000	1.423608
N	2.813117	0.000000	-4.562224
N	-2.813117	0.000000	-4.562224
C	0.000000	0.000000	3.944559
C	0.000000	0.000000	-8.203292
C	2.363168	0.000000	-7.019594
C	-2.363168	0.000000	-7.019594
C	2.280911	0.000000	7.972559
C	-2.280911	0.000000	7.972559
C	2.296562	0.000000	5.358762
C	-2.296562	0.000000	5.358762
C	0.000000	0.000000	9.304072
H	4.055577	0.000000	8.997926
H	-4.055577	0.000000	8.997926
H	4.059773	0.000000	4.317695
H	-4.059773	0.000000	4.317695
H	4.682070	0.000000	-4.152423
H	-4.682070	0.000000	-4.152423
H	3.991296	0.000000	-8.285458
H	-3.991296	0.000000	-8.285458
H	0.000000	0.000000	-10.246593
H	0.000000	0.000000	11.351021

Table A.10: Cartesian coordinates for system B Fe(III) $^6A_1$.

Atom	X	Y	Z
Co	0.000000	0.000000	1.686681
N	0.000000	0.000000	4.733168
N	2.492603	0.000000	-0.801446
N	-2.492603	0.000000	-0.801446
C	2.296581	0.000000	-3.292952
C	-2.296581	0.000000	-3.292952
C	0.000000	0.000000	-4.576147
H	4.302709	0.000000	-0.175382
H	-4.302709	0.000000	-0.175382
H	4.030728	0.000000	-4.401407
H	-4.030728	0.000000	-4.401407
H	0.000000	0.000000	6.666691
H	0.000000	0.000000	-6.617792

Table A.11: Cartesian coordinates for system A Co(III) $^1A_1$.

A.2 Co(III)

A.2.1 System A

Atom	X	Y	Z
Co	0.000000	0.000000	1.690893
N	0.000000	0.000000	5.034917
N	2.699941	0.000000	-0.886398
N	-2.699941	0.000000	-0.886398
C	2.339565	0.000000	-3.357829
C	-2.339565	0.000000	-3.357829
C	0.000000	0.000000	-4.577217
H	4.552942	0.000000	-0.406317
H	-4.552942	0.000000	-0.406317
H	4.005507	0.000000	-4.572005
H	-4.005507	0.000000	-4.572005
H	0.000000	0.000000	6.952644
H	0.000000	0.000000	-6.620192

Table A.12: Cartesian coordinates for system A Co(III) $^3B_1$.

Atom	X	Y	Z
Co	0.000000	0.000000	1.685137
N	0.000000	0.000000	4.931055
N	2.657282	0.000000	-0.856374
N	-2.657282	0.000000	-0.856374
C	2.327530	0.000000	-3.329346
C	-2.327530	0.000000	-3.329346
C	0.000000	0.000000	-4.567281
H	4.499721	0.000000	-0.341962
H	-4.499721	0.000000	-0.341962
H	4.011144	0.000000	-4.517325
H	-4.011144	0.000000	-4.517325
H	0.000000	0.000000	6.852042
H	0.000000	0.000000	-6.609468

Table A.13: Cartesian coordinates for system A Co(III) $^3B_2$.

Atom	X	Y	Z
Co	0.000000	0.000000	1.719662
N	0.000000	0.000000	4.987982
N	2.759256	0.000000	-0.907306
N	-2.759256	0.000000	-0.907306
C	2.352148	0.000000	-3.369194
C	-2.352148	0.000000	-3.369194
C	0.000000	0.000000	-4.571935
H	4.619747	0.000000	-0.460738
H	-4.619747	0.000000	-0.460738
H	3.997617	0.000000	-4.613647
H	-3.997617	0.000000	-4.613647
H	0.000000	0.000000	6.898825
H	0.000000	0.000000	-6.615090

Table A.14: Cartesian coordinates for system A Co(III) $^5A_1$.

Atom	X	Y	Z
Co	0.000000	0.000000	1.689810
N	0.000000	0.000000	4.963745
N	2.774597	0.000000	-0.877960
N	-2.774597	0.000000	-0.877960
C	2.357636	0.000000	-3.339818
C	-2.357636	0.000000	-3.339818
C	0.000000	0.000000	-4.534537
H	4.634839	0.000000	-0.432439
H	-4.634839	0.000000	-0.432439
H	3.999092	0.000000	-4.587965
H	-3.999092	0.000000	-4.587965
H	0.000000	0.000000	6.874562
H	0.000000	0.000000	-6.577959

Table A.15: Cartesian coordinates for system A Co(III) $^5A_2$.

Atom	X	Y	Z
Co	0.000000	0.000000	-1.868694
N	0.000000	0.000000	1.328597
N	2.508939	0.000000	-4.350281
N	-2.508939	0.000000	-4.350281
C	0.000000	0.000000	3.865015
C	0.000000	0.000000	-8.121987
C	2.298648	0.000000	-6.840161
C	-2.298648	0.000000	-6.840161
C	2.287710	0.000000	7.857765
C	-2.287710	0.000000	7.857765
C	2.302683	0.000000	5.244425
C	-2.302683	0.000000	5.244425
C	0.000000	0.000000	9.176791
H	4.057383	0.000000	8.888645
H	-4.057383	0.000000	8.888645
H	4.056313	0.000000	4.189890
H	-4.056313	0.000000	4.189890
H	4.322386	0.000000	-3.736150
H	-4.322386	0.000000	-3.736150
H	4.028737	0.000000	-7.955773
H	-4.028737	0.000000	-7.955773
H	0.000000	0.000000	-10.163593
H	0.000000	0.000000	11.223832

Table A.16: Cartesian coordinates for system B Co(III) $^1A_1$.

A.2.2 System B

Atom	X	Y	Z
Co	0.000000	0.000000	-1.912756
N	0.000000	0.000000	1.462680
N	2.705387	0.000000	-4.498865
N	-2.705387	0.000000	-4.498865
C	0.000000	0.000000	3.962847
C	0.000000	0.000000	-8.187705
C	2.340545	0.000000	-6.969166
C	-2.340545	0.000000	-6.969166
C	2.292553	0.000000	7.989611
C	-2.292553	0.000000	7.989611
C	2.307355	0.000000	5.380867
C	-2.307355	0.000000	5.380867
C	0.000000	0.000000	9.308792
H	4.059364	0.000000	9.026630
H	-4.059364	0.000000	9.026630
H	4.061406	0.000000	4.325979
H	-4.061406	0.000000	4.325979
H	4.560511	0.000000	-4.027914
H	-4.560511	0.000000	-4.027914
H	4.004427	0.000000	-8.186981
H	-4.004427	0.000000	-8.186981
H	0.000000	0.000000	-10.230885
H	0.000000	0.000000	11.356216

Table A.17: Cartesian coordinates for system B Co(III) $^3B_1$.

Atom	X	Y	Z
Co	0.000000	0.000000	-1.880621
N	0.000000	0.000000	1.373485
N	2.641745	0.000000	-4.418369
N	-2.641745	0.000000	-4.418369
C	0.000000	0.000000	3.912511
C	0.000000	0.000000	-8.136083
C	2.323715	0.000000	-6.893141
C	-2.323715	0.000000	-6.893141
C	2.270688	0.000000	7.908006
C	-2.270688	0.000000	7.908006
C	2.297055	0.000000	5.290757
C	-2.297055	0.000000	5.290757
C	0.000000	0.000000	9.246130
H	4.051925	0.000000	8.920939
H	-4.051925	0.000000	8.920939
H	4.064827	0.000000	4.260444
H	-4.064827	0.000000	4.260444
H	4.482620	0.000000	-3.897415
H	-4.482620	0.000000	-3.897415
H	4.012677	0.000000	-8.072823
H	-4.012677	0.000000	-8.072823
H	0.000000	0.000000	-10.178040
H	0.000000	0.000000	11.291864

Table A.18: Cartesian coordinates for system B Co(III) $^3B_2$.

Atom	X	Y	Z
Co	0.000000	0.000000	-1.887923
N	0.000000	0.000000	1.453827
N	2.751985	0.000000	-4.517622
N	-2.751985	0.000000	-4.517622
C	0.000000	0.000000	3.957816
C	0.000000	0.000000	-8.185629
C	2.350509	0.000000	-6.980069
C	-2.350509	0.000000	-6.980069
C	2.286201	0.000000	7.982889
C	-2.286201	0.000000	7.982889
C	2.304487	0.000000	5.372523
C	-2.304487	0.000000	5.372523
C	0.000000	0.000000	9.310332
H	4.057702	0.000000	9.012589
H	-4.057702	0.000000	9.012589
H	4.064671	0.000000	4.327497
H	-4.064671	0.000000	4.327497
H	4.612276	0.000000	-4.069500
H	-4.612276	0.000000	-4.069500
H	3.999076	0.000000	-8.220287
H	-3.999076	0.000000	-8.220287
H	0.000000	0.000000	-10.228829
H	0.000000	0.000000	11.357171

Table A.19: Cartesian coordinates for system B Co(III) $^5A_1$.

Atom	X	Y	Z
Co	0.000000	0.000000	-1.910273
N	0.000000	0.000000	1.424912
N	2.780024	0.000000	-4.464476
N	-2.780024	0.000000	-4.464476
C	0.000000	0.000000	3.930764
C	0.000000	0.000000	-8.118431
C	2.358887	0.000000	-6.925745
C	-2.358887	0.000000	-6.925745
C	2.285559	0.000000	7.955214
C	-2.285559	0.000000	7.955214
C	2.303939	0.000000	5.344518
C	-2.303939	0.000000	5.344518
C	0.000000	0.000000	9.283027
H	4.057365	0.000000	8.984373
H	-4.057365	0.000000	8.984373
H	4.064773	0.000000	4.300689
H	-4.064773	0.000000	4.300689
H	4.641190	0.000000	-4.023678
H	-4.641190	0.000000	-4.023678
H	3.998985	0.000000	-8.175479
H	-3.998985	0.000000	-8.175479
H	0.000000	0.000000	-10.161922
H	0.000000	0.000000	11.329827

Table A.20: Cartesian coordinates for system B Co(III) $^5A_2$.

Atom	X	Y	Z
Ni	0.000000	0.000000	1.701133
N	0.000000	0.000000	4.976916
N	2.623589	0.000000	-0.872207
N	-2.623589	0.000000	-0.872207
C	2.327116	0.000000	-3.348346
C	-2.327116	0.000000	-3.348346
C	0.000000	0.000000	-4.590566
H	4.466576	0.000000	-0.349741
H	-4.466576	0.000000	-0.349741
H	4.014308	0.000000	-4.533971
H	-4.014308	0.000000	-4.533971
H	0.000000	0.000000	6.899795
H	0.000000	0.000000	-6.633909

Table A.21: Cartesian coordinates for system A Ni(III) $^2B_1$.

A.3 Ni(III)

A.3.1 System A

Atom	X	Y	Z
Ni	0.000000	0.000000	1.662707
N	0.000000	0.000000	4.803840
N	2.548587	0.000000	-0.799180
N	-2.548587	0.000000	-0.799180
C	2.303804	0.000000	-3.276377
C	-2.303804	0.000000	-3.276377
C	0.000000	0.000000	-4.553132
H	4.359557	0.000000	-0.183927
H	-4.359557	0.000000	-0.183927
H	4.024600	0.000000	-4.407791
H	-4.024600	0.000000	-4.407791
H	0.000000	0.000000	6.729436
H	0.000000	0.000000	-6.595141

Table A.22: Cartesian coordinates for system A Ni(III) $^2B_2$.

Atom	X	Y	Z
Ni	0.000000	0.000000	1.696754
N	0.000000	0.000000	5.016584
N	2.706324	0.000000	-0.883726
N	-2.706324	0.000000	-0.883726
C	2.338939	0.000000	-3.350254
C	-2.338939	0.000000	-3.350254
C	0.000000	0.000000	-4.573305
H	4.559901	0.000000	-0.408899
H	-4.559901	0.000000	-0.408899
H	4.002946	0.000000	-4.570490
H	-4.002946	0.000000	-4.570490
H	0.000000	0.000000	6.937133
H	0.000000	0.000000	-6.616109

Table A.23: Cartesian coordinates for system A Ni(III) $^4A_1$.

Atom	X	Y	Z
Ni	0.000000	0.000000	1.653750
N	0.000000	0.000000	5.193146
N	2.637924	0.000000	-0.879727
N	-2.637924	0.000000	-0.879727
C	2.327021	0.000000	-3.354362
C	-2.327021	0.000000	-3.354362
C	0.000000	0.000000	-4.595491
H	4.482786	0.000000	-0.363771
H	-4.482786	0.000000	-0.363771
H	4.012465	0.000000	-4.542155
H	-4.012465	0.000000	-4.542155
H	0.000000	0.000000	7.114564
H	0.000000	0.000000	-6.638046

Table A.24: Cartesian coordinates for system A Ni(III) $^4B_2$.

Atom	X	Y	Z
Ni	0.000000	0.000000	1.626557
N	0.000000	0.000000	4.884689
N	2.809773	0.000000	-0.806543
N	-2.809773	0.000000	-0.806543
C	2.365195	0.000000	-3.262083
C	-2.365195	0.000000	-3.262083
C	0.000000	0.000000	-4.445360
H	4.672127	0.000000	-0.374905
H	-4.672127	0.000000	-0.374905
H	3.995536	0.000000	-4.525632
H	-3.995536	0.000000	-4.525632
H	0.000000	0.000000	6.802729
H	0.000000	0.000000	-6.488925

Table A.25: Cartesian coordinates for system A Ni(III) $^4A_2$.

Atom	X	Y	Z
Ni	0.000000	0.000000	-1.899008
N	0.000000	0.000000	1.440176
N	2.630617	0.000000	-4.476725
N	-2.630617	0.000000	-4.476725
C	0.000000	0.000000	3.939233
C	0.000000	0.000000	-8.195173
C	2.326881	0.000000	-6.952505
C	-2.326881	0.000000	-6.952505
C	2.294048	0.000000	7.962640
C	-2.294048	0.000000	7.962640
C	2.308631	0.000000	5.354145
C	-2.308631	0.000000	5.354145
C	0.000000	0.000000	9.278883
H	4.059693	0.000000	9.001038
H	-4.059693	0.000000	9.001038
H	4.061233	0.000000	4.297038
H	-4.061233	0.000000	4.297038
H	4.474769	0.000000	-3.960371
H	-4.474769	0.000000	-3.960371
H	4.013026	0.000000	-8.140216
H	-4.013026	0.000000	-8.140216
H	0.000000	0.000000	-10.238172
H	0.000000	0.000000	11.326394

Table A.26: Cartesian coordinates for system B Ni(III) $^2B_1$.

A.3.2 System B

Atom	X	Y	Z
Ni	0.000000	0.000000	-1.868963
N	0.000000	0.000000	1.311150
N	2.546029	0.000000	-4.324327
N	-2.546029	0.000000	-4.324327
C	0.000000	0.000000	3.823254
C	0.000000	0.000000	-8.079594
C	2.303328	0.000000	-6.801560
C	-2.303328	0.000000	-6.801560
C	2.283472	0.000000	7.824354
C	-2.283472	0.000000	7.824354
C	2.307734	0.000000	5.213743
C	-2.307734	0.000000	5.213743
C	0.000000	0.000000	9.153382
H	4.057075	0.000000	8.849869
H	-4.057075	0.000000	8.849869
H	4.067627	0.000000	4.170459
H	-4.067627	0.000000	4.170459
H	4.357592	0.000000	-3.710902
H	-4.357592	0.000000	-3.710902
H	4.025278	0.000000	-7.931311
H	-4.025278	0.000000	-7.931311
H	0.000000	0.000000	-10.120462
H	0.000000	0.000000	11.199610

Table A.27: Cartesian coordinates for system B Ni(III) $^2B_2$.

Atom	X	Y	Z
Ni	0.000000	0.000000	-1.908497
N	0.000000	0.000000	1.451906
N	2.710778	0.000000	-4.486844
N	-2.710778	0.000000	-4.486844
C	0.000000	0.000000	3.948735
C	0.000000	0.000000	-8.174486
C	2.339674	0.000000	-6.952070
C	-2.339674	0.000000	-6.952070
C	2.288867	0.000000	7.967851
C	-2.288867	0.000000	7.967851
C	2.309946	0.000000	5.359608
C	-2.309946	0.000000	5.359608
C	0.000000	0.000000	9.292934
H	4.058573	0.000000	8.999849
H	-4.058573	0.000000	8.999849
H	4.067776	0.000000	4.311379
H	-4.067776	0.000000	4.311379
H	4.565344	0.000000	-4.016978
H	-4.565344	0.000000	-4.016978
H	4.002033	0.000000	-8.174365
H	-4.002033	0.000000	-8.174365
H	0.000000	0.000000	-10.217221
H	0.000000	0.000000	11.339674

Table A.28: Cartesian coordinates for system B Ni(III) $^4A_1$.

Atom	X	Y	Z
Ni	0.000000	0.000000	-2.024795
N	0.000000	0.000000	1.564436
N	2.644900	0.000000	-4.542022
N	-2.644900	0.000000	-4.542022
C	0.000000	0.000000	4.088752
C	0.000000	0.000000	-8.254065
C	2.329386	0.000000	-7.016589
C	-2.329386	0.000000	-7.016589
C	2.271909	0.000000	8.088344
C	-2.271909	0.000000	8.088344
C	2.301338	0.000000	5.472792
C	-2.301338	0.000000	5.472792
C	0.000000	0.000000	9.424494
H	4.052411	0.000000	9.102023
H	-4.052411	0.000000	9.102023
H	4.069833	0.000000	4.444389
H	-4.069833	0.000000	4.444389
H	4.492227	0.000000	-4.034648
H	-4.492227	0.000000	-4.034648
H	4.013996	0.000000	-8.205109
H	-4.013996	0.000000	-8.205109
H	0.000000	0.000000	-10.296793
H	0.000000	0.000000	11.470013

Table A.29: Cartesian coordinates for system B Ni(III) $^4B_2$.

Atom	X	Y	Z
Ni	0.000000	0.000000	-1.916203
N	0.000000	0.000000	1.473043
N	2.686389	0.000000	-4.506724
N	-2.686389	0.000000	-4.506724
C	0.000000	0.000000	3.963011
C	0.000000	0.000000	-8.202685
C	2.336516	0.000000	-6.974428
C	-2.336516	0.000000	-6.974428
C	2.290653	0.000000	7.990138
C	-2.290653	0.000000	7.990138
C	2.311370	0.000000	5.382671
C	-2.311370	0.000000	5.382671
C	0.000000	0.000000	9.314424
H	4.058987	0.000000	9.024264
H	-4.058987	0.000000	9.024264
H	4.069840	0.000000	4.335628
H	-4.069840	0.000000	4.335628
H	4.535967	0.000000	-4.016953
H	-4.535967	0.000000	-4.016953
H	4.006941	0.000000	-8.185019
H	-4.006941	0.000000	-8.185019
H	0.000000	0.000000	-10.245453
H	0.000000	0.000000	11.361350

Table A.30: Cartesian coordinates for system B Ni(III) $^4A_2$.

Appendix B

DFT Geometries

This appendix contains sets of Cartesian coordinates for all systems used in chapter 6. All values are in a_0 and rounded to six decimal places.

B.1 Trigonal Bipyramid

Atom	X	Y	Z
Cr	0.000000	0.000000	0.000888
N	6.185403	0.000000	0.002776
N	-6.185403	0.000000	0.002776
N	0.000000	-5.325204	-3.080723
N	0.000000	5.325204	-3.080723
N	0.000000	0.000000	6.153650
C	3.964524	0.000000	0.001988
C	-3.964524	0.000000	0.001988
C	0.000000	-3.409517	-1.972909
C	0.000000	3.409517	-1.972909
C	0.000000	0.000000	3.940616

Table B.1: Cartesian coordinates for $[Cr^{II}(CN)_5]^{3-}$ trigonal bipyramid $^1A_1$ (A).

Atom	X	Y	Z
Cr	0.000000	0.000000	0.003910
N	5.312176	0.000000	-3.098419
N	-5.312176	0.000000	-3.098419
N	0.000000	-6.187864	0.012490
N	0.000000	6.187864	0.012490
N	0.000000	0.000000	6.157592
C	3.402041	0.000000	-1.980726
C	-3.402041	0.000000	-1.980726
C	0.000000	-3.967123	0.008363
C	0.000000	3.967123	0.008363
C	0.000000	0.000000	3.944438

Table B.2: Cartesian coordinates for $[Cr^{II}(CN)_5]^{3-}$ trigonal bipyramid $^1A_1$ (B).

Atom	X	Y	Z
Cr	0.000000	0.000000	-0.253044
N	6.169411	0.000000	-1.291628
N	-6.169411	0.000000	-1.291628
N	0.000000	-6.155953	-1.360673
N	0.000000	6.155953	-1.360673
N	0.000000	0.000000	5.837247
C	4.019373	0.000000	-0.771288
C	-4.019373	0.000000	-0.771288
C	0.000000	-4.016228	-0.799388
C	0.000000	4.016228	-0.799388
C	0.000000	0.000000	3.615633

Table B.3: Cartesian coordinates for $[Cr^{II}(CN)_5]^{3-}$ trigonal bipyramid $^1A_1$ (C).

Atom	X	Y	Z
Cr	0.000000	0.000000	-0.193764
N	6.198585	0.000000	-1.089461
N	-6.198585	0.000000	-1.089461
N	0.000000	-6.180937	-1.669674
N	0.000000	6.180937	-1.669674
N	0.000000	0.000000	5.939614
C	4.028404	0.000000	-0.645923
C	-4.028404	0.000000	-0.645923
C	0.000000	-4.064440	-1.041664
C	0.000000	4.064440	-1.041664
C	0.000000	0.000000	3.722631

Table B.4: Cartesian coordinates for $[Cr^{II}(CN)_5]^{3-}$ trigonal bipyramid $^3B_1$ (A).

Atom	X	Y	Z
Cr	0.000000	0.000000	0.029974
N	6.250760	0.000000	0.311139
N	-6.250760	0.000000	0.311139
N	0.000000	-4.958836	-3.673356
N	0.000000	4.958836	-3.673356
N	0.000000	0.000000	6.631068
C	4.039556	0.000000	0.192616
C	-4.039556	0.000000	0.192616
C	0.000000	-3.139071	-2.414890
C	0.000000	3.139071	-2.414890
C	0.000000	0.000000	4.423669

Table B.5: Cartesian coordinates for $[Cr^{II}(CN)_5]^{3-}$ trigonal bipyramid $^3B_1$ (B).

Atom	X	Y	Z
Cr	0.000000	0.000000	-0.192984
N	6.181551	0.000000	-1.668146
N	-6.181551	0.000000	-1.668146
N	0.000000	-6.197576	-1.093773
N	0.000000	6.197576	-1.093773
N	0.000000	0.000000	5.940608
C	4.065099	0.000000	-1.039876
C	-4.065099	0.000000	-1.039876
C	0.000000	-4.028038	-0.647248
C	0.000000	4.028038	-0.647248
C	0.000000	0.000000	3.723658

Table B.6: Cartesian coordinates for $[Cr^{II}(CN)_5]^{3-}$ trigonal bipyramid $^3B_2$ (A).

Atom	X	Y	Z
Cr	0.000000	0.000000	0.033656
N	4.962446	0.000000	-3.664237
N	-4.962446	0.000000	-3.664237
N	0.000000	-6.251702	0.289747
N	0.000000	6.251702	0.289747
N	0.000000	0.000000	6.635083
C	3.140830	0.000000	-2.408394
C	-3.140830	0.000000	-2.408394
C	0.000000	-4.039629	0.188138
C	0.000000	4.039629	0.188138
C	0.000000	0.000000	4.427634

Table B.7: Cartesian coordinates for $[Cr^{II}(CN)_5]^{3-}$ trigonal bipyramid $^3B_2$ (B).

Atom	X	Y	Z
Cr	0.000000	0.000000	0.005715
N	6.356550	0.000000	0.016703
N	-6.356550	0.000000	0.016703
N	0.000000	-5.626497	-3.283591
N	0.000000	5.626497	-3.283591
N	0.000000	0.000000	6.517321
C	4.149858	0.000000	0.013004
C	-4.149858	0.000000	0.013004
C	0.000000	-3.718337	-2.169683
C	0.000000	3.718337	-2.169683
C	0.000000	0.000000	4.307805

Table B.8: Cartesian coordinates for $[Cr^{II}(CN)_5]^{3-}$ trigonal bipyramid $^5A_1$.

B.2 Square Pyramid

Atom	X	Y	Z
Cr	0.000000	0.000000	-0.165608
N	0.000000	0.000000	6.075542
N	4.382324	4.271707	-1.425118
N	-4.382324	-4.271707	-1.425118
N	-4.382324	4.271707	-1.425118
N	4.382324	-4.271707	-1.425118
C	0.000000	0.000000	3.863482
C	2.879004	2.735233	-0.895988
C	-2.879004	-2.735233	-0.895988
C	-2.879004	2.735233	-0.895988
C	2.879004	-2.735233	-0.895988

Table B.9: Cartesian coordinates for $[Cr^{II}(CN)_5]^{3-}$ square based pyramid $^1A_1$ (A).

Atom	X	Y	Z
Cr	0.000000	0.000000	-0.162479
N	0.000000	0.000000	6.079370
N	4.273233	4.379891	-1.430092
N	-4.273233	-4.379891	-1.430092
N	-4.273233	4.379891	-1.430092
N	4.273233	-4.379891	-1.430092
C	0.000000	0.000000	3.867408
C	2.736186	2.879081	-0.895672
C	-2.736186	-2.879081	-0.895672
C	-2.736186	2.879081	-0.895672
C	2.736186	-2.879081	-0.895672

Table B.10: Cartesian coordinates for $[Cr^{II}(CN)_5]^{3-}$ square based pyramid $^1A_1$. (B)

Atom	X	Y	Z
Cr	0.000000	0.000000	-0.249599
N	0.000000	0.000000	5.828028
N	4.355613	4.359042	-1.325856
N	-4.355613	-4.359042	-1.325856
N	-4.355613	4.359042	-1.325856
N	4.355613	-4.359042	-1.325856
C	0.000000	0.000000	3.605822
C	2.840198	2.841194	-0.784269
C	-2.840198	-2.841194	-0.784269
C	-2.840198	2.841194	-0.784269
C	2.840198	-2.841194	-0.784269

Table B.11: Cartesian coordinates for $[Cr^{II}(CN)_5]^{3-}$ square based pyramid $^1A_1$. (C)

Atom	X	Y	Z
Cr	0.000000	0.000000	0.285032
N	0.000000	0.000000	6.808466
N	4.749299	4.732618	-1.722844
N	-4.749299	-4.732618	-1.722844
N	-4.749299	4.732618	-1.722844
N	4.749299	-4.732618	-1.722844
C	0.000000	0.000000	4.608224
C	3.191295	3.188954	-1.436359
C	-3.191295	-3.188954	-1.436359
C	-3.191295	3.188954	-1.436359
C	3.191295	-3.188954	-1.436359

Table B.12: Cartesian coordinates for $[Cr^{II}(CN)_5]^{3-}$ square pyramid $^3A_1$.

Atom	X	Y	Z
Cr	0.000000	0.000000	-0.225619
N	0.000000	0.000000	5.989566
N	4.352256	4.351877	-1.354396
N	-4.352256	-4.351877	-1.354396
N	-4.352256	4.351877	-1.354396
N	4.352256	-4.351877	-1.354396
C	0.000000	0.000000	3.782411
C	2.824115	2.823882	-0.868181
C	-2.824115	-2.823882	-0.868181
C	-2.824115	2.823882	-0.868181
C	2.824115	-2.823882	-0.868181

Table B.13: Cartesian coordinates for $[Cr^{II}(CN)_5]^{3-}$ square pyramid $^3A_2$.

Atom	X	Y	Z
Cr	0.000000	0.000000	-0.015551
N	0.000000	0.000000	6.207073
N	4.728660	4.732698	-1.523701
N	-4.728660	-4.732698	-1.523701
N	-4.728660	4.732698	-1.523701
N	4.728660	-4.732698	-1.523701
C	0.000000	0.000000	4.004000
C	3.209412	3.210044	-1.016901
C	-3.209412	-3.210044	-1.016901
C	-3.209412	3.210044	-1.016901
C	3.209412	-3.210044	-1.016901

Table B.14: Cartesian coordinates for $[Cr^{II}(CN)_5]^{3-}$ square pyramid $^5A_1$.

Atom	X	Y	Z
Cr	0.000000	0.000000	-0.242106
N	0.000000	0.000000	6.561377
N	4.429410	4.429723	-1.481910
N	-4.429410	-4.429723	-1.481910
N	-4.429410	4.429723	-1.481910
N	4.429410	-4.429723	-1.481910
C	0.000000	0.000000	4.350175
C	2.904690	2.904831	-1.010282
C	-2.904690	-2.904831	-1.010282
C	-2.904690	2.904831	-1.010282
C	2.904690	-2.904831	-1.010282

Table B.15: Cartesian coordinates for $[Cr^{II}(CN)_5]^{3-}$ square pyramid $^5A_2$.

B.3 Transition State

Atom	X	Y	Z
Cr	0.000000	0.000000	-0.148747
N	0.000000	6.352558	-0.490588
N	0.000000	-6.352558	-0.490588
N	5.939151	0.000000	-2.693648
N	-5.939151	0.000000	-2.693648
N	0.000000	0.000000	6.512272
C	0.000000	4.150429	-0.348786
C	0.000000	-4.150429	-0.348786
C	3.919227	0.000000	-1.799727
C	-3.919227	0.000000	-1.799727
C	0.000000	0.000000	4.301975

Table B.16: Cartesian coordinates for $[Cr^{II}(CN)_5]^{3-}$ transition state $^5A_1$.

Appendix C

Python Code

```
1  #! /usr/bin/env python2.2
2  #sym = number of symmetry distinct orbital types
3  #Lon is a list of numbers used to test if files are compatable
4  #St=string of top of file, Sb=string of bottom of file
5  import sys
6  import os
7  output=open(sys.argv[-1],'w')
8  Lin=sys.argv[1:-1]
9  Fsym=open(Lin[0],'r')
10 Lsym=Fsym.readlines()
11 Fsym.close()
12 Ssym=Lsym[3]
13 sym=int(Ssym[-5:-1])
14 Son=Lsym[4]
15 Son=Son[:-1].replace('␣','')
16 Lon=list(Son)
17 Lt=Lsym[:7]
18 St=''.join(Lt)
19 Ib=Lsym.index('#OCC\n')
20 Lb=Lsym[Ib:]
21 Sb=''.join(Lb)
22 temp=open('temp','w')
23 temp.write(St)
24 Lty=['Inactive','Active','Virtual']
25
26
27 def chop(A,B,C,D,E,F):#A=symetry B=Inputlist C=orbital type D=filename
28                       #E=Keybord input list F=input file List
29     if C=='Inactive':
30         d=F.index(D)
31         x=int(E[((d*6)+0)])
32         y=int(E[((d*6)+1)])
33     elif C=='Active':
34         d=Lin.index(D)
35         x=int(E[((d*6)+2)])
36         y=int(E[((d*6)+3)])
37     elif C=='Virtual':
38         d=Lin.index(D)
39         x=int(E[((d*6)+4)])
40         y=int(E[((d*6)+5)])
41     z=int(y)+1
42     try:
```

```
43          if int(x) in range(1,10): #loop to correctly format search
44              X='   '+str(x)
45          elif int(x) in range(10,100):
46              X='  '+str(x)
47          elif int(x) in range(100,1000):
48              X=' '+str(x)
49          else:
50              X=x
51          if int(z) in range(1,10):
52              Z='   '+str(z)
53          elif int(z) in range(10,100):
54              Z='  '+str(z)
55          elif int(z) in range(100,1000):
56              Z=' '+str(z)
57          else:
58              Z=z
59          V=B.index('* ORBITAL    %s %s\n'%(A,X)) #search for first
                orbital
60          if ('* ORBITAL    %s %s\n'%(A,Z))not in B and \
61          ('* ORBITAL    %s %s\n'%(str(A+1),'   1')) not in B:
62              W=B.index('#OCC\n')
63          elif('* ORBITAL    %s %s\n'%(A,Z)) not in B:
64              W=B.index('* ORBITAL    %s %s\n'%(str(A+1),'   1'))
65          else:
66              W=B.index('* ORBITAL    %s %s\n'%(A,Z))#search for last
                    orbital
67      except ValueError:
68          pass
69      else:
70          L=B[V:W] #compile list of lines between first orbital and last
                orbital
71          S=''.join(L) #convert to string for output
72          return S
73
74
75  def orblist(A,B,C):
76      #A=symetry, B=order of group C=inputlist
77      Lorb=[]
78      c=C[4]
79      d=int((-5+(A*8)))
80      e=int(c[d:(d+5)])
81      for a in range(1,(e+1)):
82          if int(a) in range(10):#formatting for strings
83              a1='   '+str(a)
84          elif int(a) in range(10,100):#formatting for strings
85              a1='  '+str(a)
86          elif int(a) in range(100,1000):#formatting for strings
87              a1=' '+str(a)
88          else:
89              a1=str(a)
90          orb=('* ORBITAL    %s %s\n'%(A,a1))
91          #creates string based on syn and orbital number
92          if (str(orb) not in C):continue #excludes strings not present
93          Z=C.count(orb)#set up veriables
94          L1=C#set up veriables
95          X=0#set up veriables
96          W=0#set up veriables
97          while Z!=0:#finds all copies of string orb
```

```
 98                 Y=L1[X:].index(str(orb))
 99                 X=Y+1+W
100                 V=Y+W
101                 W=X
102                 Lorb.append(V)#writes values to list
103                 Z=Z-1
104         return Lorb
105
106
107 def imp(A):#A=sym
108         S=raw_input("Enter orbitals in sym %s for all files.\n\
109 format = file1 Inactive Active Virtual file2 Inactive ...\n\
110 eg. 1-2 5-7 20-72 1-12 15-20 0-0\n"%(A))
111         S=S.replace(' ',',')
112         S=S.replace('-',',')
113         L=S.split(',')
114         return L
115
116
117 for SYM in range (1,(sym+1)):
118         Limp=imp(SYM)
119         Simp=str(Limp)
120         for type in Lty:
121             for files in Lin:
122                 input=open(files,'r')
123                 Lf=input.readlines()
124                 try:
125                     Sout=chop(SYM,Lf,type,files,Limp,Lin)
126                     temp.write(Sout)
127                     input.close()
128                 except TypeError:
129                     pass
130
131 temp.write(Sb)
132 temp.close()
133 temp=open('temp','r')
134 Ltemp=temp.readlines()
135 temp.close()
136 os.remove('temp')
137
138 for SYM in range(1,(sym+1)):#runs orblist for each sym
139         Lorb=orblist(SYM,sym,Ltemp)
140         Lorb.sort()
141         L2=Ltemp
142         i=1
143         for N in Lorb:#renumbers all orbitals in Lorb
144             P=L2[N]
145             Q=P[13:19]
146             R=P[13]
147             if int(i) in range(10):#formatting for strings
148                 I='   '+str(i)
149             elif int(i) in range(10,100):#formatting for strings
150                 I='  '+str(i)
151             elif int(i) in range(100,1000):#formatting for strings
152                 I=' '+str(i)
153             else:
154                 I=str(i)
155             P=P.replace(Q,'%s %s'%(R,I))
```

```
156             L2[N]=P
157             i+=1
158
159 S2=''.join(L2)
160 output.write(S2)#creates output file
161 output.close()
```

Appendix D

Unpublished Basis Sets By B. J. Persson

This appendix contains the unpublished basis sets By B. J. Persson used in chapter 3.

D.1 Chromium ANO-CC

Basis set:CR.ANO-CC...6S5P4D3F2G.

Type s

No. Exponent Contraction Coefficients

1 0.617719400E+07 0.000004 -0.000001 0.000000 0.000000 0.000000 0.000000

2 0.924929500E+06 0.000035 -0.000011 0.000004 -0.000001 0.000003 -0.000004

3 0.210486500E+06 0.000184 -0.000060 0.000020 -0.000005 0.000017 -0.000019

4 0.596200500E+05 0.000776 -0.000254 0.000085 -0.000021 0.000071 -0.000080

5 0.194507600E+05 0.002818 -0.000924 0.000311 -0.000079 0.000266 -0.000287

6 0.702205600E+04 0.009120 -0.003004 0.001008 -0.000251 0.000833 -0.000947

7 0.273876300E+04 0.026608 -0.008893 0.003001 -0.000763 0.002593 -0.002772

8 0.113581400E+04 0.069498 -0.023878 0.008076 -0.002005 0.006624 -0.007641

9 0.495092300E+03 0.156649 -0.057531 0.019793 -0.005069 0.017374 -0.018353

10 0.224748700E+03 0.281854 -0.117842 0.041361 -0.010214 0.033551 -0.039996

11 0.105383600E+03 0.343293 -0.188346 0.070016 -0.018332 0.064775 -0.066985

12 0.501935900E+02 0.210846 -0.158518 0.062141 -0.014599 0.044418 -0.063477

13 0.222495700E+02 0.040261 0.156084 -0.070678 0.015002 -0.047833 0.112199

14 0.109826500E+02 0.011445 0.557867 -0.352991 0.103192 -0.377425 0.349248

15 0.538366500E+01 0.011615 0.406279 -0.385732 0.097087 -0.471546 0.828321

16 0.234368500E+01 0.000652 0.054853 0.276041 -0.068543 1.045255 -2.883225

17 0.110520200E+01 0.000240 -0.001830 0.700360 -0.340150 0.953130 1.800090

18 0.487848000E+00 -0.000066 0.001466 0.312845 -0.148764 -1.547483 0.635137

19 0.895990000E-01 0.000020 -0.000147 0.010331 0.793858 -0.523837 -2.121314

20 0.334230000E-01 -0.000013 0.000172 -0.003616 0.343540 1.085978 1.931237

21 0.133690000E-01 0.000005 -0.000047 0.001369 0.005848 -0.141625 -0.258912

Type p

No. Exponent Contraction Coefficients

22 0.626892100E+04 0.000187 -0.000066 0.000041 -0.000066 0.000101

23 0.148511800E+04 0.001644 -0.000579 0.000371 -0.000628 0.000899

24 0.481914600E+03 0.009121 -0.003237 0.001998 -0.003233 0.005021

25 0.183514200E+03 0.037197 -0.013353 0.008596 -0.014612 0.021259

26 0.771900500E+02 0.114927 -0.042597 0.026425 -0.042989 0.069704

27 0.346517800E+02 0.256932 -0.098945 0.065578 -0.115060 0.176448
28 0.161484600E+02 0.383370 -0.157646 0.094271 -0.141524 0.217465
29 0.771093900E+01 0.304749 -0.109486 0.093868 -0.195065 0.126850
30 0.360715400E+01 0.082417 0.188870 -0.245529 0.656726 -1.683373
31 0.166736200E+01 0.002707 0.476993 -0.422694 0.586670 1.366644
32 0.739088000E+00 0.001438 0.401964 0.117820 -1.007875 0.652913
33 0.301326000E+00 -0.000335 0.103722 0.354895 -0.408024 -1.507169
34 0.120530000E+00 0.000229 -0.001723 0.516858 0.671315 0.455408
35 0.482120000E-01 -0.000101 0.002718 0.174657 0.263617 0.399288
36 0.192850000E-01 0.000032 -0.000775 -0.002539 0.000089 0.009929
Type d
No. Exponent Contraction Coefficients
37 0.150834100E+03 0.001180 -0.000919 0.000989 -0.002037
38 0.449972300E+02 0.009662 -0.007337 0.008310 -0.025734
39 0.169608800E+02 0.041387 -0.031569 0.033429 -0.078930
40 0.704015400E+01 0.121174 -0.089373 0.094397 -0.334423
41 0.310387800E+01 0.242019 -0.260640 0.430821 -0.588093
42 0.137589600E+01 0.323287 -0.256559 0.142758 0.859847
43 0.592282000E+00 0.317542 0.035444 -0.505063 0.311581
44 0.242138000E+00 0.238377 0.332972 -0.371184 -0.602585
45 0.912840000E-01 0.102539 0.393703 0.192579 -0.264320
46 0.365140000E-01 0.020258 0.326170 0.603974 0.578242
Type f
No. Exponent Contraction Coefficients
47 0.771390000E+01 0.043396 -0.056567 0.171922
48 0.305750000E+01 0.345885 -0.596916 0.781785
49 0.121190000E+01 0.521835 -0.087036 -0.963703
50 0.480300000E+00 0.267992 0.560156 0.021202
51 0.190400000E+00 0.101462 0.337806 0.534772
52 0.755000000E-01 0.015388 0.094919 0.181549
Type g
No. Exponent Contraction Coefficients
53 0.436270000E+01 0.298904 -0.594246
54 0.171480000E+01 0.652143 -0.119623
55 0.674000000E+00 0.228769 0.670057
56 0.264900000E+00 0.063260 0.291155

D.2 Iron ANO-CC

Basis set:FE.ANO-CC...6S5P4D3F2G.
Type s
No. Exponent Contraction Coefficients
1 0.431626500E+07 0.000009 -0.000003 0.000001 0.000000 0.000001 -0.000001
2 0.646342400E+06 0.000067 -0.000020 0.000008 -0.000002 0.000004 -0.000008
3 0.147089700E+06 0.000355 -0.000107 0.000040 -0.000010 0.000022 -0.000041
4 0.416615200E+05 0.001495 -0.000450 0.000168 -0.000042 0.000094 -0.000170
5 0.135907700E+05 0.005415 -0.001637 0.000610 -0.000153 0.000339 -0.000635

6 0.490575000E+04 0.017366 -0.005300 0.001979 -0.000497 0.001111 -0.001993
7 0.191274600E+04 0.049578 -0.015499 0.005795 -0.001449 0.003212 -0.006086
8 0.792604300E+03 0.123134 -0.040591 0.015288 -0.003847 0.008633 -0.015331
9 0.344806500E+03 0.249517 -0.092306 0.035153 -0.008799 0.019497 -0.037750
10 0.155899900E+03 0.358982 -0.168076 0.066035 -0.016756 0.038037 -0.066173
11 0.722309100E+02 0.277942 -0.190326 0.078418 -0.019682 0.043458 -0.093644
12 0.327250600E+02 0.067086 0.044168 -0.019191 0.004285 -0.009651 0.059665
13 0.156676200E+02 -0.002410 0.515471 -0.303737 0.082409 -0.189080 0.283591
14 0.750348300E+01 0.000708 0.505180 -0.460716 0.127617 -0.361072 1.011031
15 0.331222300E+01 -0.001119 0.092339 0.136313 -0.043181 0.325539 -1.876230
16 0.155847100E+01 0.000398 -0.002471 0.711951 -0.280861 0.931779 -0.621890
17 0.683914000E+00 -0.000160 0.002270 0.404006 -0.256345 -0.557031 2.273460
18 0.146757000E+00 0.000066 -0.000516 0.028082 0.455829 -1.656893 -1.612246
19 0.705830000E-01 -0.000062 0.000579 -0.013133 0.530904 1.103844 0.136242
20 0.314490000E-01 0.000030 -0.000239 0.007527 0.183439 0.461931 0.730640
21 0.125800000E-01 -0.000008 0.000066 -0.001578 0.000728 0.079640 0.032998
Type p
No. Exponent Contraction Coefficients
22 0.772148900E+04 0.000177 -0.000064 0.000028 -0.000063 0.000060
23 0.182912600E+04 0.001551 -0.000562 0.000256 -0.000593 0.000588
24 0.593628000E+03 0.008640 -0.003154 0.001401 -0.003109 0.002992
25 0.226205400E+03 0.035488 -0.013110 0.005992 -0.013934 0.013960
26 0.952614500E+02 0.110824 -0.042259 0.018859 -0.042028 0.041317
27 0.428592000E+02 0.251583 -0.099910 0.046612 -0.111483 0.117685
28 0.200497100E+02 0.381689 -0.161770 0.071289 -0.149700 0.132119
29 0.962088500E+01 0.309893 -0.115245 0.064243 -0.189081 0.187402
30 0.454137100E+01 0.087794 0.184776 -0.148623 0.572228 -1.021074
31 0.211350000E+01 0.003674 0.474958 -0.299826 0.669380 0.226398
32 0.947201000E+00 0.001471 0.403980 -0.032601 -0.815788 1.126442
33 0.391243000E+00 -0.000296 0.107285 0.243076 -0.583740 -0.787307
34 0.156497000E+00 0.000215 -0.001049 0.549688 0.376858 -0.607421
35 0.625990000E-01 -0.000094 0.002638 0.307216 0.378923 0.590474
36 0.250400000E-01 0.000030 -0.000754 0.033034 0.083538 0.415532
Type d
No. Exponent Contraction Coefficients
37 0.217368800E+03 0.000913 -0.000716 0.001096 -0.002234
38 0.649997600E+02 0.007796 -0.005788 0.008269 -0.022892
39 0.247731400E+02 0.035289 -0.027414 0.042297 -0.096130
40 0.104361400E+02 0.107333 -0.077682 0.101884 -0.319420
41 0.467965300E+01 0.225122 -0.209342 0.415057 -0.605483
42 0.212562200E+01 0.314769 -0.263111 0.250338 0.799408
43 0.945242000E+00 0.314962 -0.054114 -0.521781 0.414047
44 0.402685000E+00 0.245525 0.273504 -0.436837 -0.631971
45 0.156651000E+00 0.121226 0.414633 0.144199 -0.300063
46 0.626600000E-01 0.041346 0.394669 0.574895 0.597769
Type f
No. Exponent Contraction Coefficients
47 0.112749000E+02 0.030228 -0.034845 0.097121

48 0.446900000E+01 0.270107 -0.506922 0.815033
49 0.177130000E+01 0.525407 -0.284306 -0.704627
50 0.702100000E+00 0.321884 0.527971 -0.315841
51 0.278300000E+00 0.131815 0.394485 0.602167
52 0.110300000E+00 0.026413 0.126559 0.229477
Type g
No. Exponent Contraction Coefficients
53 0.637680000E+01 0.186958 -0.433468
54 0.250640000E+01 0.630572 -0.409085
55 0.985100000E+00 0.339896 0.630925
56 0.387200000E+00 0.100343 0.403580

D.3 Nickel ANO-CC

Basis set:NI.ANO-CC...6S5P4D3F2G.
Type s
No. Exponent Contraction Coefficients
1 0.504801000E+07 0.000009 -0.000003 0.000001 0.000000 0.000001 -0.000001
2 0.755918100E+06 0.000066 -0.000022 0.000008 -0.000002 0.000006 -0.000007
3 0.172026200E+06 0.000349 -0.000113 0.000040 -0.000009 0.000032 -0.000037
4 0.487245700E+05 0.001473 -0.000479 0.000170 -0.000040 0.000136 -0.000151
5 0.158948900E+05 0.005333 -0.001740 0.000617 -0.000143 0.000493 -0.000568
6 0.573746800E+04 0.017107 -0.005631 0.002002 -0.000467 0.001605 -0.001772
7 0.223705100E+04 0.048861 -0.016456 0.005865 -0.001363 0.004687 -0.005460
8 0.927030200E+03 0.121470 -0.043024 0.015497 -0.003621 0.012474 -0.013641
9 0.403346100E+03 0.246526 -0.097505 0.035728 -0.008317 0.028685 -0.034147
10 0.182428200E+03 0.355388 -0.176338 0.067404 -0.015875 0.055157 -0.059246
11 0.845891700E+02 0.275846 -0.198360 0.080570 -0.018844 0.065952 -0.086914
12 0.384229300E+02 0.069004 0.042452 -0.019331 0.004125 -0.018493 0.058254
13 0.184687900E+02 0.007444 0.519460 -0.313771 0.078913 -0.272502 0.261918
14 0.886819000E+01 0.010282 0.503637 -0.462103 0.119171 -0.591069 0.985165
15 0.391887000E+01 0.000634 0.091330 0.154607 -0.046954 0.740171 -2.188548
16 0.183985300E+01 0.000345 -0.002295 0.709505 -0.256324 1.181032 0.240535
17 0.804663000E+00 -0.000111 0.002229 0.396268 -0.234621 -1.219349 1.758502
18 0.169846000E+00 0.000050 -0.000496 0.026910 0.377750 -1.141027 -2.127599
19 0.793700000E-01 -0.000046 0.000479 -0.013467 0.566158 1.068052 0.812935
20 0.347000000E-01 0.000023 -0.000228 0.007432 0.213963 0.149415 0.523147
21 0.138800000E-01 -0.000006 0.000062 -0.001670 -0.000579 0.076600 0.098055
Type p
No. Exponent Contraction Coefficients
22 0.914879600E+04 0.000174 -0.000064 0.000030 -0.000063 0.000073
23 0.216717100E+04 0.001527 -0.000562 0.000273 -0.000589 0.000698
24 0.703385700E+03 0.008523 -0.003163 0.001499 -0.003105 0.003648
25 0.268134200E+03 0.035142 -0.013201 0.006429 -0.013917 0.016699
26 0.113007800E+03 0.110276 -0.042789 0.020391 -0.042406 0.051183
27 0.509133900E+02 0.251742 -0.101884 0.050631 -0.112419 0.142253
28 0.238774000E+02 0.382534 -0.165440 0.078389 -0.155368 0.171960

29 0.114892400E+02 0.308917 -0.114200 0.067750 -0.185666 0.203333
30 0.543688400E+01 0.087141 0.192553 -0.169266 0.597158 -1.350551
31 0.253383700E+01 0.003858 0.475674 -0.320791 0.640662 0.620657
32 0.113530900E+01 0.001511 0.397937 -0.000685 -0.837665 1.129670
33 0.467891000E+00 -0.000253 0.106795 0.263241 -0.574651 -1.197881
34 0.187156000E+00 0.000213 -0.000965 0.533178 0.433644 -0.235407
35 0.748620000E-01 -0.000090 0.002665 0.304384 0.387403 0.627753
36 0.299450000E-01 0.000029 -0.000764 0.016880 0.038201 0.179250
Type d
No. Exponent Contraction Coefficients
37 0.258866700E+03 0.000958 -0.000898 0.001162 -0.002193
38 0.774960400E+02 0.008226 -0.007371 0.009350 -0.023199
39 0.295897200E+02 0.037527 -0.035025 0.046091 -0.095891
40 0.125152700E+02 0.113870 -0.101026 0.122019 -0.324067
41 0.562446800E+01 0.232878 -0.256510 0.400709 -0.560409
42 0.255130300E+01 0.315566 -0.279457 0.151944 0.802177
43 0.112806000E+01 0.309224 0.011467 -0.534013 0.392818
44 0.475373000E+00 0.242474 0.340059 -0.360747 -0.677505
45 0.182128000E+00 0.123553 0.398781 0.213137 -0.246325
46 0.728510000E-01 0.035331 0.302658 0.590550 0.607558
Type f
No. Exponent Contraction Coefficients
47 0.142156000E+02 0.030351 -0.044772 0.108701
48 0.563450000E+01 0.243950 -0.511995 0.786258
49 0.223330000E+01 0.514396 -0.314354 -0.673275
50 0.885200000E+00 0.346486 0.525100 -0.338303
51 0.350900000E+00 0.146727 0.381028 0.615772
52 0.139100000E+00 0.030873 0.121066 0.236110
Type g
No. Exponent Contraction Coefficients
53 0.803990000E+01 0.157216 -0.425203
54 0.316010000E+01 0.614569 -0.452658
55 0.124210000E+01 0.377925 0.617079
56 0.488200000E+00 0.105175 0.404607

D.4 Cobalt ANO-CC

Basis set:CO.ANO-CC...6S5P4D3F2G.
Type s
No. Exponent Contraction Coefficients
1 0.467670800E+07 0.000009 -0.000003 0.000001 0.000000 0.000001 -0.000001
2 0.700317200E+06 0.000067 -0.000022 0.000008 -0.000002 0.000006 -0.000007
3 0.159373000E+06 0.000351 -0.000114 0.000040 -0.000009 0.000032 -0.000037
4 0.451406700E+05 0.001478 -0.000480 0.000169 -0.000040 0.000134 -0.000154
5 0.147257500E+05 0.005353 -0.001744 0.000613 -0.000145 0.000487 -0.000580
6 0.531544800E+04 0.017169 -0.005642 0.001989 -0.000473 0.001585 -0.001799
7 0.207249800E+04 0.049025 -0.016481 0.005827 -0.001382 0.004636 -0.005582

8 0.858823100E+03 0.121805 -0.043060 0.015385 -0.003669 0.012300 -0.013811
9 0.373643700E+03 0.246946 -0.097450 0.035430 -0.008417 0.028337 -0.034925
10 0.168968200E+03 0.355373 -0.175886 0.066701 -0.016032 0.054155 -0.059556
11 0.783197100E+02 0.275015 -0.197285 0.079532 -0.018978 0.065098 -0.089581
12 0.355372400E+02 0.068595 0.042338 -0.019165 0.004166 -0.019748 0.065227
13 0.170473500E+02 0.007857 0.517317 -0.308568 0.079156 -0.262924 0.251578
14 0.817553400E+01 0.010717 0.504554 -0.461614 0.121578 -0.587223 1.019783
15 0.361157800E+01 0.000715 0.091948 0.145719 -0.045157 0.708719 -2.235969
16 0.169746800E+01 0.000346 -0.002367 0.708932 -0.261776 1.204028 0.239805
17 0.743636000E+00 -0.000111 0.002265 0.401679 -0.241328 -1.207743 1.804698
18 0.158325000E+00 0.000052 -0.000519 0.028044 0.386695 -1.198085 -2.234078
19 0.750090000E-01 -0.000048 0.000510 -0.014135 0.558871 1.126353 0.946293
20 0.330930000E-01 0.000024 -0.000236 0.007782 0.213460 0.136905 0.456993
21 0.132370000E-01 -0.000006 0.000064 -0.001684 0.001987 0.080528 0.105895
Type p
No. Exponent Contraction Coefficients
22 0.842184200E+04 0.000175 -0.000064 0.000029 -0.000062 0.000062
23 0.199500000E+04 0.001538 -0.000562 0.000264 -0.000586 0.000604
24 0.647485500E+03 0.008576 -0.003156 0.001449 -0.003083 0.003091
25 0.246779500E+03 0.035297 -0.013147 0.006206 -0.013807 0.014391
26 0.103968900E+03 0.110511 -0.042498 0.019617 -0.041901 0.042935
27 0.468105200E+02 0.251625 -0.100863 0.048588 -0.110970 0.121831
28 0.219270300E+02 0.382114 -0.163560 0.074852 -0.151735 0.140231
29 0.105371500E+02 0.309434 -0.114717 0.065905 -0.185124 0.192339
30 0.498067800E+01 0.087485 0.188688 -0.158763 0.575573 -1.088357
31 0.231982400E+01 0.003773 0.474576 -0.310849 0.654271 0.307718
32 0.103960900E+01 0.001494 0.400831 -0.013780 -0.811053 1.115680
33 0.428921000E+00 -0.000270 0.108233 0.250870 -0.581382 -0.843410
34 0.171568000E+00 0.000215 -0.000984 0.532806 0.381500 -0.549849
35 0.686270000E-01 -0.000092 0.002683 0.311951 0.388343 0.572361
36 0.274510000E-01 0.000029 -0.000768 0.032670 0.079464 0.398264
Type d
No. Exponent Contraction Coefficients
37 0.237592800E+03 0.000933 -0.000825 0.001106 -0.002152
38 0.710888100E+02 0.007988 -0.006719 0.008671 -0.022013
39 0.271190300E+02 0.036298 -0.031887 0.043317 -0.092903
40 0.114482600E+02 0.110280 -0.091170 0.110852 -0.304578
41 0.513954200E+01 0.228086 -0.238706 0.394687 -0.589757
42 0.233269400E+01 0.313463 -0.278133 0.197489 0.748842
43 0.103403000E+01 0.310691 -0.018011 -0.505694 0.460940
44 0.437899000E+00 0.246359 0.314587 -0.402289 -0.640344
45 0.168963000E+00 0.126798 0.399949 0.150039 -0.324261
46 0.675850000E-01 0.038696 0.345261 0.622049 0.624698
Type f
No. Exponent Contraction Coefficients
47 0.128403000E+02 0.029253 -0.038500 0.097823
48 0.508940000E+01 0.249511 -0.506844 0.798778
49 0.201720000E+01 0.518873 -0.312590 -0.670623

50 0.799600000E+00 0.340535 0.526345 -0.343822
51 0.316900000E+00 0.141868 0.386448 0.610766
52 0.125600000E+00 0.029439 0.124802 0.239836
Type g
No. Exponent Contraction Coefficients
53 0.726210000E+01 0.162360 -0.417109
54 0.285440000E+01 0.616090 -0.453815
55 0.112190000E+01 0.370661 0.614560
56 0.441000000E+00 0.109129 0.412990

Bibliography

[1] F. GAO, Y. WANG, J. ZHANG, D. SHI, M. WANG, R. HUMPHRY-BAKER, P. WANG, S. M. ZAKEERUDDIN, and M. GRATZEL, *Chem. Commun.* , 2635 (2008), DOI = 10.1039/b802909a.

[2] P. R. TAYLOR, *J. Inorg. Biochem.* **100**, 780 (2006), DOI = 10.1016/j.jinorgbio.2006.01.026.

[3] F. JENSEN, *Introduction to Computational Chemistry*, John Wiley and Sons Ltd, 2 edition, 2006.

[4] P.-O. WIDMARK, ED., *European Summer School in Quantum Chemistry 2005*, volume I, Lund University, 4 edition, 2005.

[5] P.-O. WIDMARK, ED., *European Summer School in Quantum Chemistry 2005*, volume II, Lund University, 4 edition, 2005.

[6] P.-O. WIDMARK, ED., *European Summer School in Quantum Chemistry 2005*, volume III, Lund University, 4 edition, 2005.

[7] J. HARVEY, Molecular Electronic Structure, `http://www.chm.bris.ac.uk/pt/harvey/elstruct/introduction.html` .

[8] H. B. SCHLEGEL and M. J. FRISCH, *Int. J. Quantum Chem.* **54**, 83 (1995), DOI = 10.1002/qua.560540202.

[9] W. KOHN and L. J. SHAM, *Phys. Rev.* **140**, A1133 (1965), DOI = 10.1103/PhysRev.140.A1133.

[10] R. O. JONES and O. GUNNARSSON, *Rev. Mod. Phys.* **61**, 689 (1989), DOI = 10.1103/RevModPhys.61.689.

[11] U. VON BARTH and L. HEDIN, *JoPC* **5**, 1629 (1972), DOI = 10.1088/0022-3719/5/13/012.

[12] A. D. BECKE, *J. Chem. Phys.* **98**, 5648 (1993), DOI = 10.1063/1.464913.

[13] C. LEE, W. YANG, and R. G. PARR, *Phys. Rev. B* **37**, 785 (1988), DOI = 10.1103/PhysRevB.37.785.

[14] B. O. ROOS, *Int. J. Quantum Chem.* **18**, 175 (1995), DOI = 10.1002/qua.560180822.

[15] S. HUZINAGA, *J. Chem. Phys.* **42**, 1293 (1965), DOI = 10.1063/1.1696113.

[16] F. B. VAN DUIJNEVELDT, *IBM Tech. Res. Rep.* , RJ945 (1971).

[17] H. PARTRIDGE, *J. Chem. Phys.* **90**, 1043 (1989), DOI = 10.1063/1.456157.

[18] T. H. DUNNING JR., *J. Chem. Phys.* **55**, 716 (1971), DOI = 10.1063/1.1676139.

[19] A. D. MCLEAN and G. S. CHANDLER, *J. Chem. Phys.* **72**, 5639 (1980), DOI = 10.1063/1.438980.

[20] T. H. DUNNING JR., *J. Chem. Phys.* **90**, 1007 (1989), DOI = 10.1063/1.456153.

[21] T. H. DUNNING JR., R. A. KENDALL, and R. J. HARRISON, *J. Chem. Phys.* **96**, 6796 (1992), DOI = 10.1063/1.462569.

[22] A. SCHÄFER, C. HUBER, and R. AHLRICHS, *J. Chem. Phys.* **100**, 5829 (1994), DOI = 10.1063/1.467146.

[23] A. SCHÄFER, H. HORN, and R. AHLRICHS, *J. Chem. Phys.* **97**, 2571 (1992), DOI = 10.1063/1.463096.

[24] F. WEIGEND, F. FURCHE, and R. AHLRICHS, *J. Chem. Phys.* **119**, 12753 (2003), DOI = 10.1063/1.1627293.

[25] J. ALMLÖF and P. R. TAYLOR, *J. Chem. Phys.* **86**, 4070 (1987), DOI = 10.1063/1.451917.

[26] A. J. H. WACHTERS, *J. Chem. Phys.* **52**, 1033 (1970), DOI = 10.1063/1.1673095.

[27] P. J. HAY, *J. Chem. Phys.* **66**, 4377 (1977), DOI = 10.1063/1.433731.

[28] R. F. STEWART, *J. Chem. Phys.* **52**, 431 (1970), DOI = 10.1063/1.1672702.

[29] C. W. BAUSCHLICHER JR., S. R. LANGHOFF, H. PARTRIDGE, and L. A. BARNES, *J. Chem. Phys.* **91**, 2399 (1989), DOI = 10.1063/1.456998.

[30] R. D. AMOS, A. BERNHARDSSON, A. BERNING, P. CELANI, D. L. COOPER, M. J. O. DEEGAN, A. J. DOBBYN, F. ECKERT, C. HAMPEL, G. HETZER, P. J. KNOWLES, T. KORONA, R. LINDH, A. W. LLOYD, S. J. MCNICHOLAS, F. R. MANBY, W. MEYER, M. E. MURA, A. NICKLASS, P. PALMIERI, R. PITZER, G. RAUHUT, M. SCHÜTZ, U. SCHUMANN, H. STOLL, A. J. STONE, R. TARRONI, T. THORSTEINSSON, and H.-J. WERNER, MOLPRO, a package of ab initio programs designed by H.-J. Werner and P. J. Knowles, version 2002.1.

[31] A. GHOSH and P. R. TAYLOR, *Curr. Opin. Chem. Biol.* **7**, 113 (2003), DOI = 10.1016/S1367-5931(02)00023-6.

[32] R. LINDH, U. RYU, and B. LIU, *J. Chem. Phys.* **95**, 5889 (1991), DOI = 10.1063/1.461610.

[33] H. WERNER and P. J. KNOWLES, *J. Chem. Phys.* **82**, 5053 (1985), DOI = 10.1063/1.448627.

[34] H. WERNER and P. J. KNOWLES, *Chem. Phys. Lett.* **115**, 259 (1985), DOI = 10.1016/0009-2614(85)80025-7.

[35] G. KARLSTRÖM, R. LINDH, P.-Å. MALMQVIST, B. O. ROOS, U. RYDE, V. VERYAZOV, P.-O. WIDMARK, M. COSSI, B. SCHIMMELPFENNIG, P. NEOGRADY, and L. SEIJO, *Comp. Mater. Sci.* **28**, 222 (2003), DOI = 10.1016/S0927-0256(03)00109-5.

[36] G. SCHAFTENAAR and J. NOORDIK, *J. Comput.-Aided Mol. Des.* **14**, 123 (2000), DOI = 10.1023/A:1008193805436.

[37] N. C. HANDY and A. J. COHEN, *Mol. Phys.* **99**, 403 (2001), DOI = 10.1080/00268970010018431.

[38] J. P. PERDEW, K. BURKE, and M. ERNZERHOF, *Phys. Rev. Lett.* **77**, 3865 (1996), DOI = 10.1103/PhysRevLett.77.3865.

[39] J. P. PERDEW, K. BURKE, and M. ERNZERHOF, *Phys. Rev. Lett.* **78**, 1396 (1997), DOI = 10.1103/PhysRevLett.78.1396.

[40] J. CONRADIE and A. GHOSH, *J. Chem. Theory Comput.* **3**, 689 (2007), DOI = 10.1021/ct600337j.

[41] X. DAI, P. KAPOOR, and T. H. WARREN, *JACS* **126**, 4798 (2004), DOI = 10.1021/ja036308i.

[42] G. BAI, P. WEI, A. DAS, and D. W. STEPHAN, *Organometallics* **25**, 5870 (2006), DOI = 10.1021/om060757k.

[43] E. KOGUT, H. L. WIENCKO, L. ZHANG, D. E. CORDEAU, and T. H. WARREN, *JACS* **127**, 11248 (2005), DOI = 10.1021/ja0533186.

[44] J. PRUST, H. HOHMEISTER, A. STASCH, H. W. ROESKY, J. MAGULL, E. ALEXOPOULOS, I. USÓN, H.-G. SCHMIDT, and M. NOLTEMEYER, *Eur. J. Inorg. Chem.* **2002**, 2156 (2002), DOI = 10.1002/1099-0682(200208)2002:8¡2156::AID-EJIC2156¿3.0.CO;2-P.

[45] M. BRUSTLE, *Nachr. Chem. Tech. Lab.* **49**, 1310 (2001).

[46] R. AHLRICHS, M. BÄR, H.-P. BARON, R. BAUERNSCHMITT, S. BÖCKER, P. DEGLMANN, M. EHRIG, K. EICHKORN, S. ELLIOTT, F. FURCHE, F. HAASE, M. HÄSER, H. HORN, C. HÄTTIG, C. HUBER, U. HUNIAR, M. KATTANNEK, A. KÖHN, C. KÖLMEL, M. KOLLWITZ, K. MAY, C. OCHSENFELD, H. ÖHM, A. SCHÄFER, U. SCHNEIDER, M. SIERKA, O. TREUTLER, B. UNTERREINER, M. VON ARNIM, F. WEIGEND, P. WEIS, and H. WEISS, Turbomole see, `http://www.chem-bio.uni-karlsruhe.de/TheoChem/turbomole/intro.en.html` .

[47] R. AHLRICHS, M. BÄR, M. HÄSER, H. HORN, and C. KÖLMEL, *Chem. Phys. Lett.* **162**, 165 (1989), DOI = 10.1016/0009-2614(89)85118-8.

[48] O. TREUTLER and R. AHLRICHS, *J. Chem. Phys.* **102**, 346 (1995), DOI = 10.1063/1.469408.

[49] M. VON ARNIM and R. AHLRICHS, *J. Chem. Phys.* **111**, 9183 (1999), DOI = 10.1063/1.479510.

[50] H. WERNER, C. HAMPEL, and P. J. KNOWLES, *J. Chem. Phys.* **99**, 5219 (1993), DOI = 10.1063/1.465990.

[51] H. WERNER, C. HAMPEL, and P. J. KNOWLES, *J. Chem. Phys.* **112**, 3106 (2000), DOI = 10.1063/1.480886.

[52] N. A. ECKERT, S. VADDADI, S. STOIAN, R. J. LACHICOTTE, T. R. CUNDARI, and P. L. HOLLAND, *Angew. Chem. Int. Ed.* **45**, 6868 (2006), DOI = 10.1002/anie.200601927.

[53] K. J. NELSON, I. D. GILES, W. W. SHUM, A. M. ARIF, and J. S. MILLER, *Angew. Chem. Int. Ed.* **44**, 3129 (2005), DOI = 10.1002/anie.200462763.

[54] M. NAKAMURA, *Angew. Chem. Int. Ed.* **48**, 2638 (2009), DOI = 10.1002/anie.200805446.

[55] R. L. LORD and M.-H. BAIK, *Inorg. Chem.* **47**, 4413 (2008), DOI = 10.1021/ic8000653.

[56] R. J. DEETH, *Eur. J. Inorg. Chem.* **2006**, 2551 (2006), DOI = 10.1002/ejic.200600137.

[57] R. S. BERRY, *J. Chem. Phys.* **32**, 933 (1960), DOI = 10.1063/1.1730820.

[58] G. M. WHITESIDES and H. L. MITCHELL, *J. Am. Chem. Soc.* **91**, 5384 (1969), DOI = 10.1021/ja01047a034.

[59] J. D. DUNITZ and V. PRELOG, *Angew. Chem. Int. Ed.* **7**, 725 (1968), DOI = 10.1002/anie.196807251.

[60] A. R. ALLOUCHE, Gabedit is a free Graphical User Interface for computational chemistry packages. It is available from `http://gabedit.sourceforge.net/` .

[61] H. F. SCHAEFER III ED., I. SHAVITT, C. F. BENDER, F. W. BOBROWICZ, G. DAS, T. H. DUNNING JR., A. A. FROST, W. A. GODDARD III, R. F. HAUSMAN JR., P. J. HAY, W. KUTZELNIGG, C. W. MCCURDY JR., V. MCKOY, W. MEYER, J. W. MOSKOWITZ, T. N. RESCIGNO, B. O. ROOS, P. E. M. SIEGBAHN, L. C. SNYDER, A. C. WAHL, and D. L. YEAGER, *Modern Theoretical Chemistry Volume 3: Methods of Electronic Structure Theory*, Plenum Press, New York, Ny, 1 edition, 1977.

[62] J. L. WHITTEN and M. HACKMEYER, *J. Chem. Phys.* **51**, 5584 (1969), DOI = 10.1063/1.1671985.

[63] J. L. WHITTEN and M. HACKMEYER, *J. Chem. Phys.* **54**, 3739 (1971), DOI = 10.1063/1.1675423.

[64] W. J. HUNT and W. A. GODDARD III, *Chem. Phys. Lett.* **3**, 414 (1969), DOI = 10.1016/0009-2614(69)80154-5.

[65] P. R. TAYLOR and P.-O. WIDMARK, ED., *European Summer School in Quantum Chemistry 2009*, volume III, Lund University, 6 edition, 2009.

[66] L. B. and A. D. McLean, *J. Chem. Phys.* **91**, 2348 (1989), DOI = 10.1063/1.457043.

[67] S. F. Boys and F. Bernardi, *Mol. Phys.* **19**, 553 (1970), DOI = 10.1080/00268977000101561.

[68] T. H. Dunning Jr. and D. E. Woon, *J. Chem. Phys.* **98**, 1358 (1993), DOI = 10.1063/1.464303.

[69] J. F. Berry, E. Bill, E. Bothe, S. D. George, B. Mienert, F. Neese, and K. Wieghardt, *Science* **312**, 1937 (2006), DOI = 10.1126/science.1128506.

[70] J. Bendix, K. Meyer, T. Weyhermüller, E. Bill, N. Metzler-Nolte, and K. Wieghardt, *Inorg. Chem.* **37**, 1767 (1998), DOI = 10.1021/ic971377h.

[71] T. Birk, H. O. Sørensen, and J. Bendix, *Acta Crystallogr., Sect. C* **C61**, m231 (2005), DOI = 10.1107/S0108270105008693.

[72] C.-C. Wang, Y. Wang, L.-K. Chou, and C.-M. Che, *J. Phys. Chem.* **99**, 13899 (1995), DOI = 10.1021/j100038a022.

[73] C.-C. Wang, T.-H. Tang, and Y. Wang, *J. Phys. Chem. A* **104**, 9566 (2000), DOI = 10.1021/jp001130x.

[74] K. Meyer, J. Bendix, E. Bill, T. Weyhermüller, and K. Wieghardt, *Inorg. Chem.* **37**, 5180 (1998), DOI = 10.1021/ic980392q.

[75] T. Birk and J. Bendix, *Inorg. Chem.* **42**, 7608 (2003), DOI = 10.1021/ic034777f.